

$\Delta F = 2$ observables and $B \rightarrow X_q \gamma$ decays in the Left-Right Model: Higgs particles striking back

Monika Blanke^a Andrzej J. Buras^{b,c} Katrin Gemmler^b and Tillmann Heidsieck^b

^aLaboratory for Elementary Particle Physics, Cornell University,
142 Sciences Drive, Ithaca, NY 14853, USA

^bPhysik Department, Technische Universität München, James-Frank-Straße,
D-85747 Garching, Germany

^cTUM Institute for Advanced Study, Lichtenbergstr. 2a, D-85747 Garching, Germany

E-mail: mb744@cornell.edu, Andrzej.Buras@ph.tum.de,

Katrin.Gemmler@ph.tum.de, Tillmann.Heidsieck@ph.tum.de

ABSTRACT: We present a complete study of $\Delta S = 2$ and $\Delta B = 2$ processes in the left-right model (LRM) based on the weak gauge group $SU(2)_L \times SU(2)_R \times U(1)_{B-L}$. This includes ε_K , ΔM_K , ΔM_q , A_{SL}^q , $\Delta \Gamma_q$ with $q = d, s$ and the mixing induced CP asymmetries $S_{\psi K_S}$ and $S_{\psi\phi}$. Compared to the Standard Model (SM) these observables are affected by tree level contributions from heavy neutral Higgs particles (H^0) as well as new box diagrams with W_R gauge boson and charged Higgs (H^\pm) exchanges. We also analyse the $B \rightarrow X_{s,d} \gamma$ decays that receive important new contributions from the $W_L - W_R$ mixing and H^\pm exchanges. Compared to the existing literature the novel feature of our analysis is the search for correlations between various observables that could help us to distinguish this model from other extensions of the SM and to obtain an insight into the structure of the mixing matrix V^R that governs right-handed currents. Moreover, we perform the full phenomenology including both gauge boson and Higgs boson contributions. We find that even for $M_{H^0} \approx M_{H^\pm} \sim \mathcal{O}(20)$ TeV, the tree level H^0 contributions to $\Delta F = 2$ observables are by far dominant and the H^\pm contributions to $B \rightarrow X_q \gamma$ can be very important, even dominant for certain parameters of the model. While in a large fraction of the parameter space this model has to struggle with the experimental constraint from ε_K , we demonstrate that there exist regions in parameter space which satisfy all existing $\Delta F = 2$, $B \rightarrow X_{s,d} \gamma$, tree level decays and electroweak precision constraints for scales $M_{W_R} \simeq 2 - 3$ TeV in the reach of the LHC. We also show that the $S_{\psi K_S} - \varepsilon_K$ tension present in the SM can be removed in the LRM. Simultaneously $\text{Br}(B \rightarrow X_s \gamma)$ can be brought closer to the data. However, we point out that with the increased lower bound on M_{W_R} , the LRM cannot help in explaining the difference between the inclusive and exclusive determinations of $|V_{ub}|$, when all constraints are taken into account, unless allowing for large fine-tuning. Finally we present a rather complete list of Feynman rules involving quarks, gauge bosons and Higgs particles.

KEYWORDS: Beyond the Standard Model

Contents

1	Introduction	1
2	Models with Left-Right gauge symmetry	4
2.1	Gauge group and fermion content	4
2.2	Higgs sector and spontaneous symmetry breaking	5
2.3	Gauge sector after electroweak symmetry breaking	6
2.4	Yukawa interactions and fermion masses	7
2.5	Parameter counting	7
3	$\Delta F = 2$ transitions	8
3.1	Preliminaries	8
3.2	Local operators	9
3.3	Effective Hamiltonian	10
3.3.1	Wilson coefficients from gauge boson box diagrams	10
3.3.2	Wilson coefficients from charged Higgs box diagrams	11
3.3.3	Wilson coefficients from tree level Higgs exchange	12
3.4	QCD corrections and hadronic matrix elements	12
3.5	Final expressions for mixing amplitudes	15
3.6	General anatomy of LR contributions	16
3.7	Special anatomy of LR contributions	17
3.8	Comparison of the operator structure in various models	19
3.9	Basic formulae for $\Delta F = 2$ observables	19
3.10	Summary	22
4	The decays $B \rightarrow X_{s,d}\gamma$	23
4.1	Preliminaries	23
4.2	Gauge boson contributions	23
4.3	Charged Higgs contributions	25
4.4	QCD corrections	26
4.5	The branching ratio	27
4.6	Dissecting the LR contributions to $\text{Br}(B \rightarrow X_s\gamma)$	28
4.7	The decay $B \rightarrow X_d\gamma$	28
4.8	CP asymmetries in $B \rightarrow X_{s,d}\gamma$	31
5	Constraints from tree level decays	31
5.1	Preliminaries	31
5.2	Constraints on the mixing matrices V^L and V^R	32
5.2.1	$u \rightarrow d$	33
5.2.2	$u \rightarrow s$	33
5.2.3	$c \rightarrow d$	33

5.2.4	$c \rightarrow s$	33
5.2.5	$b \rightarrow u$	33
5.2.6	$b \rightarrow c$	34
5.2.7	$t \rightarrow d, s$	34
5.2.8	$t \rightarrow b$	34
5.3	Charged Higgs contributions	34
5.4	A comment on $Z \rightarrow b\bar{b}$	35
5.5	Impact on CP asymmetries	35
5.5.1	CP asymmetry in $B \rightarrow DK$ and the angle γ	35
5.5.2	The impact on $S_{\psi K_S}$ and $S_{\psi\phi}$	37
5.5.3	Summary	38
6	Electroweak precision constraints	38
6.1	Preliminaries	38
6.2	Basic structure of the analysis	38
6.3	Basic constraints	40
7	Strategy for the numerical analysis	41
7.1	Preliminaries	41
7.2	Anomalies in the flavour data	41
7.2.1	The $\varepsilon_K - S_{\psi K_S}$ anomaly	42
7.2.2	$ V_{ub} $ problem	42
7.2.3	Possible solutions	42
7.2.4	Enhanced value of $S_{\psi\phi}$	43
7.3	Addressing the flavour anomalies in the LRM	43
7.3.1	Various scenarios for $ V_{ub} $	43
7.3.2	Understanding anomalies through V^R	44
7.4	Nominal input parameters	49
8	A numerical (re-)analysis of EWPT constraints	49
8.1	Numerical procedure for the EWP tests	50
8.2	Electroweak precision constraints	50
9	A general study of V^R	53
9.1	Allowed ranges for V^R	53
9.2	A fine-tuning study	54
9.3	A closer look at the “normal hierarchy” scenario	57
10	A brief discussion of flavour observables	58
10.1	A summary of possible size of NP effects in the different meson systems	58
10.2	The phase of B_s mixing and $\text{Br}(B \rightarrow X_q \gamma)$	59
10.3	The $ V_{ub} $ problem in the LRM	61
11	The role of the heavy Higgs mass	62

12 Comparison to other models	63
12.1 Preliminaries	63
12.2 LR models with additional flavour symmetries	63
12.3 2HDM with flavour blind phases: 2HDM _{MFV}	64
12.4 Right-handed MFV	64
12.5 Randall-Sundrum with custodial protection	65
12.6 Four generations: SM4	65
12.7 Littlest Higgs with T-parity	66
13 Summary	66
A Higgs potential	68
B Gauge boson masses and mixings	69
C Goldstone boson and Higgs mass eigenstates	70
D Numerical details for $\Delta F = 2$	71
E Feynman rules	72

1 Introduction

A very important property of the Standard Model (SM) regarding flavour violating processes is the left-handed structure of the charged current interactions reflecting the maximal violation of parity observed in low energy processes. Left-handed charged currents encode at the level of the Lagrangian the full information about flavour mixing and CP violation represented compactly by the CKM matrix. Due to the GIM [1] mechanism this structure has automatically profound implications for the pattern of FCNC processes that seems to be in remarkable accordance with the present data within theoretical and experimental uncertainties [2, 3], bearing in mind certain anomalies [2, 4–12], in particular in CP-violating observables which are discussed below.

As the SM is expected to be only the low-energy limit of a more fundamental theory it is conceivable that at very short distance scales parity could be a good symmetry implying the existence of right-handed (RH) charged currents. Prominent examples of such fundamental theories are left-right (LR) symmetric models on which a rich literature exists. Indeed, LR symmetric models were born 37 years ago [13–17]. Early papers mainly cover the examinations of two special cases, known as “manifest“ scenario [17] and ”pseudo-manifest“ scenario [18–21], which are characterised by no spontaneous and fully spontaneous CP violation, respectively. The right-handed counterpart of the CKM matrix appears then in a special form being either identical to or the complex-conjugate of the CKM matrix up to certain phases as e.g. summarised in [22]. The phenomenology of both scenarios has

widely been studied in the literature [23–26]. By now in both scenarios strong constraints on the heavy charged gauge boson mass $M_{W_R} \gtrsim 4 \text{ TeV}$ have been obtained [23, 27, 28] from the constraints on the $K_L - K_S$ mass difference, CP violation in kaon decays and the neutron electric dipole moment, making these scenarios difficult to access in direct searches at the LHC. In addition the "pseudo-manifest" scenario has been ruled out by both the appearance of light Higgs triplets [29] and the correlation of ε_K and $\sin(2\beta)$ [30]. This means that the right-handed mixing matrix must be different from the CKM matrix in order to reach agreement with experiment. Motivated by this fact more general studies on CP violation have been performed in [22, 31, 32]. More recent extensive analyses of many observables in the LR symmetric framework can be found in e.g. [28, 33–36].

Theoretical interest in models with an underlying $SU(2)_L \times SU(2)_R$ global symmetry has also been motivated by Higgsless models [37–40]. Moreover, the recent phenomenological interest in having another look at the right-handed currents in general originated from tensions between inclusive and exclusive determinations of the elements of the CKM matrix $|V_{ub}|$ and $|V_{cb}|$. As pointed out and analysed recently in particular in [41–43], the presence of right-handed currents could either remove or significantly weaken some of these tensions, especially in the case of $|V_{ub}|$. The implications of these findings for many observables within an effective theory approach have been studied in [44].

Yet an effective theory approach, as interesting as it may be, involves a number of unknown couplings that limit the predictive power of the theory and in particular does not allow to correlate low-energy high precision observables to high energy processes being already explored in a new domain of energy at the LHC. In this context we refer to [45, 46] where extensive analyses of LR symmetric models have been performed for early LHC data. Therefore it is of interest as a preparation for new discoveries both through high energy processes and high precision experiments in this decade to perform a detailed phenomenological analysis in a concrete class of models with right-handed currents, in particular models with LR symmetry. As manifest and pseudo-manifest LR models have already been ruled out we term the model with extended gauge group but without exact P or C symmetry *Left-Right Model* (LRM).

The goal of the present paper is to analyse the well measured FCNC observables related to the particle-antiparticle mixings $K^0 - \bar{K}^0$ and $B_{d,s}^0 - \bar{B}_{d,s}^0$ in this NP scenario. For a RH scale in the reach of the LHC the off-diagonal mixing amplitudes M_{12}^i ($i = K, d, s$) receive important and often dangerous tree level contributions from neutral heavy scalar particles (H^0) present in this model. Additionally box diagrams with exchanges of a heavy W'^{\pm} and charged Higgs (H^{\pm}) exchanges and right-handed couplings of the light W^{\pm} are present. Similarly the $W_L - W_R$ mixing can have a significant impact on the $B \rightarrow X_s \gamma$ decay that often puts a severe constraint on extensions of the SM. Also heavy charged Higgs (H^{\pm}) exchanges can contribute and in fact these contributions cannot be neglected as often done in the literature.

We would like to know whether this class of very interesting models can be made consistent with all existing data for RH scales as low as $M_{W_R} \simeq (2 - 3) \text{ TeV}$, which is still consistent with direct collider searches, while solving various anomalies observed in the quark sector.

As there have been other analyses of particle-antiparticle mixing [22, 23, 27, 28, 31, 33, 47–53] and $B \rightarrow X_s \gamma$ [54–62] in LR models, it is mandatory for us to state what is new in our paper:

- First of all we perform a simultaneous analysis of the most interesting $\Delta F = 2$ observables in the K and $B_{d,s}$ meson systems in conjunction with the decays $B \rightarrow X_s \gamma$ and $B \rightarrow X_d \gamma$. The analysis is performed in a general framework of the LRM and hence without making from the beginning particular assumptions on the structure of the right-handed mixing matrix or equality of gauge couplings. That is, in contrast to previous analyses we do not assume a certain specific form for V^R by restricting its parameters, but search for its structure by using the bounds from tree-level decays, $\Delta F = 2$ observables, $B \rightarrow X_q \gamma$ decays and imposing constraints from electroweak precision tests. This strategy differs from the existing literature which dominantly considered bounds on the parameters of LR models, in particular on the masses of W'^{\pm} and H^0 .
- In this manner we are led to new structures of the V^R matrix that are still rather simple and allow to monitor transparently which anomalies observed in the quark sector can be solved in these models. In this context we search for correlations between various observables.
- We perform the full phenomenology including both gauge boson and Higgs boson contributions finding that even for $M_{H^0} \approx M_{H^{\pm}} \sim \mathcal{O}(20)$ TeV, the tree level H^0 contributions to $\Delta F = 2$ observables are by far dominant and the H^{\pm} contributions to $B \rightarrow X_q \gamma$ can be very important and even dominant for certain parameters of the model. In this context we include the known QCD corrections.
- We analyse the issue of the element $|V_{ub}|$ in this specific model with right-handed currents, pointing out that with the increased lower bound on M_{W_R} , these models cannot help in explaining the difference between the inclusive and exclusive determinations of $|V_{ub}|$, when all constraints are taken into account, unless allowing for large fine-tuning of parameters.
- We investigate a soft lower bound on the heavy Higgs mass.
- We present a collection of Feynman rules necessary for the analysis of all flavour violating processes, in particular $\Delta F = 2$ transitions considered in the present paper. These rules could also be useful for collider physics.

Our paper is organised as follows. In section 2 we summarise briefly the main ingredients of the LRM. In section 3 we present the effective Hamiltonians for $K^0 - \bar{K}^0$, $B_d^0 - \bar{B}_d^0$ and $B_s^0 - \bar{B}_s^0$ mixings and we calculate the most interesting observables such as the CP-violating parameter ε_K , the mass differences ΔM_K and ΔM_q , the CP-asymmetries A_{SL}^q ($q = d, s$), $S_{\psi K_S}$ and $S_{\psi \phi}$ and the width differences $\Delta \Gamma_q$. In section 4 we present the analysis of the $B \rightarrow X_{s,d} \gamma$ decays including CP-violating asymmetries. In section 5 we face

tree level decays including $B^+ \rightarrow \tau^+ \nu_\tau$. In section 6 we summarise the existing constraints on the LRM from the electroweak precision tests. In section 7 we outline our strategy for the numerical analysis. In this context we review the existing anomalies in the flavour data and present a simple analytical expression for the right-handed matrix V^R that allows to see how these anomalies can be solved in a correlated manner for different values of $|V_{ub}|$. In section 8 we present the bounds on the electroweak sector of the LRM from electroweak precision tests. In section 9 a general study of the right-handed mixing matrix V^R is presented. Subsequently in section 10 a detailed numerical analysis of particle-antiparticle mixing observables and of $B \rightarrow X_{s,d} \gamma$ decays including tree-level constraints is performed. In section 11 we derive a soft lower limit on the heavy Higgs masses. In section 12 a brief comparison of the LRM with other models is presented. We summarise our results in section 13. In the appendices we provide a more detailed description of the LRM and the symmetry breaking mechanism, the Higgs sector and numerical insights into the structure of LR contributions to $\Delta F = 2$ operators. Furthermore we provide an extensive list of Feynman Rules for the LRM.

2 Models with Left-Right gauge symmetry

In this section we give a brief description of the LRM. We restrict our presentation to the key properties, which allows us to set our notation. More details on LR symmetric and asymmetric models can be found e. g. in [28, 31, 34] and references therein.

2.1 Gauge group and fermion content

Among the most popular new physics models are LR extensions

$$SU(3)_C \times SU(2)_L \times SU(2)_R \times U(1)_{B-L} \quad (2.1)$$

of the SM gauge group, as they allow for a restoration of parity symmetry at high energies. Note that the spontaneous breaking of parity does not have to be connected to the breakdown to the SM gauge group and can take place at some much higher scale. Therefore we do not restrict ourselves to the study of the parity (or alternatively charge conjugation) symmetric case but consider the generic case with independent gauge couplings g_L, g_R .

The left-handed fermions are embedded as $SU(2)_L$ doublets and $SU(2)_R$ singlets, while the right-handed fermions are $SU(2)_L$ singlets and $SU(2)_R$ doublets:

$$Q_L = \begin{pmatrix} u_L \\ d_L \end{pmatrix} \sim \left(3, 2, 1, \frac{1}{3}\right), \quad Q_R = \begin{pmatrix} u_R \\ d_R \end{pmatrix} \sim \left(3, 1, 2, \frac{1}{3}\right), \quad (2.2)$$

$$L_L = \begin{pmatrix} \nu_L \\ l_L \end{pmatrix} \sim (1, 2, 1, -1), \quad L_R = \begin{pmatrix} \nu_R \\ l_R \end{pmatrix} \sim (1, 1, 2, -1), \quad (2.3)$$

with the quantum numbers given in brackets corresponding to the gauge group in (2.1). We see that instead of the seemingly arbitrary $U(1)_Y$ charges in the SM, the fermionic $U(1)$ charges are now given by their $B - L$ quantum numbers. The resulting electric charges are

$$Q = T_{3L} + T_{3R} + \frac{B - L}{2}. \quad (2.4)$$

2.2 Higgs sector and spontaneous symmetry breaking

The spontaneous symmetry breaking of LR models takes place in two steps.

Step 1: At a high scale $\kappa_R \sim \mathcal{O}(\text{TeV})$ $SU(2)_R \times U(1)_{B-L}$ is broken to the SM hypercharge gauge group $U(1)_Y$:

$$SU(2)_R \times U(1)_{B-L} \rightarrow U(1)_Y. \quad (2.5)$$

The details of this breaking are model-dependent. The two simplest possibilities introduce either two scalar doublets or triplets, however also more complicated $SU(2)_{L,R}$ representations are phenomenologically viable. It turns out that quark flavour phenomenology does not depend on the particular structure of the Higgs sector (for more details see appendix C). Hence from now on we concentrate on the triplet model, which is appealing in the neutrino sector as it naturally generates TeV scale Majorana masses for the right-handed neutrinos [63–66] through the VEV of Δ_R defined below. Consequently the light neutrino masses are suppressed by the TeV scale see-saw mechanism.

In the triplet model, the symmetry breaking $SU(2)_R \times U(1)_{B-L} \rightarrow U(1)_Y$ is achieved by a Higgs triplet Δ_R

$$\Delta_R = \begin{pmatrix} \delta_R^+/\sqrt{2} & \delta_R^{++} \\ \delta_R^0 & -\delta_R^+/\sqrt{2} \end{pmatrix} \sim (1, 1, 3, 2), \quad (2.6)$$

which develops a VEV

$$\langle \Delta_R \rangle = \begin{pmatrix} 0 & 0 \\ \kappa_R & 0 \end{pmatrix}. \quad (2.7)$$

The most recent experimental direct W_R searches find roughly $M_{W_R} \geq 1.5 - 2 \text{ TeV}$ and this can only be satisfied with κ_R much larger than the EWSB scale v . This hierarchy of scales implies that all LR effects can be expanded in powers of the small dimensionless parameter

$$\epsilon = v/\kappa_R. \quad (2.8)$$

Throughout our phenomenological analysis we keep contributions of up to $\mathcal{O}(\epsilon^2)$, which constitute the leading corrections relative to the SM result.

Keeping up the possibility of straightforwardly incorporating the limits of manifest P or C symmetry we also introduce an $SU(2)_L$ triplet

$$\Delta_L = \begin{pmatrix} \delta_L^+/\sqrt{2} & \delta_L^{++} \\ \delta_L^0 & -\delta_L^+/\sqrt{2} \end{pmatrix} \sim (1, 3, 1, 2), \quad (2.9)$$

whose VEV

$$\langle \Delta_L \rangle = \begin{pmatrix} 0 & 0 \\ \kappa_L e^{i\theta} & 0 \end{pmatrix}, \quad (2.10)$$

is constrained to be $\kappa_L \lesssim \mathcal{O}(\text{eV})$ in order not to generate large Majorana masses for the left-handed neutrinos [63–65].

Step 2: The second step of symmetry breaking is then achieved by the bidoublet

$$\phi = \begin{pmatrix} \phi_1^0 & \phi_2^+ \\ \phi_1^- & \phi_2^0 \end{pmatrix} \sim (1, 2, 2, 0), \quad (2.11)$$

whose vacuum expectation value

$$\langle \phi \rangle = \begin{pmatrix} \kappa & 0 \\ 0 & \kappa' e^{i\alpha} \end{pmatrix}, \quad (2.12)$$

breaks $SU(2)_L \times SU(2)_R$ to its diagonal subgroup $SU(2)_V$:

$$SU(2)_L \times SU(2)_R \rightarrow SU(2)_V. \quad (2.13)$$

This step of spontaneous symmetry breaking takes place at the scale

$$v = \sqrt{\kappa^2 + \kappa'^2} = 174 \text{ GeV}. \quad (2.14)$$

Together with the spontaneous breaking $SU(2)_R \times U(1)_{B-L} \rightarrow U(1)_Y$ in (2.5) at the scale $\kappa_R \gg v$ the VEV of ϕ leads to the standard electroweak symmetry breaking (EWSB) $SU(2)_L \times U(1)_Y \rightarrow U(1)_Q$ so that finally

$$SU(2)_L \times SU(2)_R \times U(1)_{B-L} \rightarrow U(1)_Q. \quad (2.15)$$

As we see later in (2.20) in order to obtain a mass splitting between up and down type quarks $\kappa \neq \kappa'$ is required. More explicitly requiring the hierarchy $m_b \ll m_t$ to be natural implies $\kappa' \ll \kappa$. However, we do not assume that $\kappa/\kappa' = m_t/m_b$ as done in some papers. In fact such large values of κ/κ' are disfavoured by electroweak precision observables, in particular by A_{FB}^b (see section 8 for details). In our analysis we confine the values to $1 < \kappa/\kappa' < 10$. It should be stressed again that the limit $\kappa = \kappa'$ is not allowed, which can be seen explicitly from the divergent behaviour of several observables.

For our choice of scalar fields the Higgs Lagrangian is then given by

$$\mathcal{L}_{\text{Higgs}} = \text{Tr}[(D_\mu \Delta_L)^\dagger (D^\mu \Delta_L)] + \text{Tr}[(D_\mu \Delta_R)^\dagger (D^\mu \Delta_R)] + \text{Tr}[(D_\mu \phi)^\dagger (D^\mu \phi)] + V(\phi, \Delta_L, \Delta_R), \quad (2.16)$$

where the covariant derivatives are

$$\begin{aligned} D_\mu \phi &= \partial_\mu \phi + ig_L (\vec{W}_{L\mu} \cdot \vec{\tau}) \phi - ig_R \phi (\vec{W}_{R\mu} \cdot \vec{\tau}), \\ D_\mu \Delta_{(L,R)} &= \partial_\mu \Delta_{(L,R)} + ig_{(L,R)} \left[\vec{W}_{(L,R)\mu} \cdot \vec{\tau}, \Delta_{(L,R)} \right] + ig' B_\mu \Delta_{(L,R)}. \end{aligned} \quad (2.17)$$

and the Higgs potential, as being used in our analysis, is given in appendix A.

2.3 Gauge sector after electroweak symmetry breaking

After performing the two steps of symmetry breaking the gauge boson mass matrices can be constructed and diagonalised. We summarise our results in appendix B. In the process of electroweak symmetry breaking only the gluons and the photon remain massless, while the W^\pm and the Z boson and their heavy counterparts W'^\pm and Z' acquire masses as given in appendix B. The spontaneous symmetry breaking additionally introduces mixing between the light and heavy gauge bosons. In the case of the light SM like bosons W^\pm this introduces right-handed couplings at $\mathcal{O}(\epsilon^2)$. The Z boson couplings are also modified with respect to the SM but they do not enter the present analysis.

2.4 Yukawa interactions and fermion masses

The most general renormalisable Yukawa coupling of the quark fields with our choice of Higgs fields is given by

$$\mathcal{L}_{\text{Yuk}} = -y_{ij}\bar{Q}_{Li}\phi Q_{Rj} - \tilde{y}_{ij}\bar{Q}_{Li}\tilde{\phi}Q_{Rj} + \text{h.c.}, \quad (2.18)$$

where $\tilde{\phi} = \sigma_2\phi^*\sigma_2$ and flavour indices $i, j = 1, 2, 3$. Note that the quantum numbers of the other scalar fields in the theory preclude their direct coupling to quarks.¹ The resulting fermion mass matrices read

$$(M_u)_{ij} = v(Y_u)_{ij}, \quad (M_d)_{ij} = v(Y_d)_{ij}, \quad (2.19)$$

where

$$(Y_u)_{ij} = y_{ij}c + \tilde{y}_{ij}se^{-i\alpha}, \quad (Y_d)_{ij} = y_{ij}se^{i\alpha} + \tilde{y}_{ij}c, \quad (2.20)$$

and $s = \kappa'/v$ and $c = \kappa/v$. These matrices are diagonalised by the bi-unitary transformations

$$M_u^{\text{diag}} = U_L^\dagger M_u U_R, \quad (2.21)$$

$$M_d^{\text{diag}} = D_L^\dagger M_d D_R, \quad (2.22)$$

where $U_{L,R}, D_{L,R}$ are unitary matrices connecting the flavour and mass eigenstates of quarks.

As we discuss in more details below, the extended Higgs sector with respect to the SM leads to flavour changing neutral Higgs couplings already at the tree level. While the flavour violating couplings of the light SM-like Higgs are highly suppressed and therefore irrelevant for the study of $\Delta F = 2$ observables and K and B decays, the new heavy Higgses lead to dangerously large effects in FCNC observables. In particular the structure of the Yukawa coupling of the Higgs bidoublet ϕ in (2.18) leads to couplings of the down-type quarks proportional to the up-type quark mass matrix. Since up and down masses are not diagonalised simultaneously, this leads to flavour changing couplings already at the tree level, see table 18 for details.

2.5 Parameter counting

Having introduced the LR model, let us now count the parameters present in the theory.

The gauge sector is parametrised by the gauge couplings

$$g_s, \quad g_L, \quad g_R, \quad g', \quad (2.23)$$

i. e. one additional parameter relative to the SM.

The Higgs potential, see appendix A, introduces several new parameters. However we see below that for our phenomenological considerations effectively only four parameters appear to be relevant. Setting $\kappa_L = 0$ these are

$$v = \sqrt{\kappa^2 + \kappa'^2}, \quad s = \kappa'/v, \quad \kappa_R, \quad M_H, \quad (2.24)$$

¹In the triplet model $\Delta_{L,R}$ couple to the left- and right-handed leptons respectively, generating Majorana mass terms $M_{\nu_{L,R}} \sim \kappa_{L,R}$.

where the first three parametrise the Higgs VEVs² and M_H is at leading order the common mass of the heavy Higgses H_1^0 , H_2^0 and H^\pm (for more details see appendix C). Note that that the SM VEV v is given in terms of κ and κ' .

In the most general case, the Yukawa couplings y_{ij} and \tilde{y}_{ij} are arbitrary complex matrices, i.e. contain each 9 real parameters and 9 phases. However, not all of these parameters are physical but some can be removed by unitary transformations under the flavour symmetry $SU(3)_{Q_L} \times SU(3)_{Q_R}$. Finally we are left with the six quark masses and two mixing matrices in the LH and RH sectors respectively:

$$V^L = U_L^\dagger D_L, \quad V^R = U_R^\dagger D_R. \quad (2.25)$$

Adopting the standard CKM phase convention, where the 5 relative phases of the quark fields are adjusted to remove 5 complex phases from the CKM matrix V^L , we have no more freedom to remove the 6 complex phases from V^R . In the standard CKM basis V^R can be parametrised as follows [44]

$$V^R = D_U V_0^R D_D^\dagger, \quad (2.26)$$

where V_0^R is a ‘‘CKM-like’’ mixing matrix, containing only three real mixing angles and one non-trivial phase. The diagonal matrices $D_{U,D}$ contain the remaining CP-violating phases. Choosing the standard parametrisation for V_0^R we have

$$V_0^R = \begin{pmatrix} \tilde{c}_{12}\tilde{c}_{13} & \tilde{s}_{12}\tilde{c}_{13} & \tilde{s}_{13}e^{-i\phi} \\ -\tilde{s}_{12}\tilde{c}_{23} - \tilde{c}_{12}\tilde{s}_{23}\tilde{s}_{13}e^{i\phi} & \tilde{c}_{12}\tilde{c}_{23} - \tilde{s}_{12}\tilde{s}_{23}\tilde{s}_{13}e^{i\phi} & \tilde{s}_{23}\tilde{c}_{13} \\ \tilde{s}_{12}\tilde{s}_{23} - \tilde{c}_{12}\tilde{c}_{23}\tilde{s}_{13}e^{i\phi} & -\tilde{s}_{23}\tilde{c}_{12} - \tilde{s}_{12}\tilde{c}_{23}\tilde{s}_{13}e^{i\phi} & \tilde{c}_{23}\tilde{c}_{13} \end{pmatrix}, \quad (2.27)$$

and

$$D_U = \text{diag}(1, e^{i\phi_2^u}, e^{i\phi_3^u}), \quad D_D = \text{diag}(e^{i\phi_1^d}, e^{i\phi_2^d}, e^{i\phi_3^d}). \quad (2.28)$$

3 $\Delta F = 2$ transitions

3.1 Preliminaries

In what follows we use conventions and notation from our papers on various extensions of the SM. An easy comparison with the results for $\Delta F = 2$ observables in the SM, the Littlest Higgs model with T-parity (LHT) [67], the Randall-Sundrum scenario with custodial protection (RSc) [68] and the SM4 [69] is facilitated in this manner.

In the LR models the effective Hamiltonian for $\Delta F = 2$ observables is constructed by evaluating three classes of diagrams:

- The standard box diagrams with quarks and $W_L W_L$, $W_R W_R$ and $W_L W_R$ exchanges³. Among the NP contributions involving W_R only the latter matter.

²The phase α in the Higgs potential appears in the analytic expressions below. However we eventually set it to zero as the factor $\exp(i\alpha)$ always multiplies V^R and cancels out in all expressions for FCNC processes. On a more technical note: the factor $\exp(i\alpha)$ always multiplies V^R , which is a unitary matrix with six phases. Therefore we are always able to absorb α through a redefinition of all phases. Recall that a unitary matrix cannot have more than six independent phases.

³In what follows in order to make the expressions more transparent it is useful to denote W and W' by W_L by W_R , respectively, even if they differ by $\mathcal{O}(\epsilon^2)$ corrections.

- Box diagrams with charged Higgs H^\pm and gauge boson exchanges. As in LR models H^\pm have masses in the multi TeV range, among NP contributions involving H^\pm only the ones with H^\pm and W_L matter.
- Tree level neutral heavy Higgs exchanges. These contributions are problematic unless the masses of new neutral Higgs particles are significantly larger than the one of W_R . In first approximation the masses of H^\pm are equal to the masses of the neutral Higgs bosons in question.

While in the SM only one operator contributes to each $\Delta F = 2$ transition, in the model in question there are 8 such operators of dimension 6. Consequently the renormalisation group (RG) QCD analysis becomes more involved and due to the LR structure of the new operators QCD corrections play a much more important role in new physics contributions than in the SM contributions.

In what follows, after listing all contributing operators we summarise the effective Hamiltonian for $\Delta F = 2$ transitions. To this end we give the formulae for the Wilson coefficients at the matching scales and we summarise the RG QCD corrections and the results for the hadronic matrix elements. Subsequently we give the final formulae for the basic mixing amplitudes in terms of Wilson coefficients at the high scale and the effective parameters P_i that encode perturbative and non-perturbative QCD effects. Then we discuss in detail the general and special anatomy of LR contributions and compare the operator structure to the one found in other NP scenarios. We end this section with listing the relevant observables.

3.2 Local operators

The contributing operators can be split into 5 separate sectors, according to the chirality of the quark fields they contain. For definiteness, we shall first consider operators responsible for the $K^0-\bar{K}^0$ mixing. The operators belonging to the first three sectors (VLL, LR and SLL) read [70] :

$$\begin{aligned}
Q_1^{\text{VLL}}(K) &= (\bar{s}^\alpha \gamma_\mu P_L d^\alpha)(\bar{s}^\beta \gamma^\mu P_L d^\beta), \\
Q_1^{\text{LR}}(K) &= (\bar{s}^\alpha \gamma_\mu P_L d^\alpha)(\bar{s}^\beta \gamma^\mu P_R d^\beta), \\
Q_2^{\text{LR}}(K) &= (\bar{s}^\alpha P_L d^\alpha)(\bar{s}^\beta P_R d^\beta), \\
Q_1^{\text{SLL}}(K) &= (\bar{s}^\alpha P_L d^\alpha)(\bar{s}^\beta P_L d^\beta), \\
Q_2^{\text{SLL}}(K) &= (\bar{s}^\alpha \sigma_{\mu\nu} P_L d^\alpha)(\bar{s}^\beta \sigma^{\mu\nu} P_L d^\beta),
\end{aligned} \tag{3.1}$$

where $\sigma_{\mu\nu} = \frac{1}{2}[\gamma_\mu, \gamma_\nu]$ and $P_{L,R} = \frac{1}{2}(1 \mp \gamma_5)$, and summation over the colour indices $\alpha, \beta = 1, 2, 3$ is understood. The operators belonging to the two remaining sectors (VRR and SRR) are obtained from Q_1^{VLL} and Q_i^{SLL} by interchanging P_L and P_R . In the SM only the operator $Q_1^{\text{VLL}}(K)$ is present. The operators relevant for B_q ($q = d, s$) are obtained by replacing in (3.1) s by b and d by q .

3.3 Effective Hamiltonian

The effective Hamiltonian for $\Delta F = 2$ transitions can be written in a general form as follows

$$\mathcal{H}_{\text{eff}}^{\Delta F=2} = \frac{G_F^2 M_{W_L}^2}{4\pi^2} \sum_i C_i(\mu) Q_i, \quad (3.2)$$

where Q_i are the operators given in (3.1) and $C_i(\mu)$ their Wilson coefficients evaluated at a scale μ which we specify below. In what follows we collect the Wilson coefficients of these operators separating the contributions from box diagrams with W_L and W_R exchanges from box diagram charged Higgs H^\pm contributions and tree level neutral Higgs $H_{1,2}^0$ contributions so that

$$C_i = \Delta_{\text{Box}} C_i + \Delta_{H^\pm} C_i + \Delta_{H^0} C_i. \quad (3.3)$$

These coefficients depend sensitively on the elements of the matrices V^L and V^R through [49]

$$\lambda_i^{AB}(K) = V_{is}^{A*} V_{id}^B, \quad \lambda_i^{AB}(B_q) = V_{ib}^{A*} V_{iq}^B, \quad (3.4)$$

where $A, B = L, R$, $q = d, s$ and $i = u, c, t$.

3.3.1 Wilson coefficients from gauge boson box diagrams

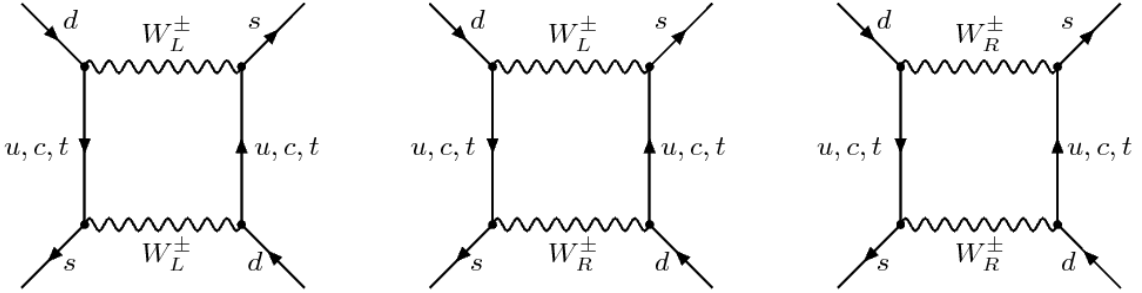


Figure 1. Feynman diagrams for contributing gauge boson box diagrams

Calculating the diagrams in figure 1, we find the following contributions to the Wilson coefficients relevant for the $K^0 - \bar{K}^0$ system at the relevant matching scales $\mu_W = \mathcal{O}(M_W, m_t)$ and $\mu_R = \mathcal{O}(M_{W_R})$

$$\Delta_{\text{Box}} C_1^{\text{VLL}}(\mu_W, K) = \sum_{i,j=c,t} \lambda_i^{\text{LL}}(K) \lambda_j^{\text{LL}}(K) S_{\text{LL}}(x_i, x_j), \quad (3.5)$$

$$\Delta_{\text{Box}} C_2^{\text{LR}}(\mu_R, K) = \sum_{i,j=u,c,t} \lambda_i^{\text{LR}}(K) \lambda_j^{\text{RL}}(K) S_{\text{LR}}(x_i, x_j, \beta), \quad (3.6)$$

$$\Delta_{\text{Box}} C_1^{\text{VRR}}(\mu_R, K) = \sum_{i,j=c,t} \lambda_i^{\text{RR}}(K) \lambda_j^{\text{RR}}(K) S_{\text{RR}}(\tilde{x}_i, \tilde{x}_j), \quad (3.7)$$

where we introduced the ratios

$$x_i = \left(\frac{m_i}{M_{W_L}} \right)^2, \quad \tilde{x}_i = \left(\frac{m_i}{M_{W_R}} \right)^2, \quad \beta = \frac{M_{W_L}^2}{M_{W_R}^2}, \quad r = \left(\frac{s_W}{c_W s_R} \right)^2. \quad (3.8)$$

Note that at $\mathcal{O}(\epsilon^2)$ there are no corrections to the Wilson coefficient of the SM Q_1^{VLL} operator. In the LR symmetric limit $g_L = g_R$ the factor r reduces to $r = 1$.

The loop functions are given as follows

$$S_{\text{LL}}(x_i, x_j) = F(x_i, x_j) + F(x_u, x_u) - F(x_i, x_u) - F(x_j, x_u), \quad (3.9)$$

$$S_{\text{LR}}(x_i, x_j, \beta) = 2\beta r \sqrt{x_i x_j} [(4 + x_i x_j \beta) I_1(x_i, x_j, \beta) - (1 + \beta) I_2(x_i, x_j, \beta)], \quad (3.10)$$

$$S_{\text{RR}}(\tilde{x}_i, \tilde{x}_j) = \beta r^2 S_{\text{LL}}(\tilde{x}_i, \tilde{x}_j), \quad (3.11)$$

$$F(x_i, x_j) = \frac{1}{4} [(4 + x_i x_j) I_2(x_i, x_j, 1) - 8x_i x_j I_1(x_i, x_j, 1)], \quad (3.12)$$

with

$$I_1(x_i, x_j, \beta) = \frac{x_i \ln(x_i)}{(1-x_i)(1-x_i\beta)(x_i-x_j)} + (i \leftrightarrow j) - \frac{\beta \ln(\beta)}{(1-\beta)(1-x_i\beta)(1-x_j\beta)}, \quad (3.13)$$

$$I_2(x_i, x_j, \beta) = \frac{x_i^2 \ln(x_i)}{(1-x_i)(1-x_i\beta)(x_i-x_j)} + (i \leftrightarrow j) - \frac{\ln(\beta)}{(1-\beta)(1-x_i\beta)(1-x_j\beta)}. \quad (3.14)$$

The remaining coefficients vanish in the absence of QCD corrections but as we discuss below they are generated by QCD effects. In obtaining the results in (3.5) and (3.7) we have used the unitarity of the matrices V^{L} and V^{R} or equivalently the GIM mechanism to eliminate the λ_u^{LL} and λ_u^{RR} terms. The GIM mechanism does not apply to the case of LR contributions. In the case of $B_q^0 - \bar{B}_q^0$ mixing we just have to replace K by B_q .

The results given above were obtained by calculating all box diagram contributions in 't Hooft-Feynman gauge keeping both gauge boson and Goldstone boson contributions. We confirm the results in the literature [28, 49, 50, 71, 72].

While S_{LL} and S_{RR} are gauge independent, this is not the case of S_{LR} as pointed out in [71]. As anticipated in that paper and explicitly demonstrated in [50, 72] a gauge independent result for S_{LR} is obtained by including vertex and self-energy corrections to the tree-level physical Higgs H_1^0 and H_2^0 exchanges that we discuss subsequently. The diagrams relevant for the cancellation of the gauge dependence of S_{LR} are the ones that include the vertices $H_i^0 G^+ G'^-$ but for consistency all vertex and self-energy corrections should be included. Detailed analyses in [50, 72] show that the main role of these additional contributions is the restoration of the gauge invariance of S_{LR} without any relevant modification of the 't Hooft-Feynman gauge result given above. Consequently we neglect these contributions in our analysis.

3.3.2 Wilson coefficients from charged Higgs box diagrams

Among various box diagrams with charged Higgs exchanges the one involving H^\pm and W_L^\pm (see left hand side in figure 2) and the corresponding diagram with W_L replaced by the Goldstone bosons are by far the most important ones. The remaining box diagrams involving only H^\pm or H^\pm and W_R^\pm can be safely neglected. A similar comment applies to box diagrams with heavy neutral Higgs particles. Calculating the relevant diagram shown in figure 2 yields

$$\Delta_{H^\pm} C_2^{\text{LR}}(\mu_H, K) = \sum_{i,j=u,c,t} \lambda_i^{\text{LR}}(K) \lambda_j^{\text{RL}}(K) S_{\text{LR}}^H(x_i, x_j, \beta_H). \quad (3.15)$$

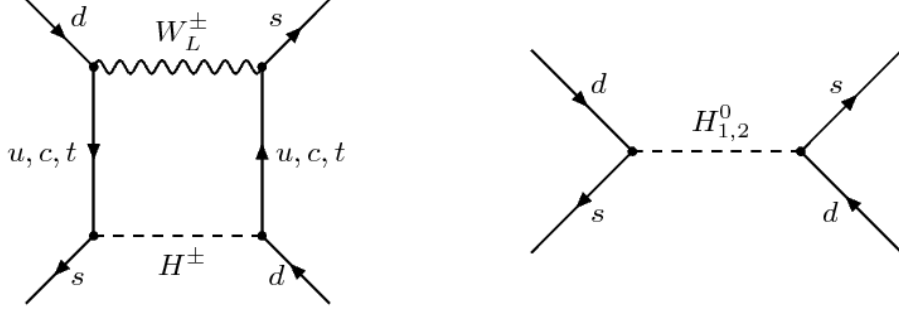


Figure 2. Feynman diagrams for Higgs contributions

with the master function S_{LR}^H defined as

$$S_{\text{LR}}^H(x_i, x_j, \beta_H) = 2u(s)\beta_H \sqrt{x_i(\mu_H)x_j(\mu_H)} [x_i x_j I_1(x_i, x_j, \beta_H) - I_2(x_i, x_j, \beta_H)]. \quad (3.16)$$

Here the function $u(s)$ and β_H are given as follows

$$u(s) = \left(\frac{1}{1-2s^2} \right)^2, \quad \beta_H = \frac{M_{W_L}^2}{M_{H^\pm}^2}. \quad (3.17)$$

We have confirmed the result of [49] except that in that paper $s \ll 1$ has been chosen. Our choice of the matching scale is explained below. Note that the quark masses in the first factor in (3.16) have to be evaluated at μ_H as this factor arises from the Yukawa couplings of H^\pm . The remaining masses have to be evaluated at scales as discussed in the context of QCD corrections below. In table 6 we provide values of the masses at different high scales.

3.3.3 Wilson coefficients from tree level Higgs exchange

Calculating the tree diagrams with neutral Higgs exchanges (right hand side in figure 2), we find that the contributions of the Higgs bosons H_1^0 and H_2^0 to $C_{1,2}^{\text{SLL}}$ and $C_{1,2}^{\text{SRR}}$ cancel each other in the limit of $M_{H_1^0} = M_{H_2^0} = M_H$. Consequently in the case of non-degenerate Higgs masses these contributions are $\mathcal{O}(\epsilon^4)$ and can be neglected. On the other hand in the same limit taking into account the overall factor in (3.2) we find

$$\Delta_{H^0} C_2^{\text{LR}}(\mu_H, K) = -\frac{16\pi^2}{\sqrt{2}M_H^2 G_F} u(s) \sum_{i,j=u,c,t} \lambda_i^{\text{LR}}(K) \lambda_j^{\text{RL}}(K) \sqrt{x_i(\mu_H)x_j(\mu_H)}, \quad (3.18)$$

with other Wilson coefficients vanishing at $\mu_H = \mathcal{O}(M_H)$ in the absence of QCD corrections. The quark masses have to be evaluated at μ_H . This result agrees with [28] except that in that paper $s \ll 1$ has been chosen. As seen in (3.17) e. g. for $s = 0.5$ the additional factor $u(s)$ provides an enhancement of a factor of 4. In the case of $B_q^0 - \bar{B}_q^0$ mixing K should be replaced by B_q . $\Delta_{H^0} C_1^{\text{LR}}$ is generated by QCD effects as discussed below.

3.4 QCD corrections and hadronic matrix elements

The complete analysis of $\Delta F = 2$ processes requires the inclusion of the QCD renormalisation group evolution. The local operators have to be evolved from their respective high

scales down low energy scales at which the hadronic matrix elements are evaluated by lattice methods. A complication arises in the model in question as three rather different high scales $\mu_W \ll \mu_R \ll \mu_H$ are involved. Before addressing this problem let us recall a very efficient method [73, 74] for the inclusion of all these QCD effects in the presence of a single high scale which we denote by μ_{in} .

Instead of evaluating the hadronic matrix elements at the low energy scale we can choose to evaluate them at the high scale μ_{in} at which heavy particles are integrated out. Thus the amplitude for $M - \bar{M}$ mixing ($M = K, B_d, B_s$) is given simply by

$$A(M \rightarrow \bar{M}) = \langle \bar{M} | \mathcal{H}_{\text{eff}}^{\Delta F=2} | M \rangle = \frac{G_F^2 M_{W_L}^2}{4\pi^2} \sum_{i,a} C_i^a(\mu_{\text{in}}) \langle \bar{M} | Q_i^a(\mu_{\text{in}}) | M \rangle. \quad (3.19)$$

Here the sum runs over all the operators listed in (3.1). The matrix elements for $B_d - \bar{B}_d$ mixing are for instance given as follows [73, 74]

$$\langle \bar{B}_d^0 | Q_i^a(\mu_{\text{in}}) | B_d^0 \rangle = \frac{2}{3} m_{B_d}^2 F_{B_d}^2 P_i^a(B_d), \quad (3.20)$$

where the coefficients $P_i^a(B_d)$ collect compactly all RG effects from scales below μ_{in} as well as hadronic matrix elements obtained by lattice methods at low energy scales. Analytic formulae for these coefficients are given in [73] while recent applications of this method can be found in [44, 75, 76]. As the Wilson coefficients $C_i(\mu_{\text{in}})$ depend directly on the loop functions, tree diagram results and fundamental parameters of a given theory, this formulation is very transparent and interesting short distance NP effects are not hidden by complicated QCD effects. The numerical values for the coefficients $P_i^a(B_q)$ and $P_i^a(K)$ that we require for our analysis are given below.

The question then arises how to generalise this method to the case at hand which involves three rather different high scales. There are three types of contributions for which the relevant high energy scales attributed to the coefficients quoted above differ from each other:

- The SM box diagrams involving W_L and the SM quarks. Here the scale is chosen to be $\mathcal{O}(m_t)$ as in [73].
- Tree diagrams mediated by neutral heavy Higgs exchanges. In this case we take $\mu_H = 15 \text{ TeV}$ as the initial scale for the RG evolution.
- The only problematic cases are the contributions from W_R and H^\pm that appear in box diagrams together with much lighter W_L and the SM quarks. Here the correct procedure would be to first integrate out W_R and H^\pm . Subsequently one would construct an effective field theory not involving them as dynamical degrees of freedom. We believe that in view of several unknown parameters in the LR models such a complicated analysis would be premature. Therefore we choose μ_R as the matching scale for box contributions involving W_R . For diagrams involving Higgs particles we set the high scale to be μ_H . As the dominant effects from the included RG evolution stem from scales below μ_t , this procedure should sufficiently well approximate the true result.

Now let us turn to the question of scales in the quark masses. In box contributions we use $m_i(m_i)$ for $i = c, b, t$ and $m_i(2\text{ GeV})$ for light quarks. An exception are the masses in the overall factor in H^\pm contribution in (3.16), as discussed previously, which originate in the Yukawa couplings of quarks to H^\pm . Here similarly to the tree level exchange of heavy neutral Higgs particles (3.18) quark masses should be evaluated at μ_H .

Having the initial conditions for Wilson coefficients at a given high scale μ_{in} we can calculate the relevant $M - \bar{M}$ amplitude by means of (3.19) provided also the corresponding hadronic matrix elements are known at this scale. As seen in (3.20) these matrix elements are directly given in terms of the parameters $P_i^a(K)$, $P_i^a(B_d)$ and $P_i^a(B_s)$. Explicit expressions for the latter in terms of RG QCD factors and the non-perturbative parameters $B_i^a(\mu_L)$ are given in equations (7.28)–(7.34) in [73] with μ_L denoting the low energy scale to be specified below.

The parameters $B_i^a(\mu_L)$ are subject to considerable uncertainties. They can be extracted from the results of [77, 78]. The parameters $B_i(\mu_L)$ ($i = 1, \dots, 5$) are given in the basis used by Ciuchini et al [79]. Both papers provide the values of the parameters B_i in the NDR scheme used in [73]. The conversion to our operator basis (3.1) is given by

$$B_1^{\text{VLL}}(\mu_L) = B_1^{\text{VRR}} = B_1(\mu_L), \quad (3.21)$$

$$B_1^{\text{LR}}(\mu_L) = B_5(\mu_L), \quad B_2^{\text{LR}}(\mu_L) = B_4(\mu_L), \quad (3.22)$$

$$B_1^{\text{SLL}}(\mu_L) = B_2(\mu_L), \quad B_2^{\text{SLL}}(\mu_L) = \frac{5}{3}B_2(\mu_L) - \frac{2}{3}B_3(\mu_L). \quad (3.23)$$

The parameters B_1^{VLL} for all meson systems are also known from most recent lattice simulations. In this case we use the RG invariant parameters \hat{B}_1^{VLL} , usually denoted by \hat{B}_K and \hat{B}_{B_q} , that are already known from the SM analyses. As these parameters are the same for the VRR contributions, we can represent the latter as corrections to the SM box function $S_0(x_t)$. In this manner the VLL and VRR contributions are governed by meson system dependent functions

$$S_i = S_0(x_t) + \Delta S_i \quad (i = K, B_d, B_s) \quad (3.24)$$

where the ΔS_i are obtained by evolving the Wilson coefficients from μ_R down to μ_t . The formula for S_i is given in (3.32).

If the unknown $\mathcal{O}(\alpha_s)$ corrections to the Wilson coefficients of non-standard operators are assumed to be small, our analysis involves only the values of the coefficients $P_2^{\text{LR}}(K)$, $P_2^{\text{LR}}(B_d)$ and $P_2^{\text{LR}}(B_s)$ calculated at $\mu_R = 2.5\text{ TeV}$ in the case of box diagrams and $\mu_H = 15\text{ TeV}$ in the case of neutral Higgs contributions. To obtain these values we only need the values of B_4 and B_5 . In the case of the K system for $\mu_L = 2\text{ GeV}$ we have [78] (see table 16 in that paper)

$$B_4 = 0.810(41)(31), \quad B_5 = 0.562(39)(46). \quad (3.25)$$

Within the uncertainties we can take the same values for B_d and B_s systems. In this case for $\mu_L = \mu_b = 4.6\text{ GeV}$ we have [77]

$$B_4 = 1.14(3)(6), \quad B_5 = 1.79(4)(18). \quad (3.26)$$

with the asymmetric errors corrected using [80]. In the case of box diagram contributions ($\mu_R = 2.5 \text{ TeV}$) we find

$$P_2^{\text{LR}}(K) = 73(4)(3), \quad P_2^{\text{LR}}(B_q) = 4.57(54)(25). \quad (\text{Box}) \quad (3.27)$$

For the Higgs contribution ($\mu_H = 15 \text{ TeV}$) we find

$$P_2^{\text{LR}}(K) = 88(5)(3), \quad P_2^{\text{LR}}(B_q) = 5.54(65)(30). \quad (\text{Higgs}) \quad (3.28)$$

For this calculation we have used the values of m_s and m_d provided by the lattice-averaging-group. We collect them in table 6. The values relevant for VLL and VRR operators are also given in table 6 and the final formulae for the mixing observables where all these matrix elements enter are presented below.

3.5 Final expressions for mixing amplitudes

We now summarise the expressions for the mixing amplitudes M_{12}^q , defined in terms of the effective Hamiltonian by

$$2m_{B_q} (M_{12}^q)^* = \langle \bar{B}_q^0 | \mathcal{H}_{\text{eff}}^{\Delta B=2} | B_q^0 \rangle. \quad (3.29)$$

We decompose them first as follows

$$M_{12}^q = (M_{12}^q)_{\text{SM}} + (M_{12}^q)_{\text{RR}} + (M_{12}^q)_{\text{LR}} \equiv \overline{(M_{12}^q)}_{\text{SM}} + (M_{12}^q)_{\text{LR}}. \quad (3.30)$$

Then

$$\overline{(M_{12}^q)}_{\text{SM}} = \frac{G_F^2}{12\pi^2} F_{B_q}^2 \hat{B}_{B_q} m_{B_q} M_W^2 [\lambda_t^{\text{LL}*}(B_q)]^2 \eta_B S_q^*(B_q), \quad (3.31)$$

where

$$S_q(B_q) = S_0(x_t) + \frac{\tilde{\eta}_B \Delta_{\text{Box}} C_1^{\text{VRR}}(\mu_R, B_q)}{\eta_B [\lambda_t^{\text{LL}}(B_q)]^2}. \quad (3.32)$$

Here η_B is the known SM QCD correction and $\tilde{\eta}_B/\eta_B \sim 0.95$ describes the QCD evolution from μ_R down to μ_W and is therefore the same for the $K^0 - \bar{K}^0$ system. $S_0(x_t)$ is given in (3.36) below.

For the LR contribution we first combine the Higgs contributions in (3.15) and (3.18) into

$$\tilde{\Delta}_{\text{Higgs}} C_2^{\text{LR}}(\mu_R, B_q) = \Delta_{\text{H}^0} C_2^{\text{LR}}(\mu_H, B_q) + \Delta_{\text{H}^+} C_2^{\text{LR}}(\mu_H, B_q). \quad (3.33)$$

Then

$$(M_{12}^q)_{\text{LR}} = \frac{G_F^2 M_W^2}{12\pi^2} F_{B_q}^2 m_{B_q} [(\Delta_{\text{Box}} C_2^{\text{LR}}(\mu_R, B_q))^* P_2^{\text{LR}}(\mu_R) + (\tilde{\Delta}_{\text{Higgs}} C_2^{\text{LR}}(\mu_H, B_q))^* P_2^{\text{LR}}(\mu_H)]. \quad (3.34)$$

In these expressions $\mu_R = \mathcal{O}(M_{W_R})$ and $\mu_H = \mathcal{O}(M_H)$. In the case of $K^0 - \bar{K}^0$ system B_q should be replaced by K and η_B by η_2 . Moreover one should add the known contributions from cc and ct box diagrams to $(M_{12}^K)_{\text{SM}}$ so that

$$(M_{12}^K)_{\text{SM}} = \frac{G_F^2}{12\pi^2} F_K^2 \hat{B}_K m_K M_W^2 [[\lambda_c^{\text{LL}*}(K)]^2 \eta_1 S_0(x_c) + [\lambda_t^{\text{LL}*}(K)]^2 \eta_2 S_0(x_t) + 2\lambda_c^{\text{LL}*}(K) \lambda_t^{\text{LL}*}(K) \eta_3 S_0(x_c, x_t)], \quad (3.35)$$

where F_K is the K -meson decay constant and m_K the K -meson mass. Here

$$S_0(x_t) \equiv S_{\text{LL}}(x_t, x_t) = \frac{4x_t - 11x_t^2 + x_t^3}{4(1-x_t)^2} - \frac{3x_t^3 \ln x_t}{2(1-x_t)^3}, \quad (3.36)$$

$$S_0(x_c) \equiv S_{\text{LL}}(x_c, x_c) \approx x_c, \quad (3.37)$$

$$S_0(x_c, x_t) \equiv S_{\text{LL}}(x_t, x_c) \approx x_c \left[\ln \frac{x_t}{x_c} - \frac{3x_t}{4(1-x_t)} - \frac{3x_t^2 \ln x_t}{4(1-x_t)^2} \right]. \quad (3.38)$$

In the last two expressions we have kept only linear terms in $x_c \ll 1$, but of course all orders in x_t .

3.6 General anatomy of LR contributions

In order to see the importance of different NP contributions we rewrite the dominant LR contribution in (3.34) by separating contributions of quark mixing matrices from the loop integral and QCD running. We obtain

$$(M_{12}^q)_{\text{LR}} = \frac{G_F^2 M_W^2}{12\pi^2} F_{B_q}^2 m_{B_q} \sum_{i,j=u,c,t} \Lambda_{ij}(B_q)^* R_{ij}(B_q), \quad (3.39)$$

where we defined

$$\begin{aligned} R_{ij}(B_q) &= S_{\text{LR}}(x_i, x_j, \beta) P_2^{\text{LR}}(B_q, \mu_R) \\ &+ S_{\text{LR}}^{\text{H}}(x_i, x_j, \beta_H) P_2^{\text{LR}}(B_q, \mu_H) \\ &- \frac{16\pi^2}{\sqrt{2} M_H^2 G_F} u(s) \sqrt{x_i(\mu_H) x_j(\mu_H)} P_2^{\text{LR}}(B_q, \mu_H), \end{aligned} \quad (3.40)$$

$$\Lambda_{ij}(B_q) = \lambda_i^{\text{LR}}(B_q) \lambda_j^{\text{RL}}(B_q). \quad (3.41)$$

Here we indicated that the QCD factors P_2^{LR} are the ones for the B_q system. In the case of $K^0 - \bar{K}^0$ system B_q should be replaced by K . Choosing $M_{W_R} = 2.5 \text{ TeV}$, $M_H = 16 \text{ TeV} \cdot u(s)^{1/4}$ and the central values for the factors P_i^a given above, we find for the matrices $\hat{R}(K)$ and $\hat{R}(B_q)$ the results collected in appendix D, for two different choices of s . This hierarchical structure of the matrix R_{ij} has an impact on the resulting structure of the mixing matrix V^{R} . We discuss this in more detail in section 3.7.

We observe that for fixed $\lambda_i^{\text{LR}} \lambda_j^{\text{RL}}$ the neutral Higgs H^0 contributions are by far dominant, followed by gauge boson contributions and rather small charged Higgs H^\pm contributions. This shows that for $M_{W_R} \geq 2.5 \text{ TeV}$ the neglect of neutral Higgs contributions for masses M_H even as high as 16 TeV, as done often in the literature, totally misrepresents the LR story in $\Delta F = 2$ transitions. In figure 3 we show the relative importance of the neutral Higgs contributions to $R_{tt}(K)$ as a function of M_H for different values of M_{W_R} and two different choices for s . We observe that even for $M_{W_R} = 400 \text{ GeV}$, which is excluded already for many years, and small s the neutral Higgs contributions for $M_H < 20 \text{ TeV}$ account for at least 20% of the total value. For realistic W_R masses $M_{W_R} > 2 \text{ TeV}$ the neutral Higgs contributions become only negligible for masses beyond 100 TeV. For large values of $s \sim 0.5$ the heavy Higgs contribution becomes even more important. As both M_{W_R} and M_H are κ_R dependent decoupling the heavy Higgs contribution would require a non-perturbative coupling α_3 in the Higgs sector.

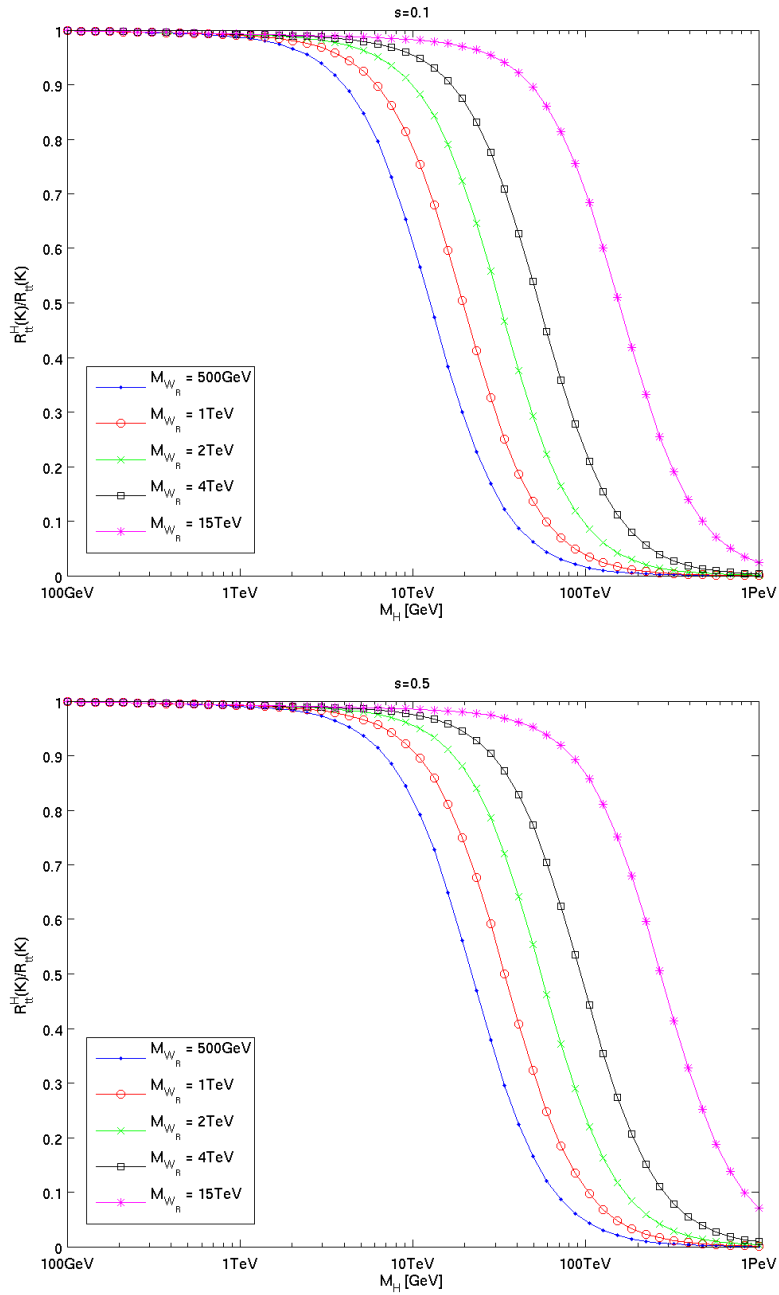


Figure 3. The relative importance of the neutral Higgs contribution R_{tt}^H (see 3.40) to $R_{tt}(K)$ as a function of M_H for different W_R masses for $s = 0.1$ and $s = 0.5$

3.7 Special anatomy of LR contributions

As can be seen from the formulae in appendix D the matrices $\hat{R}(q)$ have a very special pattern. We first restrict our discussion to the K system. Similar arguments hold for the B system but the actual hierarchies change. For now we are only interested in the order

of magnitude of the elements and especially in their relative size

$$\hat{R}(K) \sim (-1) \begin{pmatrix} 10^{-9} & 10^{-6} & 10^{-4} \\ 10^{-6} & 10^{-4} & 10^{-2} \\ 10^{-4} & 10^{-2} & 10^1 \end{pmatrix}. \quad (3.42)$$

First of all we notice the wide spread of sizes as well as the expected hierarchy towards the third generation. The relative shift for changing one generation is about two-to-three orders of magnitude. Before summation the elements of $\hat{R}(K)$ get dressed with elements of $\hat{\Lambda}(K)$ as explicitly given in (3.39). Here we define $\hat{\Lambda}(K)$ as the matrix form of $\Lambda_{ij}(K)$.

Barring fine-tuned cancellations among the various contributions, each of the LR contributions to ΔM_K and in particular ε_K has to be suppressed well below the SM contribution in order to obtain agreement with the data. Thus we can estimate rough upper bounds on some of the elements of $\hat{\Lambda}(K)$

$$|\Lambda_{tt}(K)| \lesssim 10^{-5}, \quad (3.43)$$

$$|\Lambda_{ct,tc}(K)| \lesssim 10^{-3}, \quad (3.44)$$

$$|\Lambda_{cc}(K)| \lesssim 10^{-1}, \quad (3.45)$$

while no useful bound can be obtained on the remaining elements of $\hat{\Lambda}(K)$.

On the other hand for a generic right-handed matrix V^R the matrix $\hat{\Lambda}(K)$ would exhibit the hierarchy implied by the structure of the CKM matrix only

$$|\hat{\Lambda}(K)| \sim \begin{pmatrix} 10^{-1} & 10^{-2} & 10^{-3} \\ 1 & 10^{-1} & 10^{-2} \\ 10^{-2} & 10^{-2} & 10^{-4} \end{pmatrix}. \quad (3.46)$$

Recall that

$$\Lambda_{ij}(K) = V_{is}^{L*} V_{id}^R V_{js}^{R*} V_{jd}^L. \quad (3.47)$$

Comparing the entries of (3.46) with the bounds obtained in (3.43)–(3.45) we see that the ct , tc and tt elements need an additional suppression by one order of magnitude. This can only be achieved with the help of an appropriate hierarchy in V^R , see (3.47). Explicitly we find the constraints

$$|V_{td}^R| |V_{ts}^R| \lesssim 10^{-1}, \quad |V_{td}^R| |V_{cs}^R| \lesssim 10^{-1}, \quad |V_{cd}^R| |V_{ts}^R| \lesssim 10^{-1}. \quad (3.48)$$

Following an analogous procedure for the B_d system we obtain

$$|V_{td}^R| |V_{tb}^R| \lesssim 10^{-2}, \quad (3.49)$$

while no relevant constraint can be obtained from the B_s system.

Making the plausible assumption that the diagonal elements of V^R and in particular $|V_{tb}^R|$ are $\mathcal{O}(1)$ we obtain

$$|V_{td}^R| \lesssim 10^{-2}. \quad (3.50)$$

This bound agrees surprisingly well with the one obtained from the explicit numerical analysis in section 9.2. We stress however that we have performed here a very rough estimate, keeping only the orders of magnitude. It is interesting to see that already this naive estimate allows us to understand certain patterns in our numerical analysis.

3.8 Comparison of the operator structure in various models

It is instructive to compare the operator structure in the effective Hamiltonian for $\Delta F = 2$ transitions in the specific LR model considered in the present paper with the other specific models containing RH currents considered by us like RSc models [68] or some supersymmetric flavour models [81] and in particular in the effective theory approach for the RH currents in [44]. To this end let us note that when $\mathcal{O}(\alpha_s)$ corrections at the high matching scale are neglected the following dynamics is responsible for the structure of the effective $\Delta F = 2$ Hamiltonian:

- A tree level exchange of a colourless gauge boson with LH and RH couplings generates the operators Q_1^{VLL} , Q_1^{VRR} and Q_1^{LR} . This is an example of Z' models and gauge flavour models [82].
- A tree level exchange of a gauge boson carrying colour generates the operators Q_1^{VLL} , Q_1^{VRR} , Q_1^{LR} and Q_2^{LR} . An example is the tree-level exchange of the KK-gluon in RS models.
- A tree level exchange of a colourless Higgs scalar generates the operators Q_1^{SLL} , Q_1^{SRR} and Q_2^{LR} but as we have seen above at $\mathcal{O}(\epsilon^2)$ only the last operator contributes in the model considered.
- A tree level exchange of a Higgs scalar carrying colour generates the operators $Q_{1,2}^{\text{SLL}}$, $Q_{1,2}^{\text{SRR}}$ and $Q_{1,2}^{\text{LR}}$.
- Finally box diagrams with internal charged gauge bosons or H^\pm carrying both LH and RH couplings generate the operators Q_1^{VLL} , Q_1^{VRR} and Q_2^{LR} at $\mathcal{O}(\epsilon^2)$.

With this classification in mind it is evident that the effective $\Delta F = 2$ Hamiltonian at the matching scale in [44] corresponds to a tree level exchange of a colourless gauge boson. Clearly with RH currents present in this model also the operator Q_2^{LR} is generated through box diagrams, but in the presence of QCD corrections this operator is also generated from Q_1^{LR} generated by the tree level gauge boson exchange in question. An implicit assumption in [44] was that this is the dominant mechanism for the generation of Q_2^{LR} .

In the models considered by us there are no flavour changing neutral gauge boson exchanges at tree level and the leading mechanism for the generation of Q_2^{LR} are box diagrams. The latter can also generate Q_1^{LR} at $\mathcal{O}(\epsilon^4)$ but this effect is smaller than the QCD mixing generating Q_1^{LR} from Q_2^{LR} that we include in our paper. Thus the structures of the $\Delta F = 2$ Hamiltonians considered here and in [44] are in a sense complementary to each other.

3.9 Basic formulae for $\Delta F = 2$ observables

We collect here the formulae that we used in our numerical analysis. The mixing amplitude M_{12} can be decomposed into SM and NP part ($i = K, d, s$)

$$M_{12}^i = (M_{12}^i)_{\text{SM}} + (M_{12}^i)_{\text{NP}}, \quad (3.51)$$

and is related for $i = K$ to the relevant effective Hamiltonian through

$$2m_K (M_{12}^K)^* = \langle \bar{K}^0 | \mathcal{H}_{\text{eff}}^{\Delta S=2} | K^0 \rangle, \quad (3.52)$$

with analogous expressions for $q = d, s$. A general formula for the r. h. s. is given in (3.19). The $K_L - K_S$ mass difference is then given by

$$\Delta M_K = 2 [\text{Re} (M_{12}^K)_{\text{SM}} + \text{Re} (M_{12}^K)_{\text{NP}}], \quad (3.53)$$

and the CP-violating parameter ε_K by

$$\varepsilon_K = \frac{\kappa_\varepsilon e^{i\varphi_\varepsilon}}{\sqrt{2}(\Delta M_K)_{\text{exp}}} [\text{Im} (M_{12}^K)_{\text{SM}} + \text{Im} (M_{12}^K)_{\text{NP}}], \quad (3.54)$$

where $\varphi_\varepsilon = (43.51 \pm 0.05)^\circ$ and $\kappa_\varepsilon = 0.94 \pm 0.02$ [5, 83] takes into account that $\varphi_\varepsilon \neq \pi/4$ and includes long distance effects in $\text{Im}\Gamma_{12}$ and $\text{Im}M_{12}$. The value of κ_ε given here has been calculated within the SM using the data on ε'/ε that could also contain NP contributions. As analysed in [84] these effects do not have a significant impact on our analysis. For the mass differences in the $B_{d,s}^0 - \bar{B}_{d,s}^0$ systems we have

$$\Delta M_q = 2 |(M_{12}^q)_{\text{SM}} + (M_{12}^q)_{\text{NP}}| \quad (q = d, s). \quad (3.55)$$

Let us then write [85]

$$M_{12}^q = (M_{12}^q)_{\text{SM}} + (M_{12}^q)_{\text{NP}} = (M_{12}^q)_{\text{SM}} C_{B_q} e^{2i\varphi_{B_q}}, \quad (3.56)$$

where

$$(M_{12}^d)_{\text{SM}} = |(M_{12}^d)_{\text{SM}}| e^{2i\beta}, \quad \beta \approx 22^\circ, \quad (3.57)$$

$$(M_{12}^s)_{\text{SM}} = |(M_{12}^s)_{\text{SM}}| e^{2i\beta_s}, \quad \beta_s \simeq -1^\circ. \quad (3.58)$$

Here the phases β and β_s are defined through

$$V_{td} = |V_{td}| e^{-i\beta} \quad \text{and} \quad V_{ts} = -|V_{ts}| e^{-i\beta_s}. \quad (3.59)$$

We find then

$$\Delta M_q = (\Delta M_q)_{\text{SM}} C_{B_q}, \quad (3.60)$$

and

$$S_{\psi K_S} = \sin(2\beta + 2\varphi_{B_d}), \quad (3.61)$$

$$S_{\psi\phi} = \sin(2|\beta_s| - 2\varphi_{B_s}), \quad (3.62)$$

with the latter two observables being the coefficients of $\sin(\Delta M_d t)$ and $\sin(\Delta M_s t)$ in the time dependent asymmetries in $B_d^0 \rightarrow \psi K_S$ and $B_s^0 \rightarrow \psi\phi$, respectively. Thus in the presence of non-vanishing φ_{B_d} and φ_{B_s} these two asymmetries do not measure β and β_s but $(\beta + \varphi_{B_d})$ and $(|\beta_s| - \varphi_{B_s})$, respectively. At this stage a few comments on the assumptions leading to expressions (3.61) and (3.62) are in order. These simple formulae follow only

if there are no weak phases in the decay amplitudes for $B_d^0 \rightarrow \psi K_S$ and $B_s^0 \rightarrow \psi\phi$ as is the case in the SM and also in the LHT model, where due to T-parity there are no new contributions to decay amplitudes at tree level so that these amplitudes are dominated by SM contributions [67]. In the model discussed in the present paper new contributions to decay amplitudes with non-vanishing weak phases are present at tree level. However, as we demonstrate in section 5 these contribution can be totally neglected when calculating $S_{\psi K_S}$ and $S_{\psi\phi}$.

Now in models like the LHT model and SM4, the only operators contributing to the amplitudes M_{12}^K and M_{12}^q are the SM ones, that is Q_1^{VLL} [67, 69]. Consequently the new phases φ_{B_d} and φ_{B_s} have purely perturbative character related to the fundamental dynamics at short distance scales. The situation in the LR model in question is different. As now new operators contribute to the M_{12}^q amplitudes, the parameters C_{B_q} and φ_{B_q} in (3.56) are complicated functions of fundamental short distance parameters of the model and of the non-perturbative parameters B_i present in $P_i^a(K)$ and $P_i^a(B_d)$. Thus the test of the LR models considered with the help of particle-antiparticle mixing and related CP-violation is less theoretically clean than in the case of new physics scenarios in which only the operator Q_1^{VLL} contributes.

Next, we give the expressions for the width differences $\Delta\Gamma_q$ and the semileptonic CP-asymmetries A_{SL}^q

$$\frac{\Delta\Gamma_q}{\Gamma_q} = - \left(\frac{\Delta M_q}{\Gamma_q} \right)^{\text{exp}} \left[\text{Re} \left(\frac{\Gamma_{12}^q}{M_{12}^q} \right)^{\text{SM}} \frac{\cos 2\varphi_{B_q}}{C_{B_q}} + \text{Im} \left(\frac{\Gamma_{12}^q}{M_{12}^q} \right)^{\text{SM}} \frac{\sin 2\varphi_{B_q}}{C_{B_q}} \right], \quad (3.63)$$

$$A_{\text{SL}}^q = \text{Im} \left(\frac{\Gamma_{12}^q}{M_{12}^q} \right)^{\text{SM}} \frac{\cos 2\varphi_{B_q}}{C_{B_q}} - \text{Re} \left(\frac{\Gamma_{12}^q}{M_{12}^q} \right)^{\text{SM}} \frac{\sin 2\varphi_{B_q}}{C_{B_q}}. \quad (3.64)$$

Theoretical predictions of both $\Delta\Gamma_q$ and A_{SL}^q require the non-perturbative calculation of the off-diagonal matrix element Γ_{12}^q , the absorptive part of the $B_q^0 - \bar{B}_q^0$ amplitude as well as perturbative QCD calculations. The latter are known at the NLO level [86–90]. The most recent results read [10, 91]

$$\text{Re} \left(\frac{\Gamma_{12}^d}{M_{12}^d} \right)^{\text{SM}} = -5.3(10) \cdot 10^{-3}, \quad \text{Re} \left(\frac{\Gamma_{12}^s}{M_{12}^s} \right)^{\text{SM}} = -5.0(10) \cdot 10^{-3}, \quad (3.65)$$

$$\text{Im} \left(\frac{\Gamma_{12}^d}{M_{12}^d} \right)^{\text{SM}} = -4.1(6) \cdot 10^{-4}, \quad \text{Im} \left(\frac{\Gamma_{12}^s}{M_{12}^s} \right)^{\text{SM}} = 1.9(3) \cdot 10^{-5}. \quad (3.66)$$

Finally, we recall the existence of a correlation between A_{SL}^s and $S_{\psi\phi}$ that has been pointed out in [97] and which has been investigated model-independently in [98] and in the context of the LHT model in [67]. This correlation follows analytically from (3.62) and (3.64) when the SM phase β_s and the first term in (3.64) are neglected:

$$A_{\text{SL}}^q = \text{Re} \left(\frac{\Gamma_{12}^q}{M_{12}^q} \right)^{\text{SM}} \frac{S_{\psi\phi}}{C_{B_q}}. \quad (3.67)$$

In [91] it has been pointed out recently that the accuracy of a similar correlation that uses ΔM_s and $\Delta\Gamma_s$ [99] instead of Γ_{12}^s and M_{12}^s is very poor both for small and large NP phase

observable	experimental value	SM prediction
$\phi_s = -2(\beta_s + \varphi_{B_s})$	$\in [-1.04, -0.04]$ (CDF [92]) $-0.55^{+0.38}_{-0.36}$ (D0 [93]) $+0.13(18)(7)$ (LHCb [94])	$-0.0363(17)$ [3]
$\frac{\Delta\Gamma_d}{\Gamma_d}$	$0.011(37)$ [95]	$0.0042(8)$ [10]
$\Delta\Gamma_s$	$0.075(35)(1)$ ps ⁻¹ (CDF [92]) $0.163^{+0.065}_{-0.064}$ ps ⁻¹ (D0 [93]) $0.123(29)(8)$ ps ⁻¹ (LHCb [94])	$0.087(21)$ ps ⁻¹ [10]
A_{SL}^d	$-0.12(52)\%$ [96]	$-0.041(6)\%$ [91]
A_{SL}^s	$-1.8(11)\%$ [96]	$0.0019(3)\%$ [91]
A_{SL}^b	$-0.79(20)\%$ [96]	$-0.020(3)\%$ [91]

Table 1. Theoretical and experimental values of a number of observables related to $B_{s,d} - \bar{B}_{s,d}$ mixing.

φ_{B_s} . The approximate formula (3.67) is instead very accurate for large $S_{\psi\phi}$. In order to improve the accuracy also for small values of this asymmetry, in our numerical analysis as in our previous analyses in the context of other extensions of the SM, we find such correlation numerically by using (3.62) and (3.64) without making any approximations.

3.10 Summary

In summary, in this section, we have calculated the NP contributions in the LR model in question to the amplitudes M_{12}^K and M_{12}^q . We have then given formulae for ΔM_K , ΔM_q , ε_K , $S_{\psi K_S}$, $S_{\psi\phi}$, $\Delta\Gamma_q$ and A_{SL}^q in a form suitable for the study of the size of the NP contributions. The numerical analysis of these observables is presented in section 10. While particle-antiparticle mixing in LR models has already been discussed in the literature, our analysis goes beyond these papers as in addition to the full renormalisation group analysis and inclusion of all important effects, we search for correlations between various observables that have not been studied by other authors. Most importantly, our philosophy in performing phenomenology differs from the one used in most papers. Instead for looking for bounds on the W_R and Higgs masses we investigate whether the LRM can solve certain anomalies present in the flavour data while being consistent with electroweak precision tests and the data for tree level charged currents. Moreover, we search for the oases in the large space of parameters in which the matrix V^{R} takes special forms that are dictated by the data.

4 The decays $B \rightarrow X_{s,d}\gamma$

4.1 Preliminaries

The $B \rightarrow X_s\gamma$ decay in a model with $SU(2)_L \times SU(2)_R \times U(1)$ symmetry has been analysed by many authors in the past [54–62]. There are basically two classes of contributions:

- First, the ones resulting from the mixing between W_L and W_R that imply RH couplings of the SM W^\pm to quarks. In the SM the LH structure of these couplings requires the chirality flip, necessary for $b \rightarrow s\gamma$ transition to occur, only through the mass of the initial or the final state quark. Consequently the amplitude is proportional to m_b or m_s . In contrast in LR models the RH couplings allow the chirality flip on the internal top quark line resulting in an enhancement factor m_t/m_b of the NP contribution relative to the SM one at the level of the amplitude. This is the contribution mostly studied in the literature. The relevant LO QCD corrections have been analysed for the first time within the effective field theory framework by Cho and Misiak [57] and have been checked since then by many authors, in particular by Bobeth et al. [100], where also NLO QCD corrections to the matching conditions at μ_H have been calculated. In what follows we adopt their results but include NP corrections at the LO, while taking into account the known NNLO corrections within the SM.
- The second contribution comes from charged Higgs exchanges. Although in the LR models the masses of H^\pm are $\mathcal{O}(\kappa_R)$ and numerically significantly larger than few TeV, as pointed out in [58] and also analysed in [59–61], the corresponding amplitude is also enhanced by m_t/m_b in contrast to the MSSM where it is proportional to m_b or m_s . Moreover, it does not suffer from the suppression through $W_L - W_R$ mixing as is the case of the gauge contribution. As we will see for charged Higgs masses even above 10 TeV this contribution cannot be neglected and in fact it can be dominant for certain ranges of parameters. This should be contrasted with $\Delta F = 2$ processes where it is generally subleading.

In the next two sections, we summarise the results for the Wilson coefficients of the dipole operators for these two classes of contributions at the relevant matching scales for the SM and NP. Subsequently we include RG QCD corrections to these coefficients and present the final formula for the branching ratio for the $B \rightarrow X_s\gamma$ decay. We also present the formulae for the CP-averaged branching ratio of the $B \rightarrow X_d\gamma$ decay and direct CP-asymmetries in both decays.

4.2 Gauge boson contributions

Adopting the overall normalisation of the SM effective Hamiltonian we have

$$\mathcal{H}_{\text{eff}}(b \rightarrow s\gamma) = -\frac{4G_F}{\sqrt{2}} V_{ts}^* V_{tb} [C_{7\gamma}(\mu_b) Q_{7\gamma} + C_{8G}(\mu_b) Q_{8G}] , \quad (4.1)$$

where $\mu_b = \mathcal{O}(m_b)$. The dipole operators are defined as

$$Q_{7\gamma} = \frac{e}{16\pi^2} m_b \bar{s}_\alpha \sigma^{\mu\nu} P_R b_\alpha F_{\mu\nu} , \quad Q_{8G} = \frac{g_s}{16\pi^2} m_b \bar{s}_\alpha \sigma^{\mu\nu} P_R T_{\alpha\beta}^a b_\beta G_{\mu\nu}^a . \quad (4.2)$$

In writing (4.1) we have dropped the primed operators that are obtained from (4.2) by replacing P_R by P_L . In the SM the primed operators (RL) are suppressed by m_s/m_b relative to the ones in (4.1). As we demonstrate below they can also be neglected in the LRM discussed by us.

The coefficients $C_i(\mu_b)$ are calculated from their initial values at high energy scales by means of renormalisation group methods. Before entering the discussion of QCD corrections we describe here our treatment of LR contributions at high energy scales. We first decompose the Wilson coefficients at the scale $\mu_W = \mathcal{O}(M_W)$ as the sum of the SM contribution and the NP contributions:

$$C_i(\mu_W) = C_i^{\text{SM}}(\mu_W) + \Delta^{\text{LR}}C_i(\mu_W) \quad (4.3)$$

and similarly for the primed coefficients. For the SM coefficients we have

$$C_{7\gamma}^{\text{SM}}(\mu_W) = \frac{3x_t^3 - 2x_t^2}{4(x_t - 1)^4} \ln x_t + \frac{-8x_t^3 - 5x_t^2 + 7x_t}{24(x_t - 1)^3} \equiv C_{7\gamma}^{\text{SM}}(x_t), \quad (4.4)$$

$$C_{8G}^{\text{SM}}(\mu_W) = \frac{-3x_t^2}{4(x_t - 1)^4} \ln x_t + \frac{-x_t^3 + 5x_t^2 + 2x_t}{8(x_t - 1)^3}. \quad (4.5)$$

The expressions for $\Delta^{\text{LR}}C_i(\mu_W)$ in the LRM have been found by Cho and Misiak [57]. The by far dominant contribution comes from the induced right-handed part of the W_L vertex. At the time of the work of these authors the expected values for M_{W_R} were of the order of several hundred GeV and the scale in the LR contributions could be chosen to be μ_W . With $\mu_R \gg \mu_W$ one has to take the effect of large logarithms $\log(\mu_R/\mu_W)$ into account. While a complete RG analysis would be more involved, in the present paper we take such effects only approximately into account by simply declaring the result in [57] to be valid not at μ_W but μ_R . A more involved analysis will be presented elsewhere.

Adapting the formulae of Cho and Misiak [57] to our notations we find then for the LR contributions

$$\Delta^{\text{LR}}C_{7\gamma}(\mu_R) = A^{tb} \left[\frac{3x_t^2 - 2x_t}{2(1 - x_t)^3} \ln x_t + \frac{-5x_t^2 + 31x_t - 20}{12(1 - x_t)^2} \right], \quad (4.6)$$

$$\Delta^{\text{LR}}C_{8G}(\mu_R) = A^{tb} \left[\frac{-3x_t}{2(1 - x_t)^3} \ln x_t + \frac{-x_t^2 - x_t - 4}{4(1 - x_t)^2} \right], \quad (4.7)$$

where

$$A^{tb} = \frac{m_t}{m_b} s c \epsilon^2 e^{i\alpha} \left(\frac{V_{tb}^{\text{R}}}{V_{tb}^{\text{L}}} \right) + \mathcal{O}(\epsilon^4). \quad (4.8)$$

The Wilson coefficients of the primed operators can be obtained from (4.6), (4.7) by replacing A^{tb} with $(A^{ts})^*$, where

$$A^{ts} = \frac{m_t}{m_b} s c \epsilon^2 e^{i\alpha} \left(\frac{V_{ts}^{\text{R}}}{V_{ts}^{\text{L}}} \right) + \mathcal{O}(\epsilon^4). \quad (4.9)$$

We observe that they are also enhanced by m_t/m_b in contrast to the primed operators in the SM. We stress that $m_t(m_t)$ and $m_b(\mu_b)$ should be used here. We now give arguments

that in order to obtain the leading $\mathcal{O}(\epsilon^2)$ corrections to the branching ratio we only have to keep the contributions in (4.6) and (4.7) while neglecting the contributions from primed operators and the LL and RR contributions from NP. Here the LL stands for pure P_L couplings in the weak gauge boson–quark couplings and analogously for RR with P_L replaced by P_R . The unprimed LR contributions result from the P_R coupling in the vertex containing the b -quark, while the corresponding primed contributions result from the P_R coupling in the vertex containing the s -quark. This is evident from the couplings A^{tb} and A^{ts} given in (4.8) and (4.9), respectively. Now, the LR contributions presented above have been obtained by including only SM internal W_L and top quark exchanges taking into account the right-handed couplings of W_L in the vertex containing the b -quark. These contributions are important due to the factor m_t/m_b that is absent in LL and RR contributions. Moreover, this LR contribution is $\mathcal{O}(\epsilon^2)$ at the amplitude level and interfering with the SM contribution gives also $\mathcal{O}(\epsilon^2)$ contribution to the branching ratio for $B \rightarrow X_s \gamma$. Concerning the primed LR contribution to the decay amplitude while being of the same order in ϵ as the unprimed LR coefficients and also enhanced by m_t/m_b , it does not interfere with the SM contributions and consequently enters the branching ratio at the ϵ^4 level. Therefore it should be neglected for the sake of consistency. Only in the case of a special hierarchy of the elements of V^R matrix could this suppression be compensated by the last factor in A^{ts} . However, then also other $\mathcal{O}(\epsilon^4)$ contributions to the rate would have to be included, which is beyond the scope of this paper. Finally, as already stressed by Cho and Misiak the diagrams with internal W_R exchanges give negligible contributions and a similar remark applies to LL and RR contributions from NP as one can easily check. Note that in this case the LL and RR contributions are governed by SM loop functions in (4.4) and (4.5) which are strongly suppressed when $x_t = m_t^2/M_W^2$ is replaced by $\tilde{x}_t = m_t^2/M_{W_R}^2$.

4.3 Charged Higgs contributions

In presenting the results for charged Higgs contributions we follow [58, 61] adjusting their formulae to our notations and overall normalisations and keeping the phase α . In the numerical analysis we set $\alpha = 0$. As in the case of the gauge boson contributions one can demonstrate that the primed operators can be neglected. We also neglect the H^\pm contribution to $C_{8G}(\mu_H)$. The dominant H^\pm contribution at μ_H is given as follows [58]⁴

$$\Delta^{H^\pm} C_{7\gamma}(\mu_H) = -u(s) \left[sc \frac{m_t}{m_b} e^{i\alpha} \left(\frac{V_{tb}^R}{V_{tb}^L} \right) A_{H^+}^1(y) + 2s^2 c^2 A_{H^+}^2(y) \right], \quad (4.10)$$

where the function $u(s)$ has been defined in (3.17) and [58]

$$A_{H^+}^1(y) = \left[\frac{3y^2 - 2y}{3(1-y)^3} \ln y + \frac{5y^2 - 3y}{6(1-y)^2} \right], \quad (4.11)$$

$$A_{H^+}^2(y) = \frac{1}{3} A_{\text{SM}}(y) - A_{H^+}^1(y), \quad (4.12)$$

$$A_{\text{SM}}(y) = -2C_{7\gamma}^{\text{SM}}(y), \quad y = \frac{m_t^2}{M_H^2}. \quad (4.13)$$

⁴In [58] $\tan \beta = \kappa/\kappa' = c/s$ has been used.

The last function is given on the r.h.s of (4.4). In these contributions we set $m_t = m_t(\mu_H)$. For large s close to the limit $s \rightarrow 1/\sqrt{2}$ a strong enhancement of the H^\pm contribution through the factor $u(s)$ is possible. As we discussed in section 2.4 taking this limit, corresponding to $\kappa' = \kappa$, is phenomenologically not viable. Interestingly, the inspection of gauge boson and charged Higgs contribution shows that provided the element V_{tb}^R has only a small phase, these contributions always enhance the branching ratio for $B \rightarrow X_s \gamma$ which brings the theoretical value in (4.23) closer to the data in (4.24).

4.4 QCD corrections

In order to complete the analysis of $B \rightarrow X_s \gamma$ we have to include QCD corrections which play a very important role in this decay. In the SM these corrections are known at the NNLO level. In the LR model a complete LO analysis has been done by Cho and Misiak [57]. On the other hand Bobeth et al provide matching conditions to the Wilson coefficients of LR operators at μ_R relevant for a NLO analysis, that is $\mathcal{O}(\alpha_s)$ corrections to the coefficients (4.6) and (4.7). However, performing a complete NLO analysis would require additional complicated calculations and in view of many parameters present in this model, such an involved analysis is certainly premature. In view of these remarks we proceed as follows:

- For the SM contribution we use the full result at the NNLO [101].
- For the LR contribution we use explicit LO formulae which we obtained on the basis of [57] and the recent paper [102]. We set the μ_b scale to the one used for the SM contributions, this means $\mu_b = 2.5$ GeV. While the NNLO SM contribution is not sensitive to this choice, some sensitivity is present in the LO LR contribution but in view of several parameters involved this uncertainty is not essential. We are aware of the approximate nature of this treatment of QCD corrections in the NP part but we think that such an approach is sufficient before the discovery of W_R .

Thus the basic formula for $C_{7\gamma}(\mu_b)$ used by us reads:

$$C_{7\gamma}(\mu_b) = C_{7\gamma}(\mu_b)^{\text{SM}} + \Delta^{\text{LR}} C_{7\gamma}(\mu_b) + \Delta^{\text{H}^\pm} C_{7\gamma}(\mu_b), \quad (4.14)$$

where

$$\Delta^{\text{LR}} C_{7\gamma}(\mu_b) = \kappa_7(\mu_R) \Delta^{\text{LR}} C_{7\gamma}(\mu_R) + \kappa_8(\mu_R) \Delta^{\text{LR}} C_{8G}(\mu_R) + A^{cb} \kappa_{\text{LR}}(\mu_R), \quad (4.15)$$

$$\Delta^{\text{H}^\pm} C_{7\gamma}(\mu_b) = \kappa_7(\mu_H) \Delta^{\text{H}^\pm} C_{7\gamma}(\mu_H). \quad (4.16)$$

Here $\Delta^{\text{LR}} C_{7\gamma}(\mu_R)$, $\Delta^{\text{LR}} C_{8G}(\mu_R)$ and $\Delta^{\text{H}^\pm} C_{7\gamma}(\mu_H)$ can be found in (4.6), (4.7) and (4.10), respectively. A^{cb} is given as follows

$$A^{cb} = \frac{m_c}{m_b} s c \epsilon^2 e^{i\alpha} \frac{V_{cb}^R}{V_{cb}^L}. \quad (4.17)$$

The term proportional to A^{cb} is absent in (4.16) as, being related to the mixing with new charged current operators, it is already included in (4.15) and above the scale μ_R this mixing does not take place.

μ_R	1 TeV	2.5 TeV	10 TeV	15 TeV
κ_7	0.457	0.427	0.390	0.380
κ_8	0.125	0.128	0.130	0.130
κ_{LR}	0.665	0.778	0.953	1.005
ρ_8	0.504	0.475	0.439	0.429
ρ_{LR}	-0.052	-0.043	-0.025	-0.019
$\tilde{\kappa}_7$	0.857	0.801	0.731	0.712
$\tilde{\kappa}_8$	0.044	0.060	0.078	0.082
$\tilde{\kappa}_{LR}$	0.063	0.099	0.156	0.175
$\tilde{\rho}_8$	0.874	0.824	0.760	0.743
$\tilde{\rho}_{LR}$	-0.033	-0.044	-0.056	-0.058

Table 2. The NP magic numbers for $\Delta C_{7\gamma}^{\text{LR}}$ and $\Delta C_{8G}^{\text{LR}}$ at $\mu_b = 2.5 \text{ GeV}$ and $\mu_t(m_t)$.

Finally, κ 's are the NP magic numbers listed in Tab. 2 [102], calculated taking $\alpha_s(M_Z = 91.1876 \text{ GeV}) = 0.118$ ⁵.

For later purposes we also give

$$\Delta^{\text{LR}}C_{8G}(\mu_b) = \rho_8(\mu_R) \Delta^{\text{LR}}C_{8G}(\mu_R) + A^{cb}\rho_{LR}(\mu_R), \quad (4.18)$$

with the NP magic numbers ρ_i listed in Tab. 2.

4.5 The branching ratio

For the branching ratio we follow the strategy of [102] which used the results of [103]. One has then

$$\text{Br}(B \rightarrow X_s\gamma) = \text{Br}(B \rightarrow X_s\gamma)_{\text{SM}} + \Delta\text{Br}, \quad (4.19)$$

where

$$\Delta\text{Br} = R \left[2\text{Re}(C_{7\gamma}(\mu_b)^{\text{SM}}\tilde{\Delta}^{\text{LR}}C_{7\gamma}(\mu_b)) + |\tilde{\Delta}^{\text{LR}}C_{7\gamma}(\mu_b)|^2 \right], \quad (4.20)$$

with

$$\tilde{\Delta}^{\text{LR}}C_{7\gamma}(\mu_b) = \Delta^{\text{LR}}C_{7\gamma}(\mu_b) + \Delta^{\text{H}\pm}C_{7\gamma}(\mu_b). \quad (4.21)$$

Next

$$R = 0.00247, \quad C_{7\gamma}(\mu_b)^{\text{SM}} = -0.353, \quad (4.22)$$

and

$$\text{Br}(B \rightarrow X_s\gamma)_{\text{SM}} = (3.15 \pm 0.23) \times 10^{-4} \quad (4.23)$$

are extracted from [103]. We refer to [102] for details. In particular in obtaining the value for $C_{7\gamma}(\mu_b)^{\text{SM}}$ we have taken the non-perturbative corrections into account. Strictly speaking the last term in (4.20) is of $\mathcal{O}(\epsilon^4)$ and should be dropped together with the contributions of primed operators. We recall that experimentally [95]

$$\text{Br}(B \rightarrow X_s\gamma)_{\text{exp}} = (3.55 \pm 0.26) \times 10^{-4}. \quad (4.24)$$

so that $\Delta\text{Br} > 0$ is favoured implying $\tilde{\Delta}^{\text{LR}}C_{7\gamma}(\mu_b) < 0$. This is guaranteed for $\text{Re}V_{tb}^{\text{R}} > 0$.

⁵We thank Emmanuel Stamou for providing this table.

4.6 Dissecting the LR contributions to $\text{Br}(B \rightarrow X_s \gamma)$

Let us next calculate the fraction of H^\pm contributions of the full NP contribution at the level of the branching ratio. As seen in (4.20) and (4.21), if we neglect the last term in (4.21) this is simply given by $\Delta^{\text{H}^\pm} C_{7\gamma}(\mu_b)/\tilde{\Delta}^{\text{LR}} C_{7\gamma}(\mu_b)$. In figure 4 we plot this ratio as a function of M_H for different values of M_{W_R} and two choices of s . For these plots we set V^{R} to be the identity matrix, making the formulae V^{R} independent. Since the main contributions from charged Higgs and gauge bosons are both proportional to V_{tb}^{R} this assumption has a very limited impact.

As in our previous discussion of $\Delta F = 2$ contributions in section 3.6, the Higgs exchanges (this time H^\pm) again turn out to be very important. For realistic W_R masses above 2 TeV and H^\pm masses below 20 TeV, the H^\pm contributions account for at least 20% ($s = 0.1$) or 50% ($s = 0.5$) of the total NP effect. As expected for the large value of $s = 0.5$ the H^\pm contribution is dominant.

4.7 The decay $B \rightarrow X_d \gamma$

Of considerable interest is also the decay $B \rightarrow X_d \gamma$ for which the measured CP-averaged branching ratio reads [95]

$$\langle \text{Br}(B \rightarrow X_d \gamma) \rangle = (1.41 \pm 0.49) \times 10^{-5}, \quad (4.25)$$

to be compared with the most recent SM value [36]

$$\langle \text{Br}(B \rightarrow X_d \gamma) \rangle_{\text{SM}} = (1.54_{-0.31}^{+0.26}) \times 10^{-5}. \quad (4.26)$$

While the data agree with the latter estimate there is still significant room for NP contributions. Yet already these results can imply important constraints on the extensions of the SM. Indeed, it was recently pointed out by Crivellin and Mercalli [36] that the contributions of primed operators to $\langle \text{Br}(B \rightarrow X_d \gamma) \rangle$ could be significantly constrained implying a bound on $|V_{td}^{\text{R}}|$. This bound is approximately 3.5 times stronger than what is found for the best-fit solution in [44], where this decay has not been considered. In the notation of the present paper the bound in [36] reads ⁶

$$s c \epsilon^2 |V_{td}^{\text{R}}| \leq 1.4 \times 10^{-4}. \quad (4.27)$$

As our numerical analysis shows the electroweak precision tests imply $s c \epsilon^2 \lesssim 1 \cdot 10^{-3}$. Therefore as long as $|V_{td}^{\text{R}}| \leq 0.14$ the bound in [36] is satisfied in our paper. Moreover as we can see in section 10 the typical values for $|V_{td}^{\text{R}}|$ that are consistent with ϵ_K are below

$$|V_{td}^{\text{R}}| \leq \begin{cases} 0.047 & (s = 0.5) \\ 0.113 & (s = 0.1) \end{cases}, \quad (4.28)$$

when no fine-tuning constraint is taken into account. Otherwise the allowed ranges for $|V_{td}^{\text{R}}|$ become even smaller. For further details see section 9.2. In all cases $|V_{td}^{\text{R}}|$ is well below the

⁶Note that this bound does not take into account the charged Higgs contribution.

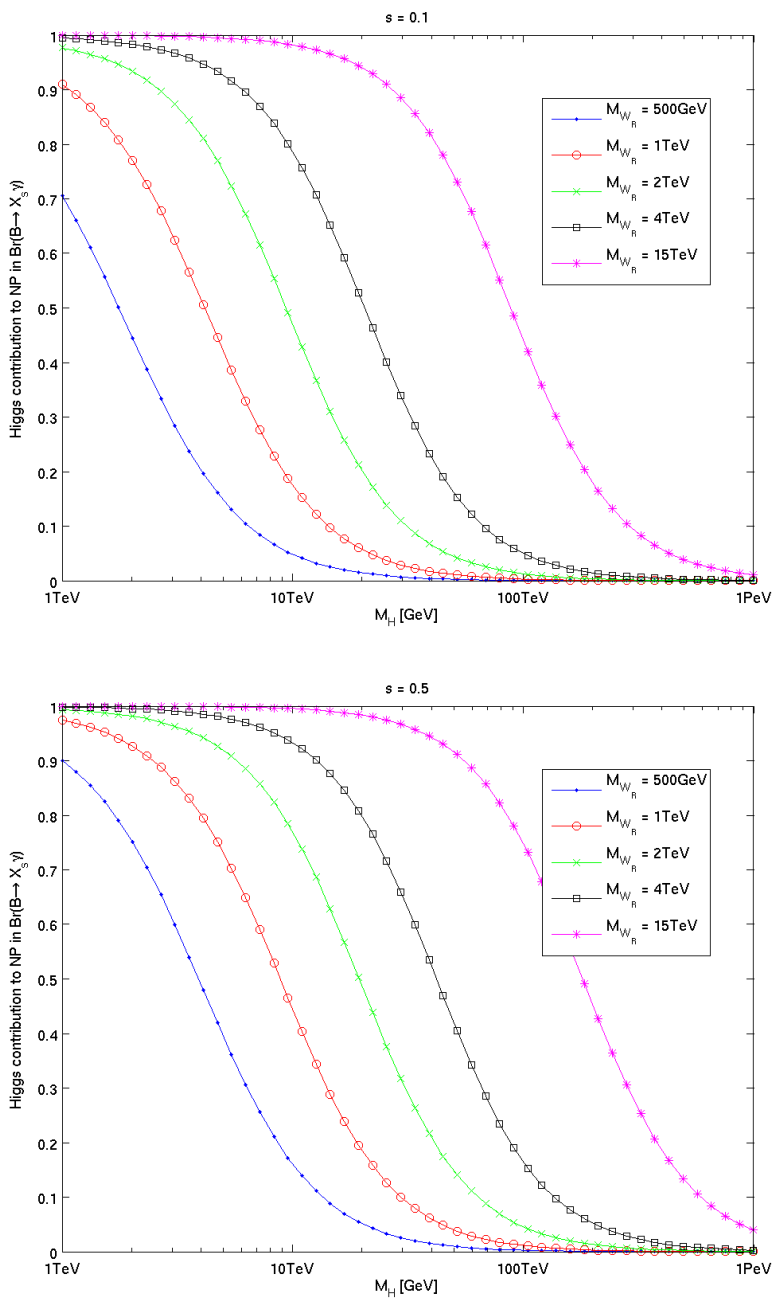


Figure 4. The relative importance of the charged Higgs diagrams in the NP contributions to $\text{Br}(B \rightarrow X_s \gamma)$ for $s = 0.1$ (top panel) and $s = 0.5$ (bottom panel) as a function of the Higgs mass for different W_R masses.

bound in [36], since e.g. a large s implies small values for $|V_{td}^R|$. As we explained before, in our model the contributions of primed operators are $\mathcal{O}(\epsilon^4)$ and consistently neglected in our analysis. While a detailed analysis of $\mathcal{O}(\epsilon^4)$ contributions to $\text{Br}(B \rightarrow X_d \gamma)$ would be required to assess the numerical importance of primed operators in this case, the discussion

a	$a_{\epsilon\epsilon}$	a_{ϵ}^r	a_{77}	a_7^r	$a_{7\epsilon}^r$	a_{88}	a_8^r
7.8221	0.4384	-1.6981	0.8161	4.8802	-0.7827	0.0197	0.5680
$a_{8\epsilon}^r$	a_{87}^r	a_7^i	a_8^i	a_{ϵ}^i	a_{87}^i	$a_{7\epsilon}^i$	$a_{8\epsilon}^i$
-0.0601	0.1923	0.3546	-0.0987	2.4997	-0.0487	-0.9067	-0.0661

Table 3. The relevant a_i parameters from [105].

above indicates that in our model they are well below the NP contributions of unprimed operators when all additional constraints are taken into account.

Clearly, the improved data on the CP-averaged branching ratio in (4.25) and the finding of [104] that the CP-averaged branching ratio contains only small hadronic uncertainties, invites us to consider this decay as well. In analysing it we use, as done in [36], the formulae of [105]. In doing this we should emphasise that these formulae strictly speaking apply only to cases where the RG evolution below the μ_W scale is the same as in the SM. Due to the presence of new LR current-current operators, additional contributions to the Wilson coefficients of the dipole operators are present. They are represented by the last term in (4.15). However, in the model considered by us these contributions are very small and can be neglected. We find then

$$\langle \text{Br}(B \rightarrow X_d \gamma) \rangle = \frac{\mathcal{N}}{100} \left| \frac{V_{td}^{L*} V_{tb}^L}{V_{cb}^L} \right|^2 [\tilde{a} + P_7 + P_8 + P_{78}], \quad (4.29)$$

where $\mathcal{N} = 2.57 \times 10^{-3}$ and

$$\tilde{a} = a + a_{\epsilon\epsilon} |\epsilon_d|^2 + a_{\epsilon}^r \text{Re}(\epsilon_d), \quad (4.30)$$

$$P_7 = a_{77} |R_7|^2 + a_7^r \text{Re}(R_7) + a_{7\epsilon}^r \text{Re}(R_7 \epsilon_d^*), \quad (4.31)$$

$$P_8 = a_{88} |R_8|^2 + a_8^r \text{Re}(R_8) + a_{8\epsilon}^r \text{Re}(R_8 \epsilon_d^*), \quad (4.32)$$

$$P_{78} = a_{87}^r \text{Re}(R_8 R_7^*). \quad (4.33)$$

The values of the a_i parameters are collected in table 3 and

$$R_7 = \frac{C_{7\gamma}(\mu_t)}{C_{7\gamma}^{\text{SM}}(\mu_W)}, \quad R_8 = \frac{C_{8G}(\mu_t)}{C_{8G}^{\text{SM}}(\mu_W)}, \quad (4.34)$$

where the $C_{7\gamma}(\mu_t), C_{8G}(\mu_t)$ denotes the total Wilson coefficients including both the SM contributions without QCD corrections, as given in (4.4) and (4.5) and the NP contributions as in (4.15) and (4.18) but evaluated at μ_t and not μ_b :

$$\Delta^{\text{LR}} C_{7\gamma}(\mu_t) = \tilde{\kappa}_7(\mu_R) \Delta^{\text{LR}} C_{7\gamma}(\mu_R) + \tilde{\kappa}_8(\mu_R) \Delta^{\text{LR}} C_{8G}(\mu_R) + A^{cb} \tilde{\kappa}_{\text{LR}}(\mu_R), \quad (4.35)$$

$$\Delta^{\text{H}^\pm} C_{7\gamma}(\mu_t) = \tilde{\kappa}_7(\mu_H) \Delta^{\text{H}^\pm} C_{7\gamma}(\mu_H), \quad (4.36)$$

and

$$\Delta^{\text{LR}} C_{8G}(\mu_t) = \tilde{\rho}_8(\mu_R) \Delta^{\text{LR}} C_{8G}(\mu_R) + A^{cb} \tilde{\rho}_{\text{LR}}(\mu_R). \quad (4.37)$$

The NP magic numbers $\tilde{\kappa}_i$ and $\tilde{\rho}_i$ are listed in table 2. Finally

$$\epsilon_d = \frac{V_{ud}^{L*} V_{ub}^L}{V_{td}^{L*} V_{tb}^L}. \quad (4.38)$$

For $B \rightarrow X_s \gamma$ one should just replace d by s .

4.8 CP asymmetries in $B \rightarrow X_{s,d} \gamma$

A very sensitive observable to NP CP violating effects is represented by the direct CP asymmetry in $b \rightarrow s \gamma$, i.e. $A_{\text{CP}}(b \rightarrow s \gamma)$ [106], in particular as the perturbative contributions within the SM amount to only +0.5% [105]. The corresponding asymmetry in $b \rightarrow d \gamma$ transition is much larger but could in principle also provide a useful test. These asymmetries are defined by $q = (s, d)$

$$A_{\text{CP}}(b \rightarrow q \gamma) \equiv \frac{\Gamma(\overline{B} \rightarrow X_{\overline{q}} \gamma) - \Gamma(B \rightarrow X_q \gamma)}{\Gamma(\overline{B} \rightarrow X_{\overline{q}} \gamma) + \Gamma(B \rightarrow X_q \gamma)}, \quad (4.39)$$

and have been studied in particular in [107, 108] and more recently in [105], where further references can be found. In the context of the LR models these asymmetries have been analysed in [60]. Unfortunately, a recent analysis [109] shows that these asymmetries, similar to other direct CP asymmetries suffer from hadronic uncertainties originating here in the hadronic component of the photon. These uncertainties lower the predictive power of these observables and in the case of $b \rightarrow s \gamma$ the authors conclude that only if experimentally $A_{\text{CP}}(b \rightarrow s \gamma)$ was found below -2% , one could consider it as a signal of NP. In order to get a rough idea whether in the models considered by us the perturbative part could be affected strongly by NP, we use the formulae in [105], which are compatible with [107, 108]. The formulae with hadronic contributions that are rather uncertain can be found in [109]. We have then

$$A_{\text{CP}}(b \rightarrow q \gamma) = \frac{\mathcal{N}}{100} \left| \frac{V_{tq}^{L*} V_{tb}^L}{V_{cb}^L} \right|^2 \frac{\text{Im}(a_7^i R_7 + a_8^i R_8 + a_\epsilon^i \epsilon_q + a_{87}^i R_8 R_7^* + a_{7\epsilon}^i R_7 \epsilon_q^* + a_{8\epsilon}^i R_8 \epsilon_q^*)}{\langle \text{Br}(B \rightarrow X_q \gamma) \rangle}, \quad (4.40)$$

with the values of a_i collected in table 3.

5 Constraints from tree level decays

5.1 Preliminaries

In this section we address the constraints from tree level decays. The possible new tree level contributions arise from the new right-handed couplings of the W_L gauge boson, from the exchange of the heavy W_R gauge boson, and from the heavy charged Higgs boson. For a detailed consideration of leptonic and semi-leptonic decays it is necessary to have a closer look at the lepton sector within the LR model. In this context in order to derive the Feynman rules we use the findings of [63, 64]. After transformation to mass eigenstates the light neutrinos are dominated by their left-handed contribution with a small right-handed admixture, while the heavy Majorana neutrinos are mainly given by the right-handed

$\text{Br}(\pi \rightarrow \mu\nu) = 0.9998770(4)$	[112]	$f_\pi = 129.5(17) \text{ MeV}$
$f_+(0) V_{us} ^{K \rightarrow \pi \ell \nu} = 0.2163(5)$		$f_+(0) = 0.9584(44)$
$f_K/f_\pi V_{us}/V_{ud} ^{K \rightarrow \mu\nu} = 0.2758(5)$	[113]	$f_K/f_\pi = 1.1931(53)$
$\text{Br}(D_s \rightarrow \tau\nu) = 0.0529(28)$		$f_{D_s} = 248.9(39) \text{ MeV}$
$\text{Br}(B \rightarrow \tau\nu) = 1.64(34) \cdot 10^{-4}$		$f_B = 205(12) \text{ MeV}$ [114]
$F(1) V_{cb} ^{B \rightarrow D^* \ell \nu} = 0.03604(52)$		$F(1) = 0.908(17)$ [115]
$G(1) V_{cb} ^{B \rightarrow D \ell \nu} = 0.0423(15)$	[95]	$G(1) = 1.074(24)$ [116]

Table 4. Values of the most important experimental and theoretical quantities used as input parameters for the constraints on tree level charged currents.

neutrinos again modified by a small left-handed contribution. This mixing angle can be constrained by the masses of heavy and light neutrinos. Assuming reasonable masses for the light neutrinos and the heavy neutrinos not to be lighter than 100 GeV, the Yukawa couplings have to be very small and cause this mixing to be at most $\mathcal{O}(10^{-6})$ [110]. In agreement with [111] we find these mixing effects to be negligible. This is in particular a good assumption taking into account that they have to compete with effects of $\mathcal{O}(\epsilon^2)$ being roughly of $\mathcal{O}(10^{-3})$. Furthermore tree level decays will only take place into the light neutrinos. As the W_R coupling to light neutrinos appears first at $\mathcal{O}(\epsilon^2)$ and the W_R propagator yields another $\mathcal{O}(\epsilon^2)$ suppression factor, we conclude that for the lepton couplings to charged gauge bosons at $\mathcal{O}(\epsilon^2)$ only the SM couplings are relevant for the tree-level decays in question. Concerning the tree level contributions of charged Higgs bosons it is sufficient to include only leading order couplings. In [44] a detailed analysis of the constraints on the elements of the matrix V^R (denoted there by \tilde{V}) and implications for the CKM matrix V^L have been presented. As the charged Higgs contributions to tree level decays in the present model turn out to be negligible (see below), basically all the results obtained in [44] can be taken over by making the following identification:

$$\varepsilon_L = \mathcal{O}(\epsilon^4), \quad \varepsilon_R = cse^2, \quad \tilde{V} = e^{i\alpha}V^R, \quad (5.1)$$

where the quantities on the l.h.s are the ones used in [44]. For completeness we summarise these results in our notation, extending the discussion of the impact of the right-handed currents in tree level decays on the mixing induced asymmetries $S_{\psi K_S}$ and $S_{\psi\phi}$ and on the CKM phase γ as extracted from $B \rightarrow D$ decays within the SM. We use our findings from [44] with updated numerical values.

5.2 Constraints on the mixing matrices V^L and V^R

In what follows we use the notation

$$|V_{ij}|_V = |V_{ij}^L + cse^{i\alpha}\epsilon^2V_{ij}^R|, \quad |V_{ij}|_A = |V_{ij}^L - cse^{i\alpha}\epsilon^2V_{ij}^R|, \quad (5.2)$$

for the combinations of left- and right-handed contributions entering vector and axial vector couplings. As G_F enters tree level decays we note that the correction to the width of the μ -decay in this model are at $\mathcal{O}(\epsilon^4)$ and have no impact on our estimates of V^R .

5.2.1 $u \rightarrow d$

The study of super-allowed $0^+ \rightarrow 0^+$ transitions yields the constraint on the $u \rightarrow d$ vector current [112]

$$|V_{ud}|_V = 0.97425(22). \quad (5.3)$$

A constraint on the axial component can be obtained from the pion decay $\pi^+ \rightarrow \mu^+\nu$, including the known radiative corrections [117], with the result

$$|V_{ud}|_A = 0.981(13). \quad (5.4)$$

5.2.2 $u \rightarrow s$

The vector current $s \rightarrow u$ transition can be obtained from $K \rightarrow \pi\ell\nu$ decays [113] with the result

$$|V_{us}|_V = 0.2257(12). \quad (5.5)$$

The axial $s \rightarrow u$ transition can be constrained by combining $K \rightarrow \mu\nu$ and $\pi \rightarrow \mu\nu$. The result reads

$$|V_{us}|_A = 0.2268(32). \quad (5.6)$$

5.2.3 $c \rightarrow d$

The constraint

$$|V_{cd}|_V = 0.229(25) \quad (5.7)$$

can be obtained from the decays $D \rightarrow K\ell\nu$ and $D \rightarrow \pi\ell\nu$ [112]. $|V_{cd}|$ can also be obtained from neutrino and anti-neutrino charm production off valence d quarks. As interference terms between left- and right-handed quarks are suppressed by m_d , we can safely neglect them. We can therefore directly apply the constraint to left-handed $c \rightarrow d$ transitions and get [112]

$$|V_{cd}^L| = 0.230(11). \quad (5.8)$$

Due to the large uncertainties these data do not provide significant constraints on the LR parameter space but we include them in our numerical analysis. The situation should change in the future when more precise data and lattice inputs will be available. Similar comments apply also to $c \rightarrow s$ transitions discussed below.

5.2.4 $c \rightarrow s$

From semileptonic D decays and $D_s \rightarrow \tau^+\nu$ one finds

$$|V_{cs}|_V = 0.98(10), \quad |V_{cs}|_A = 0.978(31). \quad (5.9)$$

5.2.5 $b \rightarrow u$

This is a place where the RH currents could enter in a potentially important manner. If the SM value for $|V_{ub}|$ is determined from the inclusive semileptonic mode $B \rightarrow X_u\ell\nu$, the interference term between LH and RH contributions is totally negligible, so that the SM result carries over to the LR model. We have [112]

$$|V_{ub}^L| = 4.27(38) \cdot 10^{-3}, \quad (5.10)$$

which should be regarded as the true value of this CKM element. The vector $b \rightarrow u$ transition can be probed by $B \rightarrow \pi \ell \nu$. This implies the constraint [112]

$$|V_{ub}|_V = 3.38(36) \cdot 10^{-3}. \quad (5.11)$$

Finally the axial $b \rightarrow u$ coupling is determined from $\text{Br}(B \rightarrow \tau \nu)$ implying the constraint

$$|V_{ub}|_A = 4.70(56) \cdot 10^{-3}. \quad (5.12)$$

5.2.6 $b \rightarrow c$

Similar to the case of $b \rightarrow u$ transitions, the inclusive determination of $|V_{cb}|$ in the SM carries over to the LR models, where we have

$$|V_{cb}^L| = 41.54(73) \cdot 10^{-3}. \quad (5.13)$$

On the other hand from $B \rightarrow D \ell \nu$ and $B \rightarrow D^* \ell \nu$ transitions one finds the constraints

$$|V_{cb}|_V = 39.4(17) \cdot 10^{-3}, \quad |V_{cb}|_A = 39.70(92) \cdot 10^{-3}. \quad (5.14)$$

The good agreement between the two exclusive determinations suggests a small contribution from right-handed currents and consequently LR effects cannot explain the tension between inclusive and exclusive determinations.

5.2.7 $t \rightarrow d, s$

The $t \rightarrow d$ and $t \rightarrow s$ transitions cannot be measured from tree level decays, so that no constraint is obtained on $V_{td,ts}^L$ and $V_{td,ts}^R$.

5.2.8 $t \rightarrow b$

In the SM $|V_{tb}|$ can be determined from the ratio of branching ratios $\text{Br}(t \rightarrow bW)/\text{Br}(t \rightarrow qW) = |V_{tb}|^2$ assuming unitarity of the CKM matrix. As interference terms are suppressed by m_q/m_t ($q = d, s, b$), this method can directly be applied to LR models. The best available constraint stems from D0 [118] and reads

$$|V_{tb}^L| = 0.95(2). \quad (5.15)$$

This measurement is 2.5σ below the SM expectation $V_{tb}^L \approx 1$. Since as we see later the tight tree level constraints on other elements on the CKM matrix do not allow for a significant deviation of V_{tb}^L from its SM value, this tension persists in the LRM. The improved data from the LHC will tell us whether this is a real problem.

5.3 Charged Higgs contributions

The charged Higgs couplings are given by combinations of the Yukawa couplings of the fermions participating in the interaction. Therefore for all processes not involving the top quark the charged Higgs contribution is very small and turns out to be negligible in all cases. The only decay where this is not completely obvious is $B^+ \rightarrow \tau^+ \nu_\tau$ due to the chiral

suppression of the W^+ contribution. However it turns out that the H^+ contribution is negligible also in that case. Indeed, the Higgs tree level diagrams appear with a suppression factor of m_B^2/M_H^2 and hence in the LR models in which H^\pm is very heavy this contribution is negligibly small in comparison to the effects from right-handed charged gauge boson couplings discussed above.

5.4 A comment on $Z \rightarrow b\bar{b}$

Even if the electroweak precision tests are considered in the next section it is useful to discuss already here the impact of new contributions on the $Z \rightarrow f\bar{f}$ couplings. Denoting the effective diagonal couplings of the Z to down-type quarks as follows

$$\mathcal{L}_{\text{eff}}^Z = \frac{g}{c_W} (g_L^{ii} \bar{d}_L^i \gamma^\mu d_L^i + g_R^{ii} \bar{d}_R^i \gamma^\mu d_R^i) Z_\mu, \quad (5.16)$$

we find (see appendix) at tree level

$$(g_L^{ii}) = \left(-\frac{1}{2} + \frac{1}{3}s_W^2 \right) - \frac{1}{24}s_R^2 c_R^2 \epsilon^2, \quad (5.17)$$

$$(g_R^{ii}) = \frac{1}{3}s_W^2 - \frac{c_R^2}{8} (c_R^2 + \frac{1}{3}s_R^2) \epsilon^2, \quad (5.18)$$

where the first terms are the SM contributions. The experimental determination of the effective couplings of the Z bosons to light down quarks resulting from the global fit of electroweak data collected by the LEP and the SLD experiments is in a very good agreement with the SM. For b quark couplings one finds [119]

$$(g_L^{bb})_{\text{exp}} = -0.4182 \pm 0.0015, \quad (5.19)$$

$$(g_R^{bb})_{\text{exp}} = +0.0962 \pm 0.0063. \quad (5.20)$$

While the result for the LH coupling is consistent with the SM prediction, there is a large disagreement between data and SM expectation in the RH sector:

$$(\Delta g_R^{bb})_{\text{exp}} = (g_R^{bb})_{\text{exp}} - (g_R^{bb})_{\text{SM}} = (1.9 \pm 0.6) \times 10^{-2}, \quad (5.21)$$

It is evident from the formulae above that with $\epsilon^2 = \mathcal{O}(10^{-3})$ as required by our analysis of electroweak precision constraints the corrections to $Z \rightarrow q\bar{q}$ are marginal and that while not spoiling the agreement of the SM with the data for the remaining couplings, these corrections cannot help in removing the anomaly in question. In this context we would like to emphasise that the flavour independence of the corrections would preclude the solution anyway without spoiling the agreement for the remaining couplings. Finally, the sign of corrections being strictly negative would make the disagreement with the data even worse.

5.5 Impact on CP asymmetries

5.5.1 CP asymmetry in $B \rightarrow DK$ and the angle γ

In the SM the angle

$$\gamma = \arg(-V_{ud}V_{ub}^*/V_{cd}V_{cb}^*), \quad (5.22)$$

can be measured by means of CP asymmetries associated with tree level $B \rightarrow DK$ decays. The theoretically cleanest method has been proposed in [120]: Studying $B^\pm \rightarrow DK^\pm$ together with a Dalitz plot analysis of a following multibody D decay allows for determining the weak phase γ without prior assumptions on the hadronic parameters involved. Belle [121] obtained

$$\gamma = 77(11)^\circ, \quad (5.23)$$

where we combined the several uncertainties in quadrature. The details of the Dalitz plot analysis can be found in [120] – as they are relevant mostly for the extraction of the hadronic parameters from the data we do not repeat them here. The measurement relies on the interference between the two modes

$$A(B^- \rightarrow D^0 K^-) \equiv A_B, \quad (5.24)$$

$$A(B^- \rightarrow \bar{D}^0 K^-) \equiv A_B r_B e^{i(\delta_B - \gamma_{\text{eff}})}, \quad (5.25)$$

with relative absolute value r_B , relative strong phase δ_B and relative weak phase γ_{eff} . In the SM the two amplitudes are governed by the operators $(\bar{c}b)_{V-A}(\bar{s}u)_{V-A}$ and $(\bar{u}b)_{V-A}(\bar{s}c)_{V-A}$ mediated by the W boson, respectively. Therefore in this approximation $\gamma_{\text{eff}} = \gamma$.

In LR models there are two new contributions to $B^\pm \rightarrow DK^\pm$ decays:

1. The small RH coupling of W leads to contributions of $(V - A) \otimes (V + A)$ structure. Unless the corresponding hadronic matrix elements are strongly enhanced with respect to the standard $(V - A) \otimes (V - A)$ ones, this contribution is subleading with respect to the one obtained from W' exchange as it is suppressed by an additional factor $sc \leq 1/2$. We neglect this contribution in view of the presently large uncertainties in the experimental determination of γ , keeping in mind that it should be reconsidered once precise data become available.
2. Similarly to the case of $S_{\psi K_S}$ (see below) we also have the contributions of W_R with purely right-handed couplings, that generate the $(V + A) \otimes (V + A)$ operators. As QCD is non-chiral the relevant matrix elements are equal to the SM ones. The LR contribution considered here is therefore purely perturbative.

The interfering amplitudes then get modified as follows

$$A(B^- \rightarrow D^0 K^-) = A(B^- \rightarrow D^0 K^-)_{\text{SM}} \left(1 + r \frac{M_W^2}{M_{W_R}^2} \frac{V_{cb}^R (V_{us}^R)^*}{V_{cb}^L V_{us}^{L*}} \right), \quad (5.26)$$

$$A(B^- \rightarrow \bar{D}^0 K^-) = A(B^- \rightarrow \bar{D}^0 K^-)_{\text{SM}} \left(1 + r \frac{M_W^2}{M_{W_R}^2} \frac{V_{ub}^R (V_{cs}^R)^*}{V_{ub}^L V_{cs}^{L*}} \right), \quad (5.27)$$

Here we neglected the QCD running of the LR contribution from M_{W_R} to M_W . Then the relative weak phase is given by

$$\gamma_{\text{eff}} = \gamma + \arg \left[1 + r \frac{M_W^2}{M_{W_R}^2} \left(\frac{V_{cb}^R (V_{us}^R)^*}{V_{cb}^L V_{us}^{L*}} - \frac{V_{ub}^R (V_{cs}^R)^*}{V_{ub}^L V_{cs}^{L*}} \right) \right]. \quad (5.28)$$

5.5.2 The impact on $S_{\psi K_S}$ and $S_{\psi\phi}$

In the SM the decay $B_d \rightarrow J/\psi K_S$ is dominated by one single decay amplitude arising from a tree level W exchange and giving rise to the operator $(\bar{b}c)_{V-A}(\bar{c}s)_{V-A}$. Using the conventions of [122] the weak phase of the decay amplitude $A(B_d \rightarrow J/\psi K_S)$ is to a very good approximation given by

$$\phi_D = \arg V_{cb}^{L*} V_{cs}^L \simeq 0. \quad (5.29)$$

Together with the phase of $B_d - \bar{B}_d$ mixing

$$\phi_M = \arg V_{tb}^{L*} V_{td}^L \simeq -\beta \quad (5.30)$$

the time dependent CP asymmetry therefore measures ⁷

$$S_{\psi K_S} = \sin[2(\phi_D - \phi_M)] = -\sin\left[2 \arg \frac{V_{tb}^{L*} V_{td}^L}{V_{cb}^{L*} V_{cs}^L}\right] = \sin 2\beta, \quad (5.31)$$

In LR models we have new contributions to the $b \rightarrow c\bar{c}s$ tree level decay. First of all the W now has a small right-handed coupling proportional to $\epsilon^2 \sim \mathcal{O}(10^{-3})$. Second, also W_R exchanges contribute at the $\epsilon^2 \sim \mathcal{O}(10^{-3})$ level. Assuming that the QCD matrix elements do not significantly affect the hierarchy of new contributions, the direct W_R exchange is dominant, in particular if $s \ll 1$. As QCD is a non-chiral theory, we find for the matrix elements governing the decay in question

$$\langle J/\psi K_S | (\bar{b}c)_{V-A} (\bar{c}s)_{V-A} | B_d \rangle = \langle J/\psi K_S | (\bar{b}c)_{V+A} (\bar{c}s)_{V+A} | B_d \rangle. \quad (5.32)$$

Hence the LR correction to the decay amplitude can be expressed in terms of short-distance physics only. We find

$$A(B_d \rightarrow J/\psi K_S) = A(B_d \rightarrow J/\psi K_S)_{\text{SM}} \left(1 + xr \frac{M_W^2}{M_{W_R}^2} \frac{V_{cb}^{R*} V_{cs}^R}{V_{cb}^{L*} V_{cs}^L} \right). \quad (5.33)$$

Here x encodes the RG running from M_{W_R} down to M_W and $r = s_W^2/c_W^2 s_R^2 = g_R^2/g_L^2$. Consequently

$$S_{\psi K_S} = \sin[2(\beta + \varphi_{B_d} + \delta\phi_D)], \quad (5.34)$$

with

$$\delta\phi_D = \arg \left(1 + xr \frac{M_W^2}{M_{W_R}^2} \frac{V_{cb}^{R*} V_{cs}^R}{V_{cb}^{L*} V_{cs}^L} \right). \quad (5.35)$$

We estimated $x \simeq 1.1$.

The same arguments apply to $B_s \rightarrow J/\psi\phi$, hence we find

$$S_{\psi\phi} = -\sin[2(\beta_s + \varphi_{B_s} + \delta\phi_D)]. \quad (5.36)$$

Note that $\delta\phi_D$ is universal in both transitions.

⁷For the estimates of the uncertainties in this relation see [123].

5.5.3 Summary

Using the expressions above we find that the impact of new contributions on the determination of γ and of new phases φ_{B_s} and φ_{B_d} is negligible. This can be traced back primarily to W_R being much heavier than W_L .

6 Electroweak precision constraints

6.1 Preliminaries

Electroweak precision tests (EWPT) provide very strong constraints on basically any model of NP. The SM agrees to a high accuracy with the measured values of roughly 40 low-and high energy observables [112, 124, 125]. Very often such tests are performed with the help of the famous S-T variables [126], which test the allowed size of the oblique corrections, but in order to get the full picture including the LEP II data the study of all observables should be favoured.

Since a full analysis of the EWP data is clearly beyond the scope of this work we use the results of [35] where a full analysis of EWP observables in a number of models with $SU(2)_1 \times SU(2)_2 \times U(1)_X$ gauge symmetry has been performed. The model denoted there by LR-T is precisely the model studied in our paper. Most useful for our study are tables IX and X, where the authors of [35] provide formulae for corrections to the most constraining observables in a given model in terms of the *fit parameters*. These formulae allow then to find allowed regions in the space of the *fit parameters* that are consistent with the data on EWP data. This analysis is independent of the flavour parameters of the matrix V^R . On the other hand the analysis of flavour physics observables is affected by the choice of EW parameters. This is in particular the case for s , to which the $b \rightarrow s\gamma$ decay and to a certain extent also $\Delta F = 2$ processes are very sensitive. Because of its enhancement by charged Higgs contributions $b \rightarrow s\gamma$ requires $s < 0.64$. In this sense we are able to separate the EWP analysis from the flavour analysis. We first determine the allowed ranges for EW parameters and then perform the flavour analysis for a certain EW benchmark point, varying only the parameter s .

In what follows, we very briefly describe the main points of [35], simultaneously adjusting their notation to ours.

6.2 Basic structure of the analysis

As seen in (2.23) and (2.24) except for g_s , m_t , M_H and the phase α , which we set to zero without loss of generality, we have six *model parameters* that are relevant for this section. For the present analysis it is convenient to make a change of variables and to fix the following input (*reference*) parameters

$$G_F, \quad M_Z, \quad \alpha_e \equiv \alpha(M_Z^2), \quad (6.1)$$

which are most precisely measured. In what follows we use, as in [35], the value of the QED coupling constant in the \overline{MS} scheme:

$$1/\alpha(M_Z^2) = 127.916 \pm 0.015. \quad (6.2)$$

In the case of the fit parameters that parametrise NP contributions, we choose

$$\epsilon, \quad s_R, \quad s, \quad (6.3)$$

which are related to the ones in [35] through

$$\tilde{x} = \frac{1}{\epsilon^2}, \quad c_{\tilde{\phi}} = c_R, \quad \sin 2\tilde{\beta} = 2sc. \quad (6.4)$$

The goal of [35] is to find the allowed ranges for the three parameters in (6.4) by fitting 37 EWP observables to the existing data. To this end the SM contributions are included at the tree and one-loop level, while NP contributions are taken into account at the tree level. This is sufficient for our purposes. Before describing the manner in which we use the results of [35], let us make a few comments on how our choice of reference parameters affects the $\mathcal{O}(\epsilon^2)$ corrections in our formulae that have been exclusively written in terms of *model parameters*. The latter parameters have been distinguished in [35] through a *tilde*. Expressing these parameters through the parameters in (6.1) and (6.4) we find that

- G_F and M_Z , as expected, do not receive any $\mathcal{O}(\epsilon^2)$ corrections. This can be explicitly verified by expressing the model parameters in terms of the parameters (6.1) and (6.4) and inserting in the formula for M_Z given in appendix B. The $\mathcal{O}(\epsilon^2)$ correction cancels when v and s_W are defined by ⁸

$$v^2 = \frac{1}{2\sqrt{2}G_F}, \quad s_W^2 c_W^2 = \frac{\pi\alpha(M_Z^2)}{\sqrt{2}M_Z^2 G_F}. \quad (6.5)$$

- On the other hand M_W , $M_{Z'}$ and M_{W_R} are given as follows:

$$M_W = M_Z c_W \left[1 + \frac{\epsilon^2}{2} \frac{c_W^2}{c_W^2 - s_W^2} \left(\frac{c_R^4}{4} - 2s^2 c^2 \right) \right], \quad (6.6)$$

$$(M_{W_R})^2 = \frac{e^2 \kappa_R^2}{c_W^2 s_R^2}, \quad (M_{Z'})^2 = \frac{2e^2 \kappa_R^2}{c_R^2 c_W^2 s_R^2}, \quad (6.7)$$

where we have dropped $\mathcal{O}(\epsilon^2)$ corrections in the last equation, s_W and c_W are defined through (6.5) and the one-loop SM corrections have not been shown in (6.6).

The implications for our analysis are as follows:

- The formula (6.6) after the inclusion of SM electroweak loop corrections together with other observables considered in [35] can be used to constrain the fit parameters in (6.4). However in the present paper we simplify this analysis by requiring that the shift in M_W due to NP contributions is consistent within 2σ with the difference between its measured value and its SM prediction

$$\begin{aligned} (\Delta M_W)^{\text{NP}} &= \epsilon^2 \frac{M_Z}{2} \frac{c_W^3}{c_W^2 - s_W^2} \left(\frac{c_R^4}{4} - 2s^2 c^2 \right) = M_W^{\text{exp}} - M_W^{\text{SM}} \\ &= 0.036(34) \text{ GeV}, \end{aligned} \quad (6.8)$$

where the SM and measured value are taken from [124, 127].

⁸Our v is by $\sqrt{2}$ smaller than the one used in [35].

- On the other hand (6.7) can be used, as done in [35], to find lower bounds on the masses of these new gauge bosons. In turn incorporating the corresponding bounds from collider experiments can put additional constraints on (6.4).
- Finally, in case W_R^\pm and Z' will be discovered and their masses precisely measured, the formulae in (6.7) will allow to take these values as reference parameters reducing the number of fit parameters to one.

6.3 Basic constraints

Using the dictionary in (6.4) and tables IX and X of [35] we find the following expressions for the four observables of interest:

- σ_{had} the partial branching fraction of $Z \rightarrow q\bar{q}$ with the NP correction

$$\delta\sigma_{\text{had}}/\sigma_{\text{had,SM}} = \left[-1.13\frac{c_R^2}{4} - 0.142\frac{c_R^4}{4} + 0.0432(2s^2c^2) \right] \epsilon^2 \quad (6.9)$$

- the forward-backward asymmetry $A_{\text{FB}}(b)$

$$\delta A_{\text{FB}}(b)/A_{\text{FB,SM}}(b) = \left[-30.0\frac{c_R^2}{4} + 67.6\frac{c_R^4}{4} - 20.6(2s^2c^2) \right] \epsilon^2 \quad (6.10)$$

- the weak charge $Q_W(\text{Cs})$ of the caesium-133 nucleus

$$\delta Q_W(\text{Cs})/Q_{W,\text{SM}}(\text{Cs}) = \left[-0.855\frac{c_R^4}{4} - 0.145(2s^2c^2) \right] \epsilon^2 \quad (6.11)$$

- the left-handed coupling measured in deep inelastic ν -N scattering

$$\delta(g_L^{N\nu})^2/(g_{L,\text{SM}}^{N\nu})^2 = [0.0219 + 0.478c_R^2 + 0.210c_R^4 - 1.42(4s^2c^2)] \epsilon^2 \quad (6.12)$$

A more detailed description of the observables considered here is presented in e.g. [35, 128].

The correct treatment of the constraints is then given by the following formula

$$|\text{EXP} - \text{SM}(1 + \text{CON})| \leq \sqrt{(\Delta\text{EXP})^2 + (\Delta\text{SM}(1 + \text{CON}))^2}, \quad (6.13)$$

where EXP and SM stand for the experimental and SM value, respectively. CON stands for one of the conditions we have listed above. Furthermore we use the constraint from the W boson mass as given in (6.8), where the SM and experimental values are taken from [124, 127].

We also incorporate the direct experimental constraints from muon decay of the TWIST Collaboration [129]. They present two bounds on the ratio of g_R/g_L times the mixing angle and one on g_L/g_R with respect to the W_R mass. As $s_W/(c_W s_R) = g_R/g_L$ holds, we can make further simplifications as in the first constraint the factor g_R/g_L cancels. In our notation their results read then

$$s c \epsilon^2 < 0.020 \quad \text{and} \quad \frac{c_W s_R}{s_W} M_{W_R} > 578 \text{ GeV} \quad (6.14)$$

at 90% C.L..

Moreover we take into account the direct experimental bounds on M_{W_R} . While [130, 131] report stringent constraints > 2 TeV on the mass of heavy W' gauge bosons, these bounds only apply to the case of very light right-handed neutrinos which escape detection. In case of a non-negligible $M_{\nu_R} < M_{W_R}$ the constraints on the masses have been analysed in [132], with the bound on M_{W_R} reaching up to 1.7 TeV depending on the right-handed neutrino mass, with only 240 pb^{-1} of data analysed so far. On the other hand if $M_{\nu_R} > M_{W_R}$ the branching ratio of W_R decaying to leptons is ϵ^2 suppressed and the dominant decay mode is into quarks. In that case the searches for resonances in the dijet mass distribution [133, 134] apply, yielding the constraint $M_{W_R} > 1.5$ TeV. We note that all these bounds depend on the ratio g_L/g_R through the production cross-section for W_R . In order to keep our analysis independent of the details of the LRM neutrino sector, we will assume $M_R \geq 2$ TeV throughout our analysis.

Finally for completeness we include the bounds $g_R^2 < 4\pi$ and $g'^2 < 4\pi$ in order to guarantee perturbativity of the gauge couplings.

7 Strategy for the numerical analysis

7.1 Preliminaries

Having at hand all the relevant formulae for $\Delta F = 2$ processes, $B \rightarrow X_{d,s}\gamma$ observables, EWP observables and tree level decays in the LRM in question, we are ready to perform a numerical analysis taking all existing experimental constraints into account.

The first question which one could ask is whether there are regions in the parameter space of the LRM for which all observables can be found in their allowed ranges. As the LRM has a large number of parameters, in particular in the mixing matrix V^R , it is probable that there are such regions even for an LHC accessible mass M_{W_R} .

The next interesting question is if there are experimentally allowed simplified parametrisations for the RH mixing matrix with only a few free parameters. There are a few popular yet already excluded matrices of this kind. We however derive inspiration from those and propose a new and simple matrix.

In general regions in the parameters space fulfilling

- the fine-tuning of parameters is small,
- the anomalies in the present data are softened or removed,

are particularly interesting. These regions can be considered as different 'oases' in the parameter space which are disconnected and lead in general to different phenomenology.

7.2 Anomalies in the flavour data

Before proceeding with outlining our strategy we now review the known flavour anomalies.

7.2.1 The $\varepsilon_K - S_{\psi K_S}$ anomaly

It has been pointed out in [5, 84] that the SM prediction for ε_K implied by the measured value of $S_{\psi K_S} = \sin 2\beta$, the ratio $\Delta M_d/\Delta M_s$ and the value of $|V_{cb}|$ turns out to be too small to agree well with experiment. This tension between ε_K and $S_{\psi K_S}$ has been pointed out from a different perspective in [4, 8, 135, 136]. These findings have been confirmed by a UTfit analysis [2]. The CKMfitter group having a different treatment of uncertainties finds less significant effects in ε_K [9]. Indeed taking the experimental value of $S_{\psi K_S} = 0.679 \pm 0.020$, $|V_{cb}| = 0.0406$, the most recent value of the relevant non-perturbative parameter $\hat{B}_K = 0.737 \pm 0.020$ [137–141] resulting from unquenched lattice calculations and including long distance (LD) effects in $\text{Im}\Gamma_{12}$ and $\text{Im}M_{12}$ in the $K^0 - \bar{K}^0$ mixing [5, 83] as well as recently calculated NNLO QCD corrections to ε_K [142, 143] one finds [143]

$$|\varepsilon_K|_{\text{SM}} = (1.81 \pm 0.28) \cdot 10^{-3}, \quad (7.1)$$

visibly below the experimental value $|\varepsilon_K|_{\text{exp}} = (2.228 \pm 0.011) \cdot 10^{-3}$. On the other hand $\sin 2\beta \approx 0.85 \pm 0.05$ from SM fits of the Unitarity Triangle (UT) is significantly larger than the experimental value $S_{\psi K_S} = 0.679 \pm 0.020$. This discrepancy is to some extent caused by the desire to fit ε_K [4, 5, 8, 84, 135, 136] and $\text{Br}(B^+ \rightarrow \tau^+ \nu_\tau)$ [8]. For the most recent discussions including up to date numerics see [10, 11, 144]. As demonstrated in [5, 84], whether the NP is required in ε_K or $S_{\psi K_S}$ depends on the values of γ , $|V_{ub}|$ and $|V_{cb}|$. The phase γ should be measured precisely by LHCb in the coming years while $|V_{ub}|$ and $|V_{cb}|$ should be precisely determined by Belle II [145] and SuperB [146–148] provided also the hadronic uncertainties will be under better control. Here we concentrate briefly on $|V_{ub}|$.

7.2.2 $|V_{ub}|$ problem

As already mentioned previously there is the tension between inclusive and exclusive determinations of $|V_{ub}|$ with the exclusive ones in the ballpark of $3.4 \cdot 10^{-3}$ and the inclusive ones typically above $4.0 \cdot 10^{-3}$. As discussed in [41] an interesting possible solution to this problem is the presence of RH charged currents, which selects the inclusive value as the true value (see our discussion in section 5), implying again $\sin 2\beta \approx 0.80$ [44]. Unfortunately in the LRM the increased value of the W_R mass precludes this explanation if only points with acceptable fine-tuning are considered. Indeed the factor $sc\epsilon^2 \leq 10^{-3}$ from EWPT data and the bound on $|V_{ub}^{\text{R}}|$ from FCNC processes as found by us, see section 10.3 for details, imply that the effect of RH currents is simply too small. Therefore one cannot state that the inclusive value is the favoured one from the point of view of the LRM and both the exclusive and inclusive determinations are equally valid.

7.2.3 Possible solutions

As discussed in [4, 5] and subsequent papers of these authors a negative NP phase φ_{B_d} in $B_d^0 - \bar{B}_d^0$ mixing would solve the $\varepsilon_K - S_{\psi K_S}$ anomaly, provided such a phase is allowed by other constraints. Indeed, this is evident from (3.61). With a negative φ_{B_d} the true $\sin 2\beta$ is larger than $S_{\psi K_S}$, implying a higher value on $|\varepsilon_K|$, in reasonable agreement with data and a better UT-fit. This solution would favour the inclusive value of $|V_{ub}|$. On the

other hand as stressed in [5] a sizeable constructive NP physics contribution to ε_K would not require an increased value of $\sin 2\beta$ relative to the experimental value of $S_{\psi K_S}$ and the exclusive value of $|V_{ub}|$ would be favoured in this case. Clearly also in such an analysis $\Delta M_{d,s}$ should be considered.

7.2.4 Enhanced value of $S_{\psi\phi}$

This topic became rather hot in the last years but the situation is still unclear at present. The Tevatron data for $S_{\psi\phi}$ combined with the results for the same sign dimuon asymmetry of $D0$ indicated last spring non-standard CP violation in the B_s -system corresponding to $S_{\psi\phi} \approx 0.8$ [10–12]. On the other hand the subsequent measurements of CDF and D0 [92, 93] and the first more accurate results for $S_{\psi\phi}$ from LHCb [94] indicate consistency with the SM. Yet, the range

$$-0.1 \leq S_{\psi\phi} \leq 0.4 \quad (7.2)$$

summarised recently in [149] leaves still a lot of room for sizeable NP contributions. Let us hope that the future data from Tevatron and in particular from the LHCb, will measure this asymmetry with sufficient precision so that we will know to which extent NP is at work here.

7.3 Addressing the flavour anomalies in the LRM

Now we want to discuss how the LRM can in principle address the anomalies described above. As the LRM has a large number of parameters, in particular in the mixing matrix V^R , it is obvious that for certain choices of these parameters, most, or even all of these anomalies can be removed. Yet, as we will see the situation is more involved than one might think at first sight. In order to better understand this matter we introduce an analytic expression for V^R valid in a specific oasis of the parameter space. This matrix is given in terms of only few parameters. Other oases will be considered later on.

In this manner we see that already the present data give us some hints on possible structures of the V^R matrix. The fact that the low energy flavour data can give us such information about physics taking place at scales of few TeV is clearly remarkable and complementary to direct collider searches for NP at the LHC, where it is basically impossible to learn about the structure of V^R . With improved flavour data we should be able to find out which of the oases considered by us, if any, is favoured by nature.

7.3.1 Various scenarios for $|V_{ub}|$

In view of the fact that the LRM cannot solve the $|V_{ub}|$ problem, as mentioned above and discussed in section 9.2, we introduce two scenarios for $|V_{ub}|$. In particular, we investigate the correlations between ε_K , $S_{\psi K_S}$, $S_{\psi\phi}$, ΔM_d and ΔM_s in these two scenarios for $|V_{ub}|$ setting $\gamma = 68^\circ$. These scenarios are defined as follows:

1. Small $|V_{ub}|$

In this scenario we set

$$|V_{ub}| = 3.4 \times 10^{-3}. \quad (7.3)$$

In this scenario within the SM we find $S_{\psi K_S} \approx 0.675$ in agreement with the data but $\varepsilon_K \approx 1.8 \times 10^{-3}$ is visibly below the data.

2. Large $|V_{ub}|$

In this scenario we set

$$|V_{ub}| = 4.4 \times 10^{-3}. \quad (7.4)$$

This is the case, considering again the SM, in which ε_K is consistent with the data while $S_{\psi K_S} \approx 0.82$, significantly above the data.

We now illustrate with an example how all these discrepancies can be solved with a special form of the matrix V^R that depends only on four parameters: \tilde{s}_{13} , \tilde{s}_{23} and two phases ϕ_1 and ϕ_2 , all chosen to be in the first quadrant. We want to stress that these scenarios are only used in our discussion regarding the simplified matrix introduced in the following section. As already discussed in section 5 in our general analysis we treat the constraints on $|V_{ub}|$ and γ like any other measurement.

7.3.2 Understanding anomalies through V^R

In this section we want to propose a new simplified RH mixing matrix and subsequently illustrate how it can be used to solve the flavour anomalies. This matrix has been found with the goal to have very simple expressions for the $\Delta F = 2$ observables while satisfying all existing constraints. To this end it turned out useful to set $\tilde{s}_{12} = 0$ in V_0^R as in this manner, as seen in (2.27), five entries in this matrix simplified considerably. Moreover, the ΔM_K constraint has been relaxed in this way. The reduction of the number of phases to two turned out also to improve the transparency.

The resulting special form of V^R is then given by

$$V^R = \begin{pmatrix} -\tilde{c}_{13}e^{-i\phi_1} & 0 & \tilde{s}_{13} \\ -\tilde{s}_{23}\tilde{s}_{13}e^{i(\phi_2-2\phi_1)} & -\tilde{c}_{23}e^{-i\phi_1} & -\tilde{s}_{23}\tilde{c}_{13}e^{i(\phi_2-\phi_1)} \\ \tilde{c}_{23}\tilde{s}_{13}e^{-i\phi_1} & -\tilde{s}_{23}e^{-i\phi_2} & \tilde{c}_{23}\tilde{c}_{13} \end{pmatrix}. \quad (7.5)$$

In order to derive simple formulae we restrict the mixing angles to the phenomenologically viable ranges

$$\tilde{s}_{13} \lesssim 0.02, \quad \tilde{s}_{23} \lesssim 0.2, \quad (7.6)$$

with the constraints coming from the B_d and B_s system, respectively. Without further assumptions on the phases involved, a much stronger combined constraint

$$\tilde{s}_{13}\tilde{s}_{23} \lesssim 10^{-5} \quad (7.7)$$

can be derived from ε_K . In this range of parameters we find then to a very good approximation that the terms proportional to $\lambda_t^{\text{LR}}\lambda_t^{\text{RL}}$ dominate as far as $\Delta M_{d,s}$, ε_K , $S_{\psi K_S}$ and $S_{\psi\phi}$ are concerned. For ΔM_K also $\lambda_t^{\text{LR}}\lambda_c^{\text{RL}}$ is relevant but the appearance of the same phase ϕ_1 in V_{td}^R and V_{cs}^R makes its contribution to ε_K to be negligible. We find then

$$(\text{Im } M_{12}^K)_{\text{LR}} = |R_{tt}(K)| \times \frac{G_F^2 M_W^2}{12\pi^2} F_K^2 m_K |V_{td}^L| |V_{ts}^L| \tilde{c}_{23} \tilde{s}_{13} \tilde{s}_{23} \sin(\phi_2 - \phi_1 - \beta + \beta_s). \quad (7.8)$$

For $B_q^0 - \bar{B}_q^0$ mixing we have

$$C_{B_q} e^{2i\varphi_{B_q}} = 1 - \frac{|R_{tt}(B_q)|}{S_0(x_t)\hat{B}_{B_q}\eta_B} \left[\frac{\lambda_t^{RR}(B_q)}{\lambda_t^{LL}(B_q)} \right]^*. \quad (7.9)$$

Using the matrix (7.5) we obtain

$$\left[\frac{\lambda_t^{RR}(B_d)}{\lambda_t^{LL}(B_d)} \right]^* = \frac{\tilde{c}_{23}\tilde{s}_{13}V_{tb}^R}{|V_{td}^L|} e^{i(\phi_1 - \beta)}, \quad \left[\frac{\lambda_t^{RR}(B_s)}{\lambda_t^{LL}(B_s)} \right]^* = \frac{\tilde{s}_{23}V_{tb}^R}{|V_{ts}^L|} e^{i(\phi_2 - \beta_s)}, \quad (7.10)$$

and consequently

$$\sin 2\varphi_{B_d} = -\frac{|z_d|}{C_{B_d}} \frac{\tilde{c}_{23}\tilde{s}_{13}V_{tb}^R}{|V_{td}^L|} \sin(\phi_1 - \beta), \quad (7.11)$$

$$\sin 2\varphi_{B_s} = -\frac{|z_s|}{C_{B_s}} \frac{\tilde{s}_{23}V_{tb}^R}{|V_{ts}^L|} \sin(\phi_2 - \beta_s). \quad (7.12)$$

Here

$$z_q = \frac{R_{tt}(B_q)}{S_0(x_t)\hat{B}_{B_q}\eta_B}. \quad (7.13)$$

Setting then $M_{W_R} = 2.5$ TeV, $s = 0.1$ and $M_{H^0} = M_{H^\pm} = 16$ TeV we find then for central values of other parameters

$$|R_{tt}(K)| = 9.1, \quad |R_{tt}(B_q)| = 0.57, \quad |z_d| = 0.36, \quad |z_s| = 0.34. \quad (7.14)$$

These quantities summarise the dominant S_{LR} contribution that governs the box contributions with (W_L, W_R) and (W_L, H^\pm) as well as neutral Higgs tree level exchanges. As seen in (3.40) it includes also QCD corrections, hadronic matrix elements and depends on the masses of W_R and heavy Higgs particles. If only the box contributions involving W_L and W_R were taken into account the NP contributions to ε_K would be reduced universally by 85% allowing for larger values of the mixing parameters and phases in these three expressions. The Higgs dominance can be read off figure 3.

The fact that three quantities in question depend only on two new phases ϕ_1 and ϕ_2 implies interesting correlations in the two scenarios for $|V_{ub}|$ that we illustrate now. These correlations depend of course on the two positive real values of \tilde{s}_{13} and \tilde{s}_{23} as we see below.

- In scenario 1, $S_{\psi K_S}$ within the SM agrees well with the data implying that $\phi_1 \approx \beta$. This in turn implies that ε_K and $S_{\psi\phi}$ are governed by the phases $\phi_2 - 2\beta$ and ϕ_2 , respectively. The desire to reproduce the experimental value of ε_K requires $\phi_2 > 2\beta - \beta_s$, and $S_{\psi\phi}$ can be enhanced simultaneously.
- In scenario 2, ε_K in the SM agrees well with the data implying that $\phi_1 \approx \phi_2 - \beta + \beta_s$. Consequently $S_{\psi K_S}$ and $S_{\psi\phi}$ are this time governed by the phases $\phi_2 - 2\beta$ and ϕ_2 , respectively. The desire to reproduce the experimental value of $S_{\psi K_S}$ requires again $\phi_2 > 2\beta - \beta_s$ which also leads to an enhanced value of $S_{\psi\phi}$.

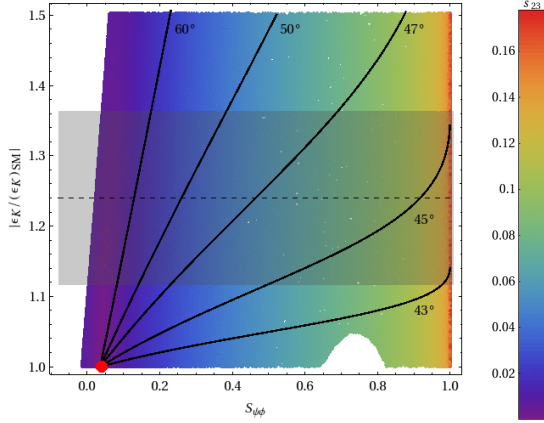


Figure 5. Correlation between $S_{\psi\phi}$ and ε_K in scenario 1, for fixed $\phi_1 = \beta$ and $\tilde{s}_{13} = 3 \cdot 10^{-3}$. The central SM value is indicated by the red dot.

In summary the phases ϕ_1 and ϕ_2 should satisfy

$$\phi_1 \simeq \begin{cases} \beta, & \text{(scenario 1)} \\ \phi_2 - \beta + \beta_s, & \text{(scenario 2)} \end{cases} \quad (7.15)$$

$$\phi_2 > 2\beta - \beta_s. \quad (7.16)$$

As we can see there are relations between the NP phases in the B_d and B_s systems but they are more involved than the ones characteristic for $2\text{HDM}_{\overline{\text{MFV}}}$ [75, 76].

In figure 5 we show the correlation between ε_K and $S_{\psi\phi}$ in scenario 1. To this end we set $\phi_1 = \beta$ and $\tilde{s}_{13} = 3 \cdot 10^{-3}$ and vary $\tilde{s}_{23} < 0.2$ and $2\beta - \beta_s < \phi_2 < \pi + 2\beta - \beta_s$, imposing the experimental constraints on ΔM_s and ΔM_d . The SM point is reached for $\tilde{s}_{23} = 0$. The black curves correspond to constant ϕ_2 values as indicated. We observe that for not too small $\tilde{s}_{23} \gtrsim 0.05$ and $45^\circ < \phi_2 < 50^\circ$ good agreement with the data for ε_K can be achieved while at the same time enhancing $S_{\psi\phi}$ w.r.t. its tiny SM value. For larger values of ϕ_2 a smaller \tilde{s}_{23} is required in order to fit the ε_K data. At the same time the effects in $S_{\psi\phi}$ become much smaller. Within scenario 1 this simple structure for V^{R} can thus solve the ε_K anomaly. The measured value of $S_{\psi\phi}$ can then be used to measure the values of \tilde{s}_{23} and ϕ_2 .

In figure 6 we show the correlation between ΔM_d and ΔM_s , normalised to their SM values, after imposing the constraint from ε_K . Again $\phi_1 = \beta$ and $\tilde{s}_{13} = 3 \cdot 10^{-3}$ are fixed, while $\tilde{s}_{23} < 0.2$ and $2\beta - \beta_s < \phi_2 < \pi + 2\beta - \beta_s$ are varied. Since the observed values for both mass differences lie below their SM predictions, a suppression is welcome also in this case. We observe that ΔM_d is very close to its experimental central value and almost constant, since it depends to very good approximation only on ϕ_1 and \tilde{s}_{13} which are fixed. Also ΔM_s can easily be suppressed and brought closer to the data, which in turn favours moderate enhancements of $S_{\psi\phi} \lesssim 0.4$ (light-blue points in the figure) or very large effects $S_{\psi\phi} \sim 1$ (red points) – the latter being disfavoured by the LHCb data.

As a specific example for how the anomalies are solved in scenario 1, we quote the

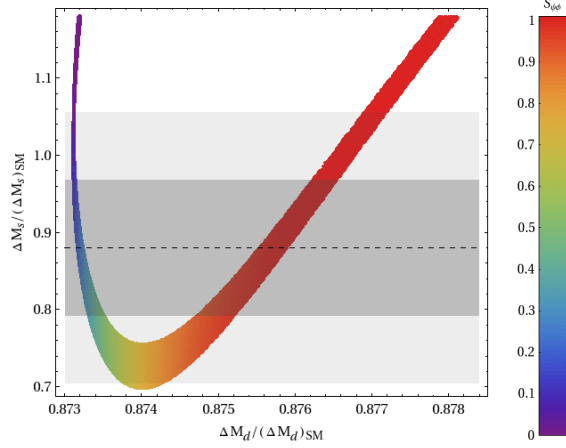


Figure 6. Correlation between ΔM_d and ΔM_s in scenario 1, for fixed $\phi_1 = \beta$ and $\tilde{s}_{13} = 3 \cdot 10^{-3}$, and imposing the constraint from ε_K .

following parameter point:

$$\tilde{s}_{13} = 3 \cdot 10^{-3}, \quad \tilde{s}_{23} = 0.03, \quad \phi_1 = \beta = 21^\circ, \quad \phi_2 = 50^\circ. \quad (7.17)$$

With this choice of parameters we find

$$S_{\psi K_S} \approx 0.67, \quad |\varepsilon_K| \approx 2.2 \cdot 10^{-3}, \quad S_{\psi\phi} \approx 0.27, \quad (7.18)$$

and

$$\Delta M_d \approx 0.51 \text{ ps}^{-1}, \quad \Delta M_s \approx 17.4 \text{ ps}^{-1} \quad (7.19)$$

barring in mind the theoretical and parametric uncertainties that have been omitted here for the sake of simplicity.

Let us stress that this solution to the flavour anomalies is in fact the simplest one possible within scenario 1. Setting any of the four parameters in (7.5) to zero would spoil the relations discussed above.

Let us now turn our attention to scenario 2, in which ε_K is in good agreement with the data, but $S_{\psi K_S}$ needs to be suppressed w. r. t. its SM value ≈ 0.82 . We show now that although this simple structure of V^R can yield some improvement over the SM situation, the tensions cannot be fully resolved in this case.

To this end we show in the left panel of figure 7 $\Delta M_d / (\Delta M_d)_{\text{SM}}$ as a function of $S_{\psi K_S}$ for different values of $\tilde{s}_{13} < 0.01$ and $2\beta - \beta_s < \phi_2 < 150^\circ$ and fixed $\phi_1 = \phi_2 - \beta + \beta_s$. We observe that in order to simultaneously fit the data on $S_{\psi K_S}$ and ΔM_d , ϕ_2 is required to lie roughly in the range $90^\circ \dots 120^\circ$.

In the right panel of figure 7 we show $\Delta M_s / (\Delta M_s)_{\text{SM}}$ as a function of $S_{\psi\phi}$ for different values of $\tilde{s}_{23} < 0.1$ and $2\beta - \beta_s < \phi_2 < 150^\circ$. Here we observe that in order to obtain a suppression of ΔM_s w. r. t. the SM prediction, as favoured by the data, a much smaller phase $\phi_2 \lesssim 70^\circ$ is required. An enhancement of $S_{\psi\phi}$ over its SM value is then obtained automatically. Such a low value for ϕ_2 would in turn allow only for a mild suppression of $S_{\psi K_S}$ with respect to its SM value. This exercise shows very clearly how important it is

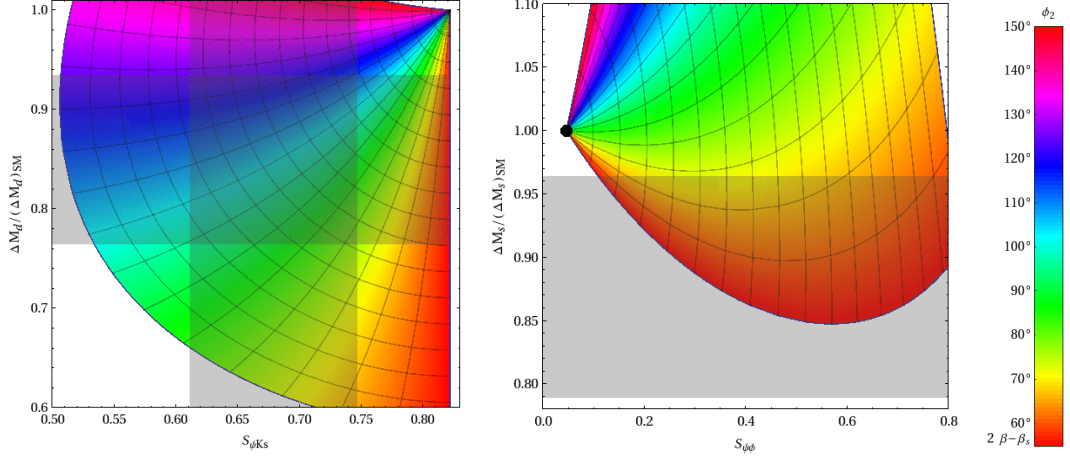


Figure 7. *left:* $\Delta M_d/(\Delta M_d)_{\text{SM}}$ as a function of $S_{\psi K_S}$ for different values of $\tilde{s}_{13} < 0.01$ and $2\beta - \beta_s < \phi_2 < 150^\circ$. *right:* $\Delta M_s/(\Delta M_s)_{\text{SM}}$ as a function of $S_{\psi\phi}$ for different values of $\tilde{s}_{23} < 0.1$ and $2\beta - \beta_s < \phi_2 < 150^\circ$. The SM values are displayed as black dots, while the experimental 1σ regions are indicated by grey bands.

to consider various observables simultaneously. Each of the panels in figure 7 taken alone allows to remove the anomalies in B_d and B_s systems, respectively. But when they are taken together a clear tension between the suppression of ΔM_s and suppression of $S_{\psi K_S}$ is present.

In view of the present non-perturbative uncertainties, it is not possible to rule out this structure of V^{R} as a solution to the flavour anomalies within scenario 2, however we note that this scenario is disfavoured since only a slight amelioration of the SM tensions is possible. On the other hand, as seen before, this simple matrix works beautifully in solving all anomalies within scenario 1.

In fact the conclusion is much more general: Within scenario 2 it is not possible to solve the flavour anomalies if the tt contribution dominates all observables in question. To see this, let us parametrise

$$V_{td}^{\text{R}} = |V_{td}^{\text{R}}|e^{-i\phi_1}, \quad V_{ts}^{\text{R}} = -|V_{ts}^{\text{R}}|e^{-i\phi_2}, \quad V_{tb}^{\text{R}} = |V_{tb}^{\text{R}}|e^{-i\phi_3}. \quad (7.20)$$

The constraint from ε_K in (7.8) again implies $\phi_1 \approx \phi_2 - \beta + \beta_s$. In the formulae for $B_{d,s}$ mixing ((7.11), (7.12)) ϕ_2 is then replaced by $\phi_2 - \phi_3$. However, since the same combination of phases appears in both meson systems it cannot help to ameliorate the tension between B_d and B_s data. Thus in order to solve the flavour anomalies in the LRM in case of a large $|V_{ub}|$ value, charm contributions have to be relevant.

These correlations are reminiscent of the ones found in the context of a 2HDM with flavour blind phases (2HDM $_{\overline{\text{MFV}}}$) [75, 76]. The difference is in the direct contribution to ε_K in scenario 1 which was absent in the 2HDM in question.

We should also emphasise that with V_{tb}^{R} being close to unity, in both scenarios the branching ratio $\text{Br}(B \rightarrow X_s \gamma)$ is also enhanced over the SM value bringing the central theoretical value of this branching ratio closer to experiment.

While showing this example we do not claim that the matrix in (7.5) is the only one that is capable of removing simultaneously (scenario 1) or ameliorating (scenario 2) all anomalies in a correlated manner, but possibly this is the simplest matrix achieving this goal. One can also check that moving to different quadrants of the mixing angles and phases would generally imply different correlations between the observables in question and this fact illustrates how one can determine V^R once the data on $S_{\psi\phi}$, $S_{\psi K_S}$ and $|V_{ub}|$ improve.

7.4 Nominal input parameters

We have collected the input parameters required for the numerical analysis in tables 5 and 6. The values of other parameters like P_i^a and the tree level constraints on the CKM matrix have been given in previous sections. At this stage it is important to recall first the theoretical uncertainties in the constraints used by us. Considerable progress in lattice calculations has been made in recent years reducing the uncertainties in F_{B_s} and F_{B_d} and also in $\sqrt{\hat{B}_{B_s}}F_{B_s}$ and $\sqrt{\hat{B}_{B_d}}F_{B_d}$ down to 5%. This implies an uncertainty of 10% in ΔM_d and ΔM_s within the SM. The numerical values and their respective errors are given in table 5. Even bigger progress has been made in the case of the CP-violating parameter ε_K , where the decay constant F_K is known with 1% accuracy. Moreover the parameter \hat{B}_K is known within 3% accuracy from lattice calculations with dynamical fermions [137–141] and an improved estimate of long distance contributions to ε_K reduced this uncertainty down to 2% [5, 83]. Also the calculation of NNLO QCD perturbative corrections to ε_K [142, 143] improved the theoretical status of ε_K by much. The situation with other B_i parameters describing the hadronic matrix elements of other operators is much worse as clearly seen in the errors of the factors P_i^a in (3.27) and (3.28). Here a significant progress is desired.

Finally let us recall that the CP-asymmetries $S_{\psi\phi}$ and $S_{\psi K_S}$ have rather small hadronic uncertainties⁹ and the hadronic uncertainties in the ratio $\Delta M_d/\Delta M_s$ amount to roughly 3%. Also the theoretical uncertainties in the rate $B \rightarrow X_s\gamma$ decay are below 10%.

On the experimental side ΔM_d , ΔM_s and ε_K are very precisely measured, so that their experimental errors can be neglected for all practical purposes, while $S_{\psi K_S}$ is known with an uncertainty of $\pm 3\%$. ΔM_K , while very accurately measured, is subject to poorly known long distance contributions and we only require that $(\Delta M_K)_{\text{exp}}$ is reproduced within $\pm 30\%$. Finally the rate for the $B \rightarrow X_s\gamma$ decay is known within the accuracy of 10%, comparable to the theoretical one.

8 A numerical (re-)analysis of EWPT constraints

In this section we revisit the constraints from EWPT following the analysis in [35] and adding a few new constraints as outlined in section 6.

⁹See [123, 150] for more details and references therein.

$G_\mu = 1.16637(1) \cdot 10^{-5} \text{ GeV}^{-2}$	$\eta_1 = 1.87(76)$ [143]
$M_W = 80.399(23) \text{ GeV}$	$\eta_3 = 0.496(47)$ [142, 151]
$\alpha(M_Z) = 1/127.9$	$\eta_2 = 0.5765(65)$ [152]
$\alpha_s(M_Z) = 0.1184(7)$	$\eta_B = 0.55(1)$ [152, 153]
$\sin^2 \hat{\theta}_W = 0.23116(13)$	$F_K = 156.0(11) \text{ MeV}$
$m_K^0 = 497.614(24) \text{ MeV}$	$\hat{B}_K = 0.737(20)$
$\Delta M_K = 0.5292(9) \cdot 10^{-2} \text{ ps}^{-1}$	$F_{B_d} = 205(12) \text{ MeV}$
$ \varepsilon_K = 2.228(11) \cdot 10^{-3}$	$F_{B_s} = 250(12) \text{ MeV}$
$m_{B_d} = 5279.5(3) \text{ MeV}$	$\hat{B}_{B_d} = 1.26(11)$
$m_{B_s} = 5366.3(6) \text{ MeV}$ [112]	$\hat{B}_{B_s} = 1.33(6)$
$\Delta M_d = 0.507(4) \text{ ps}^{-1}$	$F_{B_d} \sqrt{\hat{B}_{B_d}} = 233(14) \text{ MeV}$
$\Delta M_s = 17.77(12) \text{ ps}^{-1}$	$F_{B_s} \sqrt{\hat{B}_{B_s}} = 288(15) \text{ MeV}$
$\tau_{B_s} = 1.471(25) \text{ ps}$	$\hat{B}_{B_s} / \hat{B}_{B_d} = 1.05(7)$
$\tau_{B_d} = 1.519(7) \text{ ps}$	$\xi = 1.237(32)$ [114]
$\sin(2\beta)_{b \rightarrow c\bar{c}s} = 0.679(20)$ [95]	
$m_c(m_c) = 1.268(9) \text{ GeV}$ [114, 154]	
$m_t(m_t) = 163(1) \text{ GeV}$	
$m_b(2.5 \text{ GeV}) = 4.60(3) \text{ GeV}$	

Table 5. Values of the experimental and theoretical quantities used as input parameters.

	2GeV	4.6GeV	172GeV	2.5TeV	15TeV
$m_u(\mu)(\text{MeV})$	2.09(0)(9)	1.74(6)(7)	1.15(8)(5)	0.97(8)(4)	0.88(8)(4)
$m_d(\mu)(\text{MeV})$	4.73(0)(11)	3.94(1)(9)	2.61(2)(6)	2.19(2)(5)	2.00(2)(5)
$m_s(\mu)(\text{MeV})$	93.6(2)(11)	77.9(3)(9)	51.6(4)(6)	43.4(4)(5)	39.5(4)(5)
$m_c(\mu)(\text{MeV})$	1089(7)(0)	907(6)(0)	601(5)(0)	505(4)(0)	460(4)(0)
$m_b(\mu)(\text{GeV})$	–	4.074(19)(0)	2.702(14)(0)	2.268(12)(0)	2.068(12)(0)
$m_t(\mu)(\text{GeV})$	–	–	162.3(10)(0)	136.3(9)(0)	124.2(8)(0)

Table 6. The NLO running quark masses at different scales. The first and the second parenthesis shows the statistical and systematic error, respectively.

8.1 Numerical procedure for the EWP tests

As discussed in section 6 we can reduce the free parameters in the electroweak sector down to three. We randomly scan over the full ranges of $0 < s < 1/\sqrt{2}$, $0.1 \lesssim s_R < 1$ and $0 < \epsilon < 0.1$. For every parameter point we evaluate the χ^2 function corresponding to the constraints discussed in section 6.

8.2 Electroweak precision constraints

First of all we want to show the correlations between the three electroweak parameters we have chosen in section 6, that is ϵ , s_R and s and in this manner establish the allowed ranges for these parameters to be used in the analysis of FCNC processes. In figure 8 we show the correlation of s and ϵ while encoding $\ln(\chi^2/n_{\text{d.o.f.}})$ as a colour spectrum. As

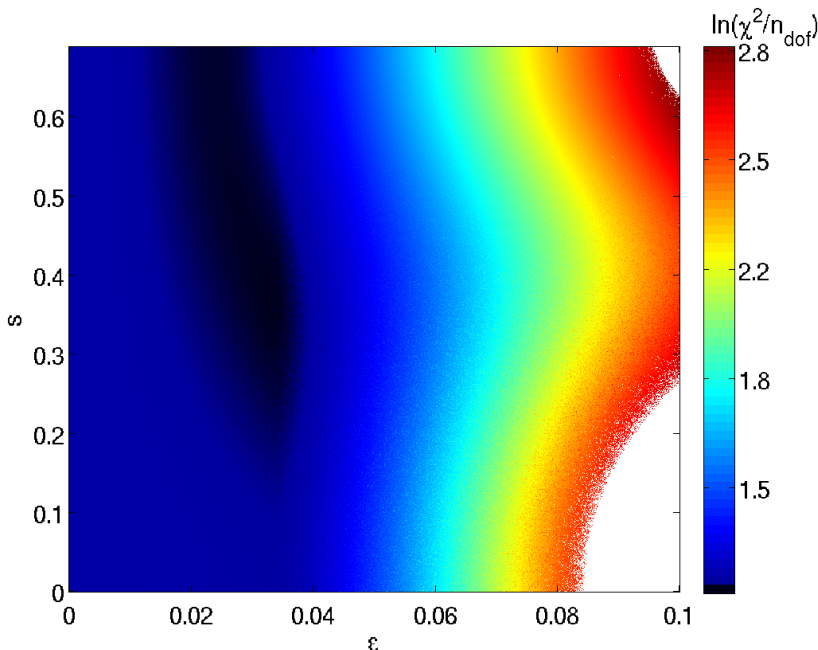


Figure 8. In this figure we show s as a function of ϵ . The colour spectrum corresponds to $\ln(\chi^2/n_{\text{d.o.f.}})$.

one can see smaller values of ϵ are clearly favoured by the data as indicated by the colour gradient. Additionally one can see an area of a slightly darker blue at $\epsilon \sim 0.03$ and non-trivial s . This area allows to soften the disagreement with A_{FB}^b as measured at LEP. This measurement has to be taken with a grain of salt because the competing SLD experiments did not measure a departure from the SM. We also note that values of ϵ above 0.08 are disfavoured.

In figure 9 we show s_R as a function of ϵ . A preference for smaller values of ϵ can again be observed. For values of $\epsilon \sim 0.03$ the value of s_R has to be non trivial and even above 0.6 in order to keep χ^2 low. As in figure 8 there is a slightly darker region for $\epsilon = 0.01 \dots 0.03$ and $s_R = 0.7 \dots 1$ where the A_{FB}^b constraint would be fulfilled within 2σ .

Figure 10 shows M_{W_R} as a function of ϵ . As expected the mass of the heavy gauge boson W_R increases with a decreasing ϵ . The wide spread is due to other parametric dependencies. Interestingly in this picture the dark blue region implies an upper limit on M_{W_R} . We conclude that in case A_{FB}^b as measured at LEP was true we would be able to put this model under pressure if M_{W_R} is not found below roughly 7 TeV.

For our analysis of $\Delta F = 2$ observables we fix two of the electroweak parameters to a point with intermediate values

$$s_R = 0.80, \quad \epsilon = 0.03. \quad (8.1)$$

The parameter s , which turns out to be very relevant for flavour observables, is varied in the range

$$0.1 < s < 0.6. \quad (8.2)$$

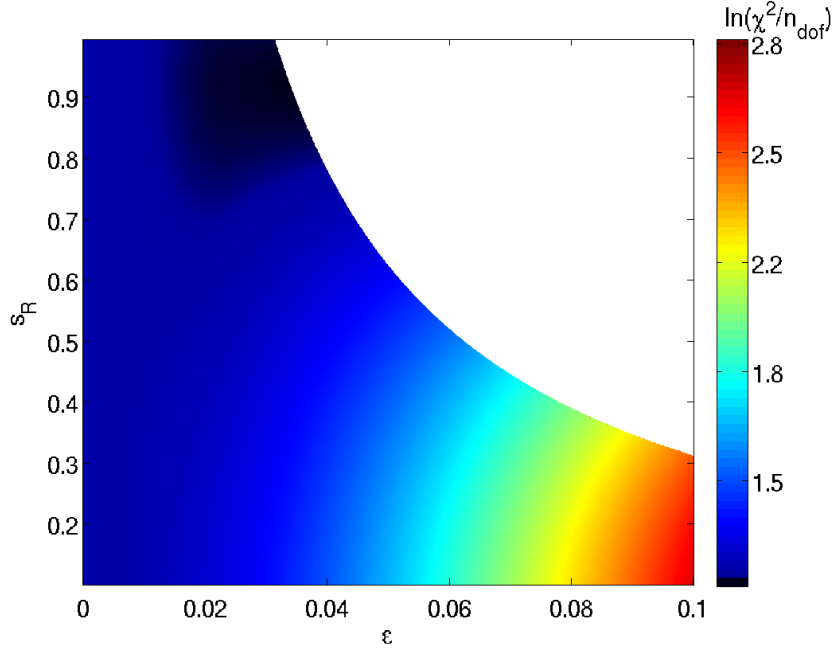


Figure 9. In this figure we show s_R as a function of ϵ . The colour spectrum corresponds to $\ln(\chi^2/n_{\text{d.o.f.}})$.

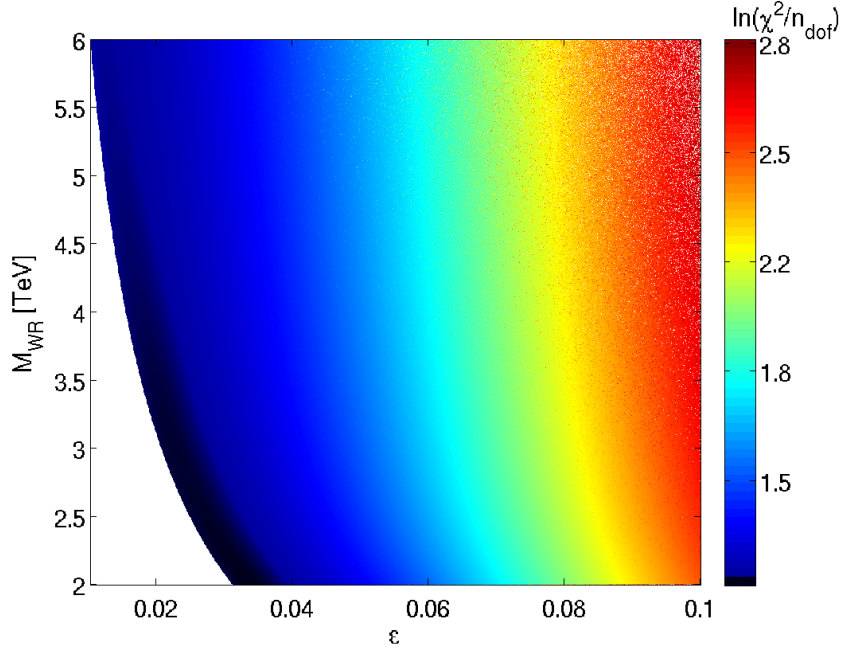


Figure 10. In this figure we show M_{W_R} as a function of ϵ . The colour spectrum corresponds to $\ln(\chi^2/n_{\text{d.o.f.}})$.

This range of parameter points is contained in the dark blue area in figures 8-10. In this way we are able to incorporate the EWP constraints into our flavour analysis in a quite

general manner. Changing the electroweak reference point (8.1) would affect mostly the masses M_{W_R} and M_H . The Higgs mass M_H additionally displays a strong dependence on the parameter s . We already studied the effect of changing the masses on $\Delta F = 2$ observables and $\text{Br}(B \rightarrow X_s \gamma)$ in sections 3.6 and 4.6, respectively. In terms of more tangible parameters our choice corresponds to the masses

$$M_{W_R} \approx 2.6 \text{ TeV}, \quad M_H \approx \frac{16}{\sqrt{1-2s^2}} \text{ TeV}, \quad (8.3)$$

where we choose $\alpha_3 = 8$ in the Higgs potential. We emphasise that increasing the value M_H by much can only be done at the price of loosing perturbativity in the scalar sector.

The parameters relevant for our flavour analysis then read

$$1.3 < \kappa/\kappa' < 9.9, \quad r = \frac{g_R^2}{g_L^2} \approx 0.48, \quad 8.9 \cdot 10^{-5} < s c c^2 < 4.3 \cdot 10^{-4}. \quad (8.4)$$

Note that using the constraints outlined in section 6 we are not able to fulfil A_{FB}^b at below 1.8σ . This can in part be accounted for by the approximate nature of the constraints used but in our opinion this should not be the dominant effect. This suggests that the LRM cannot explain the LEP A_{FB}^b anomaly, but only soften it.

9 A general study of V^{R}

In this section we study the structure of the RH matrix V^{R} . In order to perform our general analysis of V^{R} and of flavour observables we varied all 13 parameters in the V^{L} and V^{R} matrices in their allowed ranges. For the parameters of V^{R} this means $0 \dots \pi/2$ for the mixing angles and $0 \dots 2\pi$ for the phases. In the case of V^{L} parameters the situation is simpler as due to the smallness of ε_K and the tree-level constraints one is able to restrict the allowed ranges beforehand. We impose all available constraints from $\Delta F = 2$, $\text{Br}(B \rightarrow X_q \gamma)$ as well as the tree-level measurements of CKM parameters within 2σ . Our choice of electroweak parameters is described in section 8.2.

9.1 Allowed ranges for V^{R}

First we study the matrix V^{R} in full generality, aiming to identify the valid regions of parameter space. To this end we allow the parameter s to vary in the range $0.1 \dots 0.6$. Due to the unitarity of the matrix V^{R} it is sufficient to consider the allowed ranges for the absolute values of V_{us}^{R} , V_{ub}^{R} and V_{cb}^{R} in order to obtain a complete picture of the possible size of all elements. Therefore in figure 11 we show the correlations between pairs of these elements of V^{R} . The value of s is encoded in colour, where all plots show points with large s in the front layer. Generally the allowed regions grow with decreasing s . First we observe that large regions of the parameter space are already excluded. In addition all three elements can reach their maximal values ~ 1 individually, however not simultaneously. The two branches of points are easier to disentangle in the 3D version of these plots, as can be seen in figure 12 for $s = 0.1$.

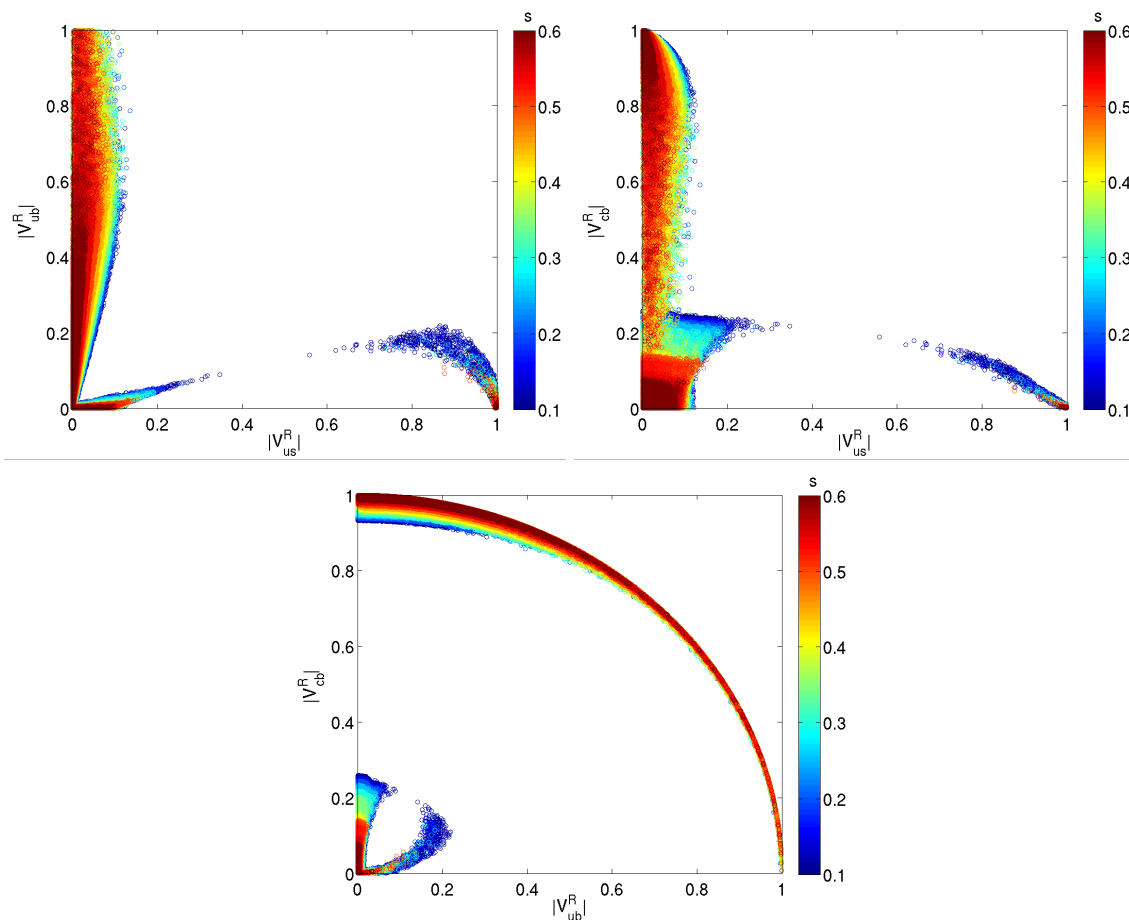


Figure 11. $|V_{us}^R|$, $|V_{ub}^R|$ and $|V_{cb}^R|$ as functions of each other with s encoded in colour

In order to keep the presentation as transparent as possible, in the following we restrict ourselves to showing results only for fixed values of s when necessary. In the course of our analysis of $\Delta F = 2$ constraints we concentrate on the case $s = 0.1$. For the study $\text{Br}(B \rightarrow X_{s,d}\gamma)$ large values of s are interesting since they lead to enhanced effects. In a few cases we consider the s dependence explicitly.

9.2 A fine-tuning study

We now turn to investigating the fine-tuning necessary for a point to fulfil all the experimental constraints.

It is well known that models which predict sizeable contributions to the LR $\Delta F = 2$ operators can lead to dangerously large fine-tuning of several observables. For example the RS model with custodial protection has to struggle with huge effects in ε_K and a potentially large fine-tuning [68, 155].

First let us define the measure of fine-tuning

$$\Delta_{\text{BG}}^{\text{mod}} = \frac{1}{N_{\text{Obs}}} \sum_{i=1}^{N_{\text{Obs}}} \Delta_{\text{BG}}(O_i) = \frac{1}{N_{\text{Obs}}} \sum_{i=1}^{N_{\text{Obs}}} \max_j \left(\left| \frac{p_j}{O_i} \frac{\partial O_i}{\partial p_j} \right| \right), \quad (9.1)$$

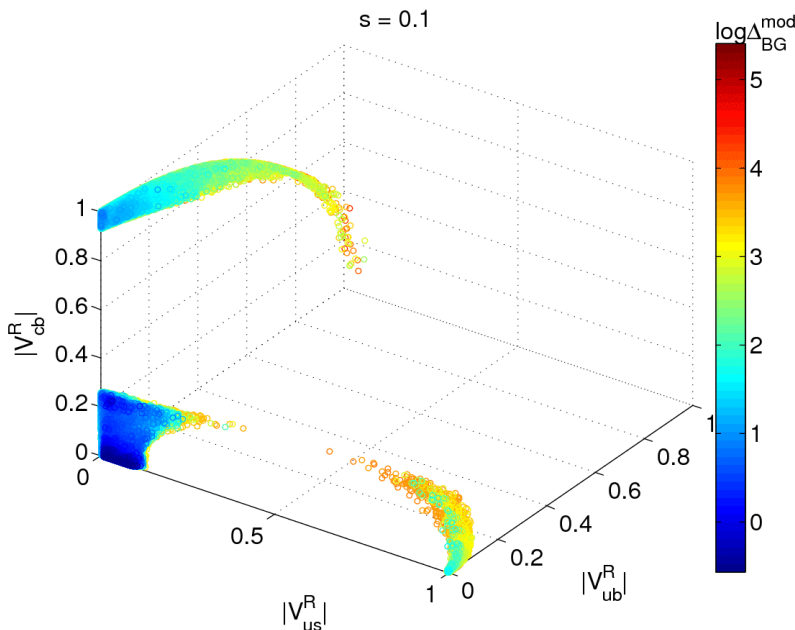


Figure 12. The absolute values of $|V_{us}^R|$, $|V_{ub}^R|$ and $|V_{cb}^R|$ with $\log \Delta_{\text{BG}}^{\text{mod}}$ encoded as the colour.

used throughout our analysis. Here Δ_{BG} is the well known Barbieri-Giudice (BG) measure of fine-tuning [156]. Note that the sum should only contain observables which are in fact fine-tuned in some part of the parameter space. The overall fine-tuning defined in equation (9.1) is compatible with the more sophisticated fine-tuning measure proposed by Athron and Miller [157]. Since the numerical application of the Athron-Miller fine-tuning measure requires much more computing power than the BG measure while not providing additional insights we decided to stick with $\Delta_{\text{BG}}^{\text{mod}}$. We note that by definition Δ_{BG} is sensitive only to fine-tuning in terms of cancellations between various contributions, but not to accidentally small parameters.

In figure 12 we show the absolute values of $|V_{us}^R|$, $|V_{ub}^R|$ and $|V_{cb}^R|$ as a three dimensional plot for $s = 0.1$. The colour corresponds to $\log \Delta_{\text{BG}}^{\text{mod}}$ and we plotted points with low fine-tuning in front of ones with large fine-tuning. This however does not preclude points with high fine-tuning to lie in regions dominated by points with low fine-tuning. First of all we observe that the constraints allow for three clearly distinct scenarios.

- In the first scenario $|V_{us}^R|$, $|V_{ub}^R|$ and $|V_{cb}^R|$ are small. The fine-tuning can be very small and increases slowly with $|V_{ub}^R|$. We call this scenario the “normal hierarchy” scenario.
- We find the second scenario in the case of small $|V_{us}^R|$ and large $|V_{cb}^R|$. This scenario is not restricted to one corner but allows points along the $|V_{ub}^R|$ axis as well. The fine-tuning is in most cases high and increases further with increasing $|V_{ub}^R|$. Taking only points with low fine-tuning this scenario corresponds to the so-called “inverted hierarchy” scenario.

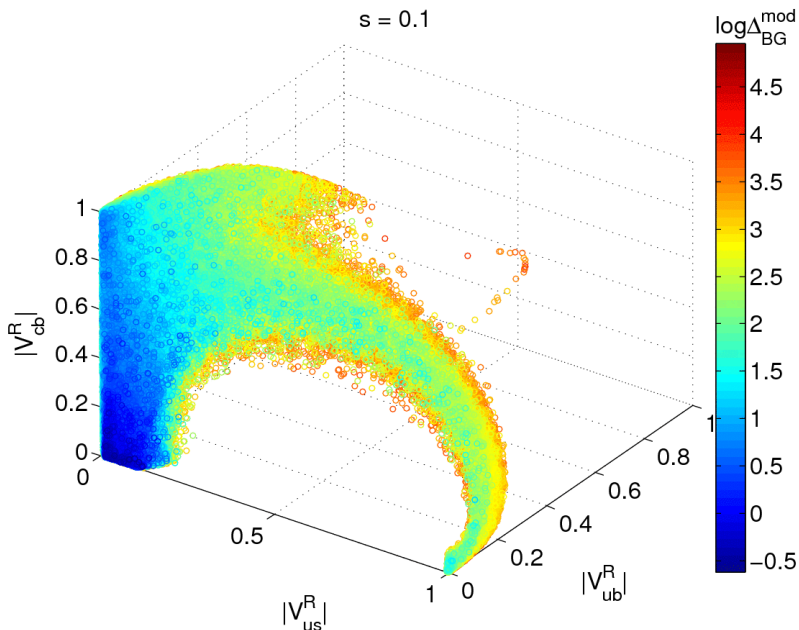


Figure 13. The 3D correlation between allowed values of $|V_{us}^R|$, $|V_{ub}^R|$ and $|V_{cb}^R|$, omitting the contributions of the heavy Higgses.

- For small $|V_{cb}^R|$, large $|V_{us}^R|$ and $|V_{ub}^R| < 0.30$ we find the third scenario. This scenario exhibits large fine-tuning for all points, hence it is completely eliminated if we require $\Delta_{BG}^{\text{mod}} < 10$. We point out that while this scenario is very fine-tuned it is also not rigorously excluded.

Second we find that while significant regions of the parameter space suffer from large fine-tuning, there exist ranges of parameters in which the fine-tuning is small and all experimental constraints, in particular the ones from ε_K and ΔM_K , can be satisfied.

In the following we restrict ourselves to points in parameter space which exhibit only a small level of fine-tuning $\Delta_{BG}^{\text{mod}} < 10$. In this case we find the following limits:

$$|V_{td}^R| < 1.2 \cdot 10^{-2} \quad \text{and} \quad |V_{us}^R| < \begin{cases} 0.18 & (s = 0.1) \\ 0.13 & (s = 0.5) \end{cases} \quad (9.2)$$

Note that the constraint on $|V_{td}^R|$ is much more stringent than the one on $|V_{ub}^R|$. The “normal” and “inverted hierarchy” scenarios introduced above are then defined by

$$\begin{aligned} |V_{cb}^R| < 0.3, & \quad (\text{normal hierarchy}) \\ |V_{cb}^R| > 0.9. & \quad (\text{inverted hierarchy}) \end{aligned} \quad (9.3)$$

The first scenario leads to a hierarchical structure of V^R with small off-diagonal elements, while the second one inverts the hierarchy of the 2, 3 submatrix giving V^R a very different structure.

Let us now consider how these results change if the heavy Higgs contributions are omitted. In figure 13 we show the allowed parameter points obtained from a scan analogous

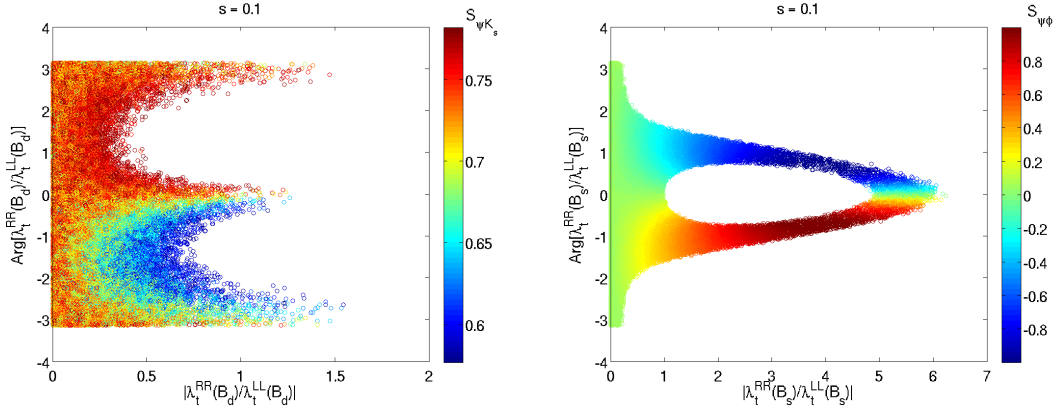


Figure 14. $\arg(\mathcal{F}_t(B_q))$ as a function of $|\mathcal{F}_t(B_q)|$ with B_d on the left-hand side and B_s on the right-hand side. The colour coding corresponds to $S_{\psi K_S}$ and $S_{\psi\phi}$ respectively.

to the one that lead to figure 12, taking into account only the gauge boson contributions. We observe that now the points cover a significantly larger region of parameter space, even if only points with low fine-tuning are considered. This drastic change reflects once more the importance of the heavy Higgs particles.

9.3 A closer look at the “normal hierarchy” scenario

Now we study in more detail the “normal hierarchy” scenario. Recall that we consider only parameter points with small fine-tuning $\Delta_{\text{BG}}^{\text{mod}} < 10$. In order to investigate the possible contributions of the matrix V^{R} to flavour processes it is useful to study the relative size of the dominant LR contribution compared to the SM contribution. From the hierarchical structure of V^{R} in this scenario together with the pattern of the matrix \hat{R} , see appendix D, we expect the tt contribution to dominate. Therefore it is convenient to define ($q = K, B_d, B_s$)

$$\mathcal{F}_t(q) = \frac{\lambda_t^{\text{LR}}(q)\lambda_t^{\text{RL}}(q)}{\lambda_t^{\text{LL}}(q)\lambda_t^{\text{LL}}(q)} = \frac{\lambda_t^{\text{RR}}(q)}{\lambda_t^{\text{LL}}(q)}. \quad (9.4)$$

In order to better understand the results obtained in this scenario it is useful to introduce a Wolfenstein-like parametrisation of the right-handed matrix by expanding in $\tilde{\lambda} = |V_{us}^{\text{R}}|$. Defining $\tilde{s}_{12} \equiv \tilde{\lambda}$, $\tilde{s}_{13} = \tilde{B}\tilde{\lambda}^2$ and $\tilde{s}_{23} = \tilde{A}\tilde{\lambda}$ and then expanding in $\tilde{\lambda}$ we arrive at

$$\begin{pmatrix} e^{i\phi_{ud}} \left(1 - \frac{\tilde{\lambda}^2}{2}\right) & e^{i\phi_{us}} \tilde{\lambda} & \tilde{B}e^{i\phi_{ub}} \tilde{\lambda}^2 \\ -e^{i(\phi_{cb} - \phi_{tb} + \phi_{ts} + \phi_{ud} - \phi_{us})} \tilde{\lambda} & e^{i(\phi_{cb} - \phi_{tb} + \phi_{ts})} \left(1 - \frac{1}{2}(\tilde{A}^2 + 1)\tilde{\lambda}^2\right) & \tilde{A}e^{i\phi_{cb}} \tilde{\lambda} \\ e^{i\phi_{ud}} \left(\tilde{A}e^{i(\phi_{ts} - \phi_{us})} - \tilde{B}e^{i(\phi_{tb} - \phi_{ub})}\right) \tilde{\lambda}^2 & -\tilde{A}e^{i\phi_{ts}} \tilde{\lambda} & e^{i\phi_{tb}} \left(1 - \frac{\tilde{A}^2}{2}\tilde{\lambda}^2\right) \end{pmatrix}. \quad (9.5)$$

Note that this matrix cannot be reduced to the matrix in V^{R} in (7.5) and is valid in a different oasis in the parameter space. In figure 14 we show the correlation of $\arg(\mathcal{F}_t(B_q))$ and $|\mathcal{F}_t(B_q)|$. On the left hand side of figure 14 we show the situation in the B_d system. In order to gain more information from this correlation we encode $S_{\psi K_S}$ as the colour of a point. First we notice that the absolute value $|\mathcal{F}_t(B_d)|$ only allows enhancements up to 1.5. The phase $\arg(\mathcal{F}_t(B_d))$ on the other hand is allowed to be in the whole $[-\pi, \pi]$

range. However there are restrictions on the phase as well. For the maximal allowed enhancement of the absolute value the phase is restricted to be close to 0 or $\pm\pi$ and for a phase of $\pm\pi/2$ the absolute value is restricted to be below roughly 0.8 and 0.5 for a phase of π ($-\pi$) respectively. The observed shape reminds us of the model-independent constraint on $(M_{12}^d)_{\text{NP}}$. Since the measured values of ΔM_d and $S_{\psi K_S}$ are in good agreement with the SM prediction (although somewhat on the low side), there is not much room left for NP. Furthermore as ΔM_d suffers from larger theoretical uncertainties than $S_{\psi K_S}$ the possible size of the NP contribution is largest if its relative phase is close to 0 or $\pm\pi$. If the tt contribution was the only contribution to $(M_{12}^d)_{\text{NP}}$, its phase would be equal to $\arg(\mathcal{F}_t(B_d))$ and we would observe strong peaks for these phases in the plot. The small “washout” indicates however that other LR contributions cannot be neglected in this case.

On the right hand side of figure 14 we show the situation in the B_s system. In this plot the colour corresponds to $S_{\psi\phi}$. We immediately see that the situation is completely different from the B_d system. The enhancement in the absolute value $|\mathcal{F}_t(B_s)|$ is allowed to be up to nearly 7 while the phase $\arg(\mathcal{F}_t(B_s))$, though allowed to be somewhere in the whole range, is very strongly correlated with the absolute value and $S_{\psi\phi}$. For $|S_{\psi\phi}|$ close to zero the absolute value is restricted to be smaller than 1.5 or bigger than 4.7 while the phase is either roughly free or very close to zero respectively. For big $|S_{\psi\phi}|$ the phase is restricted to two very specific areas (the blue and red arches in the plot). This might lead to interesting correlations in rare decays of B_s mesons. In fact the shape found in the right panel of figure 14 is familiar from the ΔM_s constraint projected onto the plane $(|(M_{12}^s)_{\text{NP}}|, \arg(M_{12}^s)_{\text{NP}})$, see e.g. figure 1 of [97]. This leads us to conclude that the NP amplitude in the present case is totally dominated by the tt contribution, and therefore governed by $\mathcal{F}_t(B_s)$. Indeed from the structure of V^{R} in (9.5) it is easy to derive that the strong hierarchy in the matrix $\hat{R}(B_q)$, see appendix D, cannot be overcompensated by hierarchies in the right-handed quark mixing.

10 A brief discussion of flavour observables

This section is dedicated to the detailed discussion of flavour violating effects in the LRM. After analysing the possible size of NP effects in the various meson systems, we study the possible enhancements of the B_s mixing phase and effects in $\text{Br}(B \rightarrow X_q \gamma)$. Finally we turn our attention to the $|V_{ub}|$ problem, which was recently discussed in the context of RH currents [41–44].

10.1 A summary of possible size of NP effects in the different meson systems

As discussed in section 9.3 the relative size of LR contributions in the various meson systems is given by the quantity $\mathcal{F}_t(q)$. In figure 15 we show the possible sizes of $|\mathcal{F}_t(q)|$ for the three meson systems as functions of each other for $s = 0.1$. We observe that in principle huge effects in the K system are possible, while the effects in the B_s system are much more moderate and the effects in the B_d system are rather small. This indicates a rough hierarchy of NP effects $B_d < B_s \ll K$ also expected for rare K and $B_{d,s}$ decays. Note that

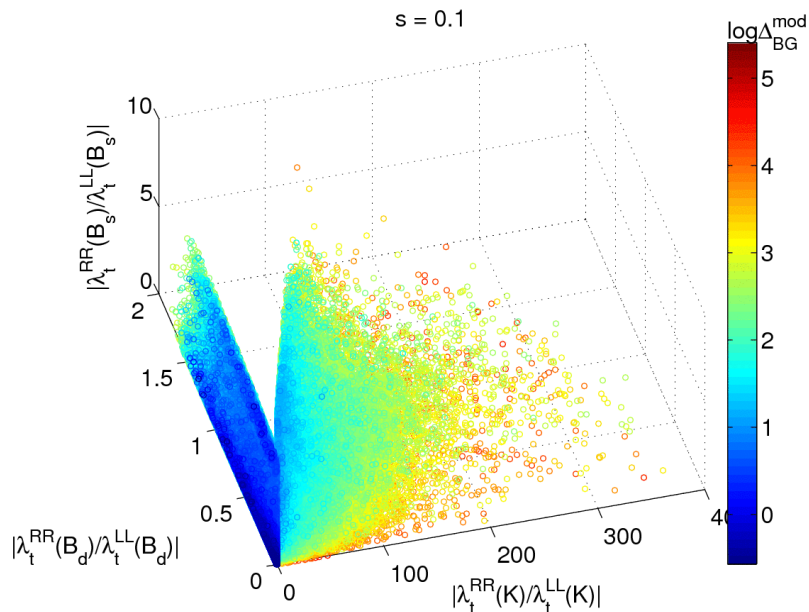


Figure 15. The absolute values of $\mathcal{F}_t(q)$ for $q = K, B_d, B_s$ as functions of each other. The colour-code corresponds to the fine-tuning Δ_{BG}^{mod} .

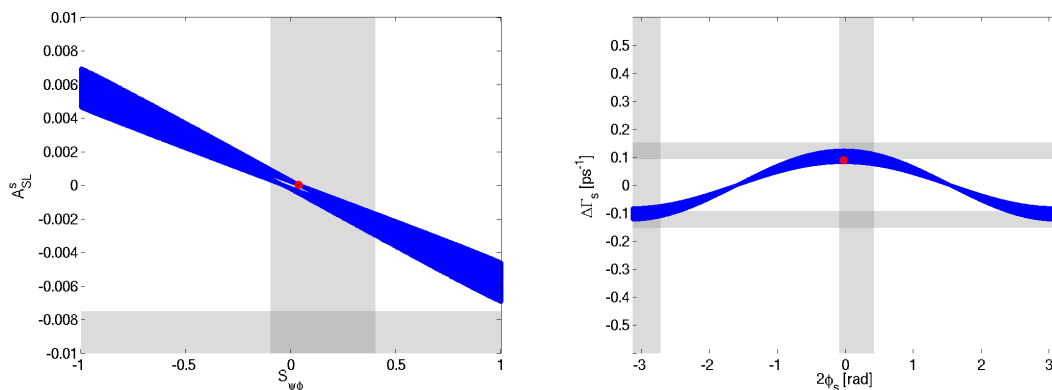


Figure 16. The model independent correlation of A_{SL}^s and $S_{\psi\phi}$ (left panel) and the correlation of $\Delta\Gamma_s$ with $2\phi_s$ (right panel)

huge effects in the K system are possible only for large fine-tuning, since in that case the large tt contribution to $K^0 - \bar{K}^0$ mixing has to be cancelled by other contributions.

10.2 The phase of B_s mixing and $\text{Br}(B \rightarrow X_q\gamma)$

Now we want to briefly discuss the results of our analysis of observables related to the phase of B_s mixing and $\text{Br}(B \rightarrow X_q\gamma)$. In the general case with and without fine-tuned points we observe no correlation between observables, except for model-independent ones such as $A_{SL}^s - S_{\psi\phi}$ and $\Delta\Gamma_s$ versus ϕ_s shown in figure 16.

In figure 17 we show the correlation between $\text{Br}(B \rightarrow X_s\gamma)$ and $\text{Br}(B \rightarrow X_d\gamma)$, en-

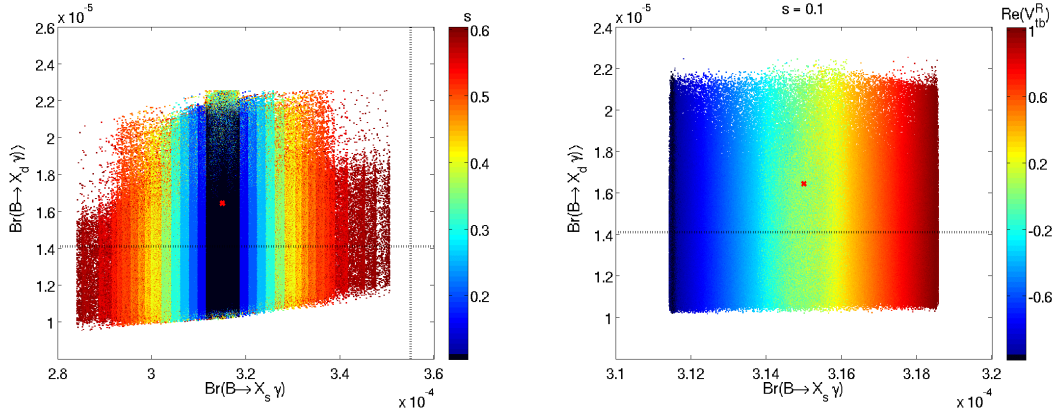


Figure 17. The correlation of $\text{Br}(B \rightarrow X_s \gamma)$ and $\langle \text{Br}(B \rightarrow X_d \gamma) \rangle$ showing the s dependence (left panel) and $\text{Re}(V_{tb}^R)$ dependence (right panel) in colour. The red cross indicates the SM values, while the experimental central values are given by the dashed lines.

coding the s dependence (left panel) and $\text{Re}(V_{tb}^R)$ dependence (right panel, for $s = 0.1$) in colour. For $s > 0.5$ the values of $\text{Br}(B \rightarrow X_s \gamma)$ cover a larger range that originates in the divergence of the function $u(s)$ in the unphysical limit $s \rightarrow 1/\sqrt{2}$, see section 4.3. For small s the branching ratios depend only linearly on this parameter and the effects are much smaller. As can be seen from the explicit formulae given in section 4.6 $\text{Br}(B \rightarrow X_s \gamma)$ depends linearly on the real part of V_{tb}^R .

Combining the information of both plots in figure 17 we conclude that in order to enhance $\text{Br}(B \rightarrow X_s \gamma)$, we would need both $s > 0.5$ and a dominantly real and positive V_{tb}^R . As the SM prediction lies somewhat below the experimental value, albeit still in good agreement, a positive NP contribution to $\text{Br}(B \rightarrow X_s \gamma)$ is welcome.

Concerning the CP asymmetries in $b \rightarrow q \gamma$ we find moderate changes relative to the SM prediction

$$A_{\text{CP}}(b \rightarrow d \gamma)^{\text{SM}} = -9.2\%, \quad (10.1)$$

$$A_{\text{CP}}(b \rightarrow s \gamma)^{\text{SM}} = 0.4\%. \quad (10.2)$$

Similar to the branching ratios also the CP asymmetries are s dependent. For $s = 0.1$ we find

$$-13.8\% < A_{\text{CP}}(b \rightarrow d \gamma) < -7.9\%, \quad (10.3)$$

$$0.3\% < A_{\text{CP}}(b \rightarrow s \gamma) < 0.6\%, \quad (10.4)$$

while for $s = 0.6$ the possible range is slightly larger

$$-14.2\% < A_{\text{CP}}(b \rightarrow d \gamma) < -8.3\%, \quad (10.5)$$

$$-0.18\% < A_{\text{CP}}(b \rightarrow s \gamma) < 1.1\%. \quad (10.6)$$

These effects will be difficult to disentangle from the SM contribution due to the large non-perturbative uncertainties present in these observables.

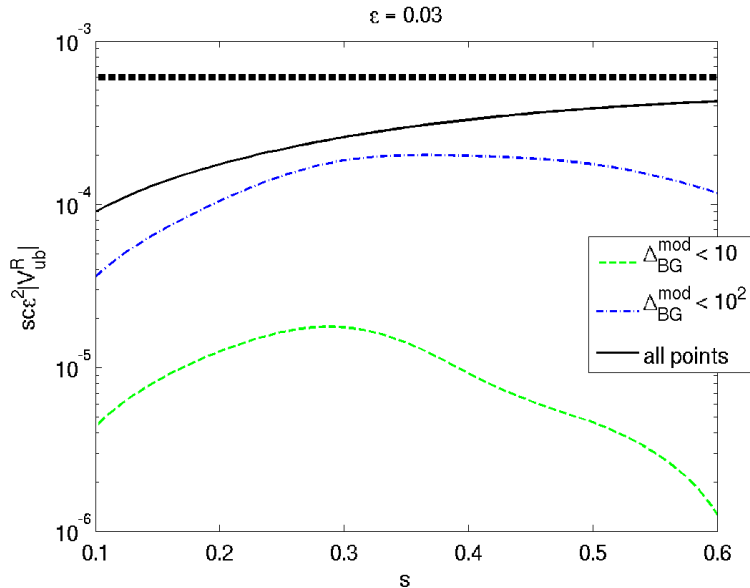


Figure 18. Maximal value for $s c e^2 |V_{ub}^R|$ as a function of s , for different allowed fine-tunings. A complete solution to the $|V_{ub}|$ problem requires values for $s c e^2 |V_{ub}^R|$ above the dashed black line.

Note that in figure 17 and in (10.3)–(10.6) we always used the maximal allowed Higgs mass (see section 11). For lower Higgs mass the constraints on the parameter space become much stronger, predicting a much more hierarchical structure for V^R . These constraints however do not suppress $\text{Br}(B \rightarrow X_{s,d}\gamma)$ since the latter decays depend only on the diagonal element V_{bb}^R . Therefore decreasing the heavy Higgs mass M_H enhances the effects in $\text{Br}(B \rightarrow X_{s,d}\gamma)$.

10.3 The $|V_{ub}|$ problem in the LRM

As already discussed in section 5 in the LRM the true value of $|V_{ub}^L|$ is given by the inclusive value of $|V_{ub}|$ in (5.10), which remains unaffected by the presence of RH currents. On the other hand the corrections from RH currents to the vector and axial-vector couplings could in principle allow to explain the different values of $|V_{ub}|$ found in exclusive decays and $B^+ \rightarrow \tau^+ \nu_\tau$ as given in (5.11) and (5.12), respectively [41–44]. A solution to the $|V_{ub}|$ problem can be provided if $s c e^2 |V_{ub}^R|$ is in the ballpark of 0.6×10^{-3} . Since we can only restrict $s c e^2 \leq 10^{-3}$, while $|V_{ub}^R|$ is not constrained if arbitrary fine-tuning is allowed, studying the s dependence of the constraints is mandatory.

Figure 18 illustrates the situation in the LRM. In general the black dashed line, necessary for a complete solution of the $|V_{ub}|$ problem, cannot be reached in the LRM. The tension increases significantly if we consider only points with small fine-tuning. While we cannot exclude that there are some models with RH currents that could solve this problem, from the point of view of the LRM considered here, this is not the case and any value of $|V_{ub}|$ among (5.10)–(5.11) could be the true value.

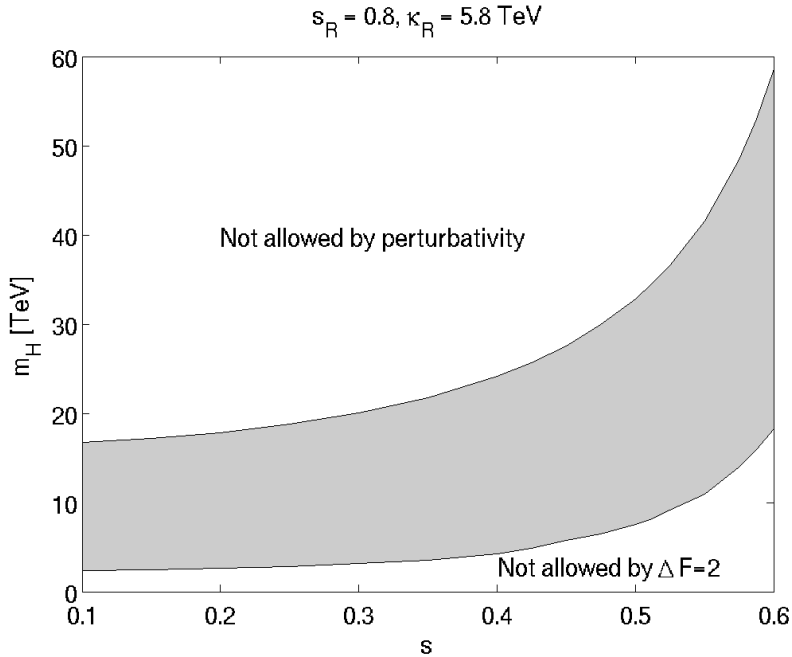


Figure 19. The allowed range for the Higgs mass M_H as a function of s for $\kappa_R \approx 5.8$ TeV and $s_R = 0.8$.

11 The role of the heavy Higgs mass

Up to now in our analysis we have set $M_H = 16/\sqrt{1 - 2s^2}$ TeV, this ensures staying in the perturbative regime of the coupling α_3 in the Higgs potential while suppressing the Higgs contributions in $\Delta F = 2$. In this section we want to investigate the lower bound on the Higgs mass from our constraints. Therefore we now allow α_3 to vary between 0.1 and 8, or equivalently the heavy Higgs mass between $2/\sqrt{1 - 2s^2}$ TeV and $16/\sqrt{1 - 2s^2}$ TeV. The result can be seen in figure 19, in particular we find the ‘soft’ lower limit on M_H to be

$$2.4 \text{ TeV} \lesssim M_H. \quad (11.1)$$

This limit is ‘soft’ in the sense that lower values are not rigorously forbidden, but our parameter scan did not reveal any points which allow for lower masses. One might suspect a very large fine-tuning for this low Higgs mass, but while the fine-tuning does increase with decreasing Higgs mass there are still points with fine-tuning $\Delta_{\text{BG}}^{\text{mod}} < 10$ even for the lowest possible mass. This is of course also a test of the idea of fine-tuning. Finally for low Higgs masses the matrix V^{R} shows a very hierarchical structure as can be expected. The mixing pattern is roughly given by

$$\tilde{s}_{12} \sim \mathcal{O}(10^{-2}), \quad \tilde{s}_{13} \sim \mathcal{O}(10^{-4}), \quad \tilde{s}_{23} \sim \mathcal{O}(10^{-3}). \quad (11.2)$$

12 Comparison to other models

12.1 Preliminaries

Now we compare the results found in the LRM to those obtained in other NP models. The first part of this section is dedicated to the comparison with two specific versions of LR models discussed in the literature. Subsequently we compare the pattern of flavour violation in the general LRM with patterns found by us in a number of extensions of the SM. A review of those analyses can be found in [6]. Our discussion below deals only with $\Delta F = 2$ transitions and $B \rightarrow X_{s,d}\gamma$ decays.

In order to increase the transparency of the comparison in question let us summarize the most characteristic features of NP contributions in the LRM:

- The dominance of the operator Q_2^{LR} in all $\Delta F = 2$ transitions: $K^0 - \bar{K}^0$, $B_d^0 - \bar{B}_d^0$ and $B_s^0 - \bar{B}_s^0$, with the biggest impact on the $K^0 - \bar{K}^0$ system.
- While both box diagrams with $W_L - W_R$ exchanges and tree level neutral Higgs contributions are the sources of the effects in $\Delta F = 2$ observables, the latter contributions are most important. Governed by the same operators and having the same quark mixing factors the trees always dominate over the boxes.
- The contributions of induced RH couplings of W_L and of H^\pm to the $B \rightarrow X_{s,d}\gamma$ decays are enhanced by the ratio m_t/m_b due to the chirality flip on the top quark propagator. Moreover H^\pm contributions receive an additional enhancement for large s .
- All effects listed above are beyond the usual MFV framework.

With this picture in mind we are in the position to make a transparent comparison with other versions of LR models and with a number of extensions of the SM.

12.2 LR models with additional flavour symmetries

Recently two different approaches have been presented to reconcile the LR models with flavour data even for relatively small symmetry breaking scales. In both cases this is achieved by introducing an additional symmetry that removes all flavour changing Higgs effects from the down quark sector.

In a first paper Guadagnoli and Mohapatra [158] suggested to extend the Higgs sector by a discrete \mathbb{Z}_4 symmetry. Eventually this leads to removing all flavour violating Higgs couplings from the down quark sector and the strongest constraints on the heavy Higgs mass then comes from $D^0 - \bar{D}^0$ mixing. $\Delta S = 2$ and $\Delta B = 2$ processes are then governed by $W_L - W_R$ box diagrams. While in [158] the manifest version of the LRSM has been considered, it is straightforward to extend this model to the general LRM leading to a potentially interesting phenomenology.

A different approach to avoid the stringent flavour constraints has been proposed in [62]. Here a gauged LR symmetric flavour group $SU(3)_{Q_L} \times SU(3)_{Q_R}$ has been introduced following the idea of Grinstein et al. [82]. In this scenario due to a different structure of the

Higgs sector only the SM Higgs boson is present and no dangerous tree level FCNH effects arise. The potentially dangerous tree level contributions from flavour gauge bosons are naturally suppressed by a see-saw-like mechanism, so that the most relevant new contributions to $\Delta F = 2$ processes arise again from $W_L - W_R$ box diagrams.

The effects in the $B \rightarrow X_{s,d}\gamma$ decays turn out to be small in this scenario. This is related to both the absence of a heavy charged Higgs and the fact that in this model W_L and W_R do not mix with each other. Consequently no chiral enhancement $\propto m_t/m_b$ is possible in this case as in the scenario considered by us. On the other hand as pointed out in [102] in such models new flavour violating neutral gauge bosons could provide an enhancement of $B \rightarrow X_{s,d}\gamma$ through a chiral enhancement $\propto m_F/m_b$, where F denotes a new vectorial neutral heavy fermion. Yet, as shown in [102] in models in which fermion masses are generated by a see-saw mechanism such contributions are strongly suppressed by the mixing between SM quarks and heavy fermions so that finally the NP contributions remain small.

12.3 2HDM with flavour blind phases: 2HDM_{MFV}

Concerning the $\Delta F = 2$ transitions the most spectacular difference in 2HDM_{MFV} [75, 76] from the LRM considered here is the absence of relevant direct contributions to ε_K . The reason is that in 2HDM_{MFV} the flavour violating neutral Higgs couplings are effectively generated at one-loop level and are necessarily proportional to the masses of external quarks ($m_{d,s}$ in this case) and not to up-quark masses as in the case of the LRM, where flavour violating Higgs couplings are present in the fundamental Lagrangian.

Therefore in 2HDM_{MFV} ε_K can only be found close to the data if $\sin 2\beta \approx 0.80$ which corresponds to scenario 2 in section 7. The interplay of flavour blind phases with the CKM phase allows then to bring $S_{\psi K_S}$ to its experimental value, while enhancing automatically $S_{\psi\phi}$ to values close to 0.3. Having less parameters than the LRM, this prediction is rather unique. Finding experimentally $S_{\psi\phi}$ to be negative would rule out 2HDM_{MFV}. For LRM this would still not be a problem as one would move then to a different oasis in the parameter space of this model than considered by us in 7.3.2.

It should also be emphasized that the neutral Higgs masses in the 2HDM_{MFV} are of the order of a few hundred GeV, whereas in the LRM they are by at least one order of magnitude larger. Therefore LHC should easily distinguish between these two scenarios.

12.4 Right-handed MFV

Recently, in [44], we have studied the effects of RH currents by means of an effective theory approach under incorporation of an extended MFV principle.

The similar symmetry pattern with respect to the LRM could lead to the premature assumption that both models can be matched by integrating out the heavy particles in the LRM. However as we have already mentioned in section 3.8, the operator structure of both models turns out to be complementary. Furthermore, due to the extended MFV mechanism the specific flavour structure precludes this possibility.

The differences display also in the phenomenology of both models. Even though the general parametrization for the RH mixing matrix is given by the same parameters, after

imposing all constraints the matrices display a different pattern. This can be seen explicitly when comparing figure 12 to the structure of the matrix given in equation (105) of [44]. The fact that the $|V_{ub}|$ problem cannot be solved in the LRM whereas this was the case in RHMFV demonstrates once more the difference in the RH mixing matrices.

Let us have a closer look at further flavour observables. While the RHMFV was originally designed to explain a large $S_{\psi\phi}$, a full theory like the LRM allows a more flexible analysis. Here no particular assumptions about $S_{\psi\phi}$ have been made and values within the full range are allowed. Since in the LRM we take into account the variation of all phases, the high number of parameters allows to find regions in parameters space where all SM tensions can be resolved. This was not the case in RHMFV where the $S_{\psi K_S} - \sin(2\beta)$ tension persists under the assumption that $S_{\psi\phi}$ is significantly enhanced over its SM value.

On the other hand the general pattern of NP effects within the different meson sectors show similarities for both models. For example in both cases we find the rough hierarchy $B_d < B_s \ll K$ for effects in the corresponding observables. The observable ε_K acts in both cases as strongest constraint. Finally both frameworks cannot explain the anomalous $Zb\bar{b}$ coupling.

12.5 Randall-Sundrum with custodial protection

In the RS model with custodial protection (RSc), $\Delta F = 2$ operators are generated already at the tree level by the exchange of heavy Kaluza-Klein gluon and electroweak gauge boson modes (see [68] for an extensive phenomenological analysis). Tree level flavour changing couplings of the SM Higgs generate $\Delta F = 2$ transitions as well, but they turn out to be subleading with respect to the aforementioned KK gauge boson contributions [159, 160]. In contrast to the LRM studied here, only $K - \bar{K}$ mixing is dominated by the chirally enhanced Q_2^{LR} operator generated by KK gluon exchange. Since the chiral enhancement is absent in the case of $B_{d,s} - \bar{B}_{d,s}$ mixing the latter processes are dominated by the operator Q_1^{VLL} and electroweak KK modes are relevant. Consequently while the constraint from ε_K generically puts strong bounds on the model in question [155], the contributions to $M_{12}^{d,s}$ are suppressed by the RS-GIM mechanism [161]. Still non-zero effects are generally expected, so that a solution of the $\varepsilon_K - S_{\psi K_S}$ tension is possible within this framework. Also $S_{\psi\phi}$ can receive large enhancements.

In contrast to $\Delta F = 2$ transitions, the dipole operators governing the $B \rightarrow X_{s,d}\gamma$ decays are generated first at the one loop level. As in the LRM the m_b suppression can be overcome by a chirality flip inside the loop. However in contrast to that model, in the RSc the primed operators $C'_{7\gamma,8G}$ are generally dominant [161–163], so that an enhanced branching ratio is generally expected.

12.6 Four generations: SM4

As opposed to the scenarios discussed so far, there are only SM operators contributing to $\Delta F = 2$ processes and the NP effects are primarily enhanced through the non-decoupling effects of the t' -quark. The presence of new mixing angles and of new phases allows then to solve the $S_{\psi K_S} - \varepsilon_K$ anomaly in a straightforward manner and simultaneously enhance

$S_{\psi\phi}$ if necessary. Moreover the agreement of theory and data can be improved in various observables.

Concerning the $B \rightarrow X_s \gamma$ decay, as seen in figure 17 of [69], the branching ratio can be enhanced up to $4 \cdot 10^{-4}$ but also significantly suppressed below $3 \cdot 10^{-4}$. Large enhancements like the ones from H^\pm in the LRM are not possible in the SM4, in particular if one wants to get interesting deviations from the SM3 predictions for $S_{\psi\phi}$ and $B_s \rightarrow \mu^+ \mu^-$.

12.7 Littlest Higgs with T-parity

As in the case of the SM4 no new operators enter in the LHT model and FCNC processes are generated first at the one-loop level [67, 164]. Still due to the absence of an intrinsic flavour structure in the mirror fermion sector the effects on $\Delta F = 2$ transitions are generally large, and in particular ε_K puts strong constraints on the new mixing parameters. At the same time the presence of new mixings and phases in the mirror sector allows to solve anomalies including a possible enhancement of $S_{\psi\phi}$. However the effects are not as strong as in the case of SM4 [165, 166]. Due to the absence of right-handed flavour violating currents, no chirality enhanced contribution to $B \rightarrow X_s \gamma$ arises and the effects remain very small.

13 Summary

In this paper we have presented a complete study of $\Delta S = 2$ and $\Delta B = 2$ processes in the LRM. This includes ε_K , ΔM_K , ΔM_s , ΔM_d , A_{SL}^q , $\Delta \Gamma_q$, and the mixing induced CP asymmetries $S_{\psi K_S}$ and $S_{\psi\phi}$. We have included the new contributions from box diagrams with W_R gauge boson and charged Higgs (H^\pm) exchanges and tree level contributions from heavy neutral Higgs exchanges. We have also analysed the $B \rightarrow X_{s,d} \gamma$ decays that receive important new contributions from the $W_L - W_R$ mixing and H^\pm exchanges. Compared to the existing literature the novel feature of our analysis is the search for correlations between various observables, simultaneous inclusion of all relevant contributions, in particular Higgs contributions and an improved treatment of QCD corrections. Our main findings are as follows:

- We find that the LRM is put under pressure by the ε_K constraint. This is due to the tree-level contributions of the neutral Higgs scalars and the related LR operators whose contributions are enhanced through renormalisation group effects and their chirally enhanced hadronic matrix elements. While this problem has been known for many years, we stress that even if the heavy Higgs masses are of order 15 – 20 TeV, these contributions are not only important but even dominant. Increasing these masses much more would make the Higgs system non-perturbative. Leaving them out from phenomenological analysis, as done in some papers, is simply wrong. Figure 3 makes this point explicitly. On the other hand we show that there are structures (hierarchical or inverted) of the matrix V^{R} where the ε_K -constraint can be satisfied without large fine-tuning of parameters.
- The contributions of W_R to $\Delta F = 2$ observables, in particular ε_K , is important but in view of the new improved lower experimental bound on its mass much less prob-

lematic than the tree level Higgs contributions, although also here the LR operators mentioned above enter. Consequently, if only these contributions were present, the matrix V^R would be somewhat less hierarchical than the CKM matrix.

- The charged Higgs H^\pm being as heavy as the neutral ones plays a subdominant role in $\Delta F = 2$ processes but can give significant contributions to $B \rightarrow X_{s,d}\gamma$ decays. These contributions are often neglected. We stress that this is not justified. Figure 4 makes this point explicitly. We find that the branching ratios for these decays can be significantly affected by new contributions but the CP-violating effects are too small to be distinguished from the SM results in view of hadronic uncertainties.
- In our analysis of FCNC processes we have taken into account all existing constraints from electroweak precision observables and tree level decays. In this context we have found that in these models the SM problem with RH $Z \rightarrow b\bar{b}$ couplings and the so-called $|V_{ub}|$ -problem cannot be solved. The increased value of M_{W_R} due to LHC combined with FCNC constraints does not allow to explain the difference in exclusive and inclusive determinations of $|V_{ub}|$ with the help of RH currents within the context of the LRM considered here.
- We have found that the NP effects are largest in the K system but large effects can also be found in the B_s system. Significant but smaller effects are found in the B_d system.
- Guided by the persisting $S_{\psi K_S} - \varepsilon_K$ tension present in the SM we have constructed a simple analytic expression for V^R , which is given in (7.5). It is given in terms of two mixing angles \tilde{s}_{13} and \tilde{s}_{23} and two corresponding phases $\phi_1 = \phi_{13}$ and $\phi_2 = \phi_{23}$ and allows to remove or soften the tension in question for scales $M_{W_R} \simeq 2 - 3$ TeV in the reach of the LHC. In this scenario for V^R interesting correlations with CP violation in the B_s system are present that depend on the value of $|V_{ub}|$ chosen as well as the numerical values of the elements of V^R . In two $|V_{ub}|$ scenarios considered by us $S_{\psi\phi}$ can be significantly enhanced over the SM value. When the data on $S_{\psi\phi}$ will improve one will be able to learn more about the structure of V^R .
- A more involved numerical analysis allows to find other structures of V^R with all its nine parameters entering the game that without large fine-tuning of these parameters allows to obtain interesting results. In particular as shown in figure 12 three oases are found in the space $(|V_{us}^R|, |V_{ub}^R|, |V_{cb}^R|)$, of which two have low fine-tuning. The pattern of flavour violation in the scenario with “normal” hierarchy in V^R has been presented in several plots in section 9 and the corresponding Wolfenstein-like parametrization has been derived.
- We find a soft lower limit for the mass of the heavy Higgses of $M_H \gtrsim 2.4$ TeV, see figure 19.

Our analysis of the LRM presented in this paper was dominated by the observables on which already good data exist. We have seen that already these data put stringent

constraints on this NP scenario. However there are other observables not discussed by us, that have not been measured yet but the experimental upper bounds on them put significant constraints on the LRM. Among them a prominent role is played by the neutron electric dipole moment (EDM). The most recent analysis in [28] demonstrates that the neutron EDM provides lower bounds on W' and heavy neutral Higgs masses that are competitive with those coming from ε_K . Determining what impact the present bounds on the neutron EDM have on the LRM considered by us would require a detailed analysis of all contributions and taking into account the significant hadronic uncertainties. We leave such an analysis for future work. Similarly, in this decade other observables, like rare B and K decay branching ratios and related CP violating observables, will be measured with sufficient precision so that we will be able to find out whether this NP scenario is viable. Of course the discovery of new gauge bosons W' and Z' at the LHC would be the most spectacular manifestation of the kind of new physics analysed in our paper.

Acknowledgements

We would like to thank Andreas Crivellin, Jennifer Girschbach, Mikolaj Misiak, Kai Schmitz and Emmanuel Stamou for very useful discussions. This research was done in the context of the ERC Advanced Grant project ‘‘FLAVOUR’’ (267104) and was partially supported by the Graduiertenkolleg GRK 1054, the German Bundesministerium für Bildung und Forschung under contract 05HT6WOA and by the U.S. National Science Foundation through grant PHY-0757868 and CAREER award PHY-0844667.

A Higgs potential

The most general renormalisable Higgs potential invariant under parity is given by [28, 29, 167, 168]

$$\begin{aligned}
V(\phi, \Delta_L, \Delta_R) = & -\mu_1^2 \text{Tr}(\phi^\dagger \phi) - \mu_2^2 \left[\text{Tr}(\tilde{\phi} \phi^\dagger) + \text{Tr}(\tilde{\phi}^\dagger \phi) \right] - \mu_3^2 \left[\text{Tr}(\Delta_L \Delta_L^\dagger) + \text{Tr}(\Delta_R \Delta_R^\dagger) \right] \\
& + \lambda_1 \left[\text{Tr}(\phi^\dagger \phi) \right]^2 + \lambda_2 \left\{ \left[\text{Tr}(\tilde{\phi} \phi^\dagger) \right]^2 + \left[\text{Tr}(\tilde{\phi}^\dagger \phi) \right]^2 \right\} \\
& + \lambda_3 \text{Tr}(\tilde{\phi} \phi^\dagger) \text{Tr}(\tilde{\phi}^\dagger \phi) + \lambda_4 \text{Tr}(\phi^\dagger \phi) \left[\text{Tr}(\tilde{\phi} \phi^\dagger) + \text{Tr}(\tilde{\phi}^\dagger \phi) \right] \\
& + \rho_1 \left\{ \left[\text{Tr}(\Delta_L \Delta_L^\dagger) \right]^2 + \left[\text{Tr}(\Delta_R \Delta_R^\dagger) \right]^2 \right\} \\
& + \rho_2 \left[\text{Tr}(\Delta_L \Delta_L) \text{Tr}(\Delta_L^\dagger \Delta_L^\dagger) + \text{Tr}(\Delta_R \Delta_R) \text{Tr}(\Delta_R^\dagger \Delta_R^\dagger) \right] \\
& + \rho_3 \text{Tr}(\Delta_L \Delta_L^\dagger) \text{Tr}(\Delta_R \Delta_R^\dagger) + \rho_4 \left[\text{Tr}(\Delta_L \Delta_L) \text{Tr}(\Delta_R^\dagger \Delta_R^\dagger) + \text{Tr}(\Delta_L^\dagger \Delta_L^\dagger) \text{Tr}(\Delta_R \Delta_R) \right] \\
& + \alpha_1 \text{Tr}(\phi^\dagger \phi) \left[\text{Tr}(\Delta_L \Delta_L^\dagger) + \text{Tr}(\Delta_R \Delta_R^\dagger) \right] \\
& + \left\{ \alpha_2 e^{i\delta_2} \left[\text{Tr}(\tilde{\phi} \phi^\dagger) \text{Tr}(\Delta_L \Delta_L^\dagger) + \text{Tr}(\tilde{\phi}^\dagger \phi) \text{Tr}(\Delta_R \Delta_R^\dagger) \right] + \text{h.c.} \right\} \\
& + \alpha_3 \left[\text{Tr}(\phi \phi^\dagger \Delta_L \Delta_L^\dagger) + \text{Tr}(\phi^\dagger \phi \Delta_R \Delta_R^\dagger) \right] + \beta_1 \left[\text{Tr}(\phi \Delta_R \phi^\dagger \Delta_L^\dagger) + \text{Tr}(\phi^\dagger \Delta_L \phi \Delta_R^\dagger) \right] \\
& + \beta_2 \left[\text{Tr}(\tilde{\phi} \Delta_R \phi^\dagger \Delta_L^\dagger) + \text{Tr}(\tilde{\phi}^\dagger \Delta_L \phi \Delta_R^\dagger) \right] + \beta_3 \left[\text{Tr}(\phi \Delta_R \tilde{\phi}^\dagger \Delta_L^\dagger) + \text{Tr}(\phi^\dagger \Delta_L \tilde{\phi} \Delta_R^\dagger) \right], \quad (\text{A.1})
\end{aligned}$$

where there are a total of 18 parameters, $\mu_{1,2,3}^2$, $\lambda_{1,2,3,4}$, $\rho_{1,2,3,4}$, $\alpha_{1,2,3}$, and $\beta_{1,2,3}$. Due to the left-right symmetry, only one of them, the coupling involving α_2 can become complex and all other couplings are real.

We have investigated the possibility of a more general Higgs potential, where no left-right symmetry is imposed. However as the parameters of the Higgs potential do not affect our flavour analysis, taking into account that leading order couplings of Higgs and quark fields are independent of these parameters, we find it sufficient to give here the left-right symmetric form. In fact among the parameters of the Higgs sector only α_3 in (A.1), determining the heavy Higgs masses, is relevant for our analysis.

B Gauge boson masses and mixings

The gauge boson mass matrices can straightforwardly be obtained from the relevant terms of equations (2.16) and (2.17). Diagonalising the resulting mass matrix for the charged gauge bosons yields the mass eigenstates

$$W^\pm = W_L^\pm + s c e^{\mp i\alpha} \frac{s_R c_W}{s_W} \epsilon^2 W_R^\pm, \quad (\text{B.1})$$

$$W'^\pm = W_R^\pm - s c e^{\pm i\alpha} \frac{s_R c_W}{s_W} \epsilon^2 W_L^\pm, \quad (\text{B.2})$$

where we defined $v = \sqrt{\kappa^2 + \kappa'^2}$, $c = \kappa/v$, $s = \kappa'/v$ and we neglected higher order terms in $\epsilon = v/\kappa_R$. We also introduced the mixing angles

$$s_R = \frac{g'}{\sqrt{g'^2 + g_R^2}}, \quad c_R = \sqrt{1 - s_R^2}, \quad s_W = \frac{s_R}{\sqrt{(g_L/g_R)^2 + s_R^2}}, \quad c_W = \sqrt{1 - s_W^2}. \quad (\text{B.3})$$

The corresponding masses read

$$(M_W)^2 = \frac{e^2 v^2}{2s_W^2} (1 - 2s^2 c^2 \epsilon^2), \quad (\text{B.4})$$

$$(M_{W_R})^2 = \frac{e^2 \kappa_R^2}{c_W^2 s_R^2} \left(1 + \frac{1}{2} \epsilon^2\right). \quad (\text{B.5})$$

For the neutral gauge bosons we can write

$$A = s_W W_L^3 + s_R c_W W_R^3 + c_R c_W B, \quad (\text{B.6})$$

$$Z = c_W W_L^3 - s_R s_W \left(1 - \frac{c_R^4}{4s_W^2} \epsilon^2\right) W_R^3 - c_R s_W \left(1 + \frac{s_R^2 c_R^2}{4s_W^2} \epsilon^2\right) B \quad (\text{B.7})$$

$$Z' = -\frac{s_R c_R^3 c_W}{4s_W} \epsilon^2 W_L^3 + c_R \left(1 + \frac{s_R^2 c_R^2}{4} \epsilon^2\right) W_R^3 - s_R \left(1 - \frac{c_R^4}{4} \epsilon^2\right) B. \quad (\text{B.8})$$

The masses are given by

$$(M_A)^2 = 0, \quad (\text{B.9})$$

$$(M_Z)^2 = \frac{e^2 v^2}{2s_W^2 c_W^2} \left(1 - \frac{c_R^4}{4} \epsilon^2\right), \quad (\text{B.10})$$

$$(M_{Z'})^2 = \frac{2e^2 \kappa_R^2}{s_R^2 c_R^2 c_W^2} \left(1 + \frac{c_R^4}{4} \epsilon^2\right). \quad (\text{B.11})$$

C Goldstone boson and Higgs mass eigenstates

The doubly charged components $\delta_{L,R}^{++}$ lead to two physical doubly charged Higgses.

The singly charged fields $\phi_{1,2}^\pm$ and $\delta_{L,R}^\pm$ form the Goldstone bosons of W^\pm and W'^\pm and two charged Higgses. The Goldstone bosons are given by

$$G^\pm = \pm i \left[c(1 - s^4 \epsilon^2) \phi_1^\pm - s e^{\mp i\alpha} (1 - c^4 \epsilon^2) \phi_2^\pm - \sqrt{2} c s e^{\mp i\alpha} \epsilon \delta_R^\pm \right], \quad (\text{C.1})$$

$$G'^\pm = \mp i \left[\left(1 - \frac{\epsilon^2}{4}\right) \delta_R^\pm + \frac{s e^{\pm i\alpha}}{\sqrt{2}} \epsilon \phi_1^\pm - \frac{c}{\sqrt{2}} \epsilon \phi_2^\pm \right]. \quad (\text{C.2})$$

The physical singly charged Higgs states are linear combinations of δ_L^\pm and

$$h^\pm = s e^{\pm i\alpha} \left(1 - \frac{(c^2 - s^2)^2}{4} \epsilon^2\right) \phi_1^\pm + c \left(1 - \frac{(c^2 - s^2)^2}{4} \epsilon^2\right) \phi_2^\pm + \frac{c^2 - s^2}{\sqrt{2}} \epsilon \delta_R^\pm. \quad (\text{C.3})$$

Finally the neutral Goldstone boson and Higgs fields are built out of $\phi_{1,2}^0$ and $\delta_{L,R}^0$. Defining $\pi^0 = c \text{Im} \phi_1^0 - s \text{Im}(e^{-i\alpha} \phi_2^0)$, the Goldstone bosons of Z and Z' read

$$G^0 = \sqrt{2} \left(1 - \frac{c_R^4}{8} \epsilon^2\right) \pi^0 - \frac{c_R^2}{\sqrt{2}} \epsilon \text{Im} \delta_R^0, \quad (\text{C.4})$$

$$G'^0 = -\sqrt{2} \left(1 - \frac{c_R^4}{8} \epsilon^2\right) \text{Im} \delta_R^0 - \frac{c_R^2}{\sqrt{2}} \epsilon \pi^0. \quad (\text{C.5})$$

In addition there are six neutral Higgs fields in the spectrum, that are linear combinations of $s \text{Im} \phi_1^0 + c \text{Im}(e^{-i\alpha} \phi_2^0)$, $\text{Re} \phi_1^0$, $\text{Re}(e^{-i\alpha} \phi_2^0)$, $\text{Re} \delta_R^0$, $\text{Re} \delta_L^0$ and $\text{Im} \delta_L^0$.

In order to make a more detailed statement about the Higgs mass eigenstates one has to diagonalize the Higgs potential (A.1). Considering the neutral 8 by 8 mass matrix, its diagonalisation can be best done by using perturbation theory. While in [28] a further hierarchy, namely $\kappa' \ll \kappa$, has been assumed, we do not restrict ourselves to this case but determine the Higgs mass eigenstates to leading order for arbitrary $s = \kappa'/v$. It turns out that the leading order Higgs couplings are not sensitive to the detailed structure of the potential and in particular the parity invariant potential yields the same result. The leading order mass eigenstates of the Higgs fields of our interest are then given by

$$h^0 = \sqrt{2} (c \text{Re} \phi_1^0 + s \text{Re}(e^{-i\alpha} \phi_2^0)) \quad (\text{C.6})$$

$$H_1^0 = \sqrt{2} (-s \text{Re} \phi_1^0 + c \text{Re}(e^{-i\alpha} \phi_2^0)) \quad (\text{C.7})$$

$$H_2^0 = \sqrt{2} (s \text{Im} \phi_1^0 + c \text{Im}(e^{-i\alpha} \phi_2^0)) \quad (\text{C.8})$$

where h_0 can be identified as the light Higgs with a mass of $\mathcal{O}(v)$, while H_1^0 and H_2^0 are two new flavour-violating neutral Higgses with masses $\mathcal{O}(\kappa_R)$. To leading order their masses are equal to each other

$$M_H^2 \equiv M_{H_1^0}^2 = M_{H_2^0}^2 = \frac{\alpha_3 \kappa_R^2}{1 - 2s^2} = \alpha_3 \kappa_R^2 \sqrt{u(s)}. \quad (\text{C.9})$$

In the course of the numerical analysis we regard M_H as a free parameter. These results agree with the ones given by the authors of [28] in the limit of small $s \ll 1$. A more explicit

analysis of the Higgs sector of this class of models can be also found in [28, 167, 168]. Charged Higgs effects in LR models are often neglected in the literature with the argument that they have to be small in FCNC processes as they have to take place at one loop order [27]. This is in fact true for the $\Delta F = 2$ processes but not for $B \rightarrow X_{s,d}\gamma$. This has already been pointed out in [54, 55, 58–61] in LR models and confirmed here by us. As in the case of the neutral Higgs sector we are only interested in leading order couplings and masses. We find that the mass of the lightest charged Higgs,

$$H^\pm = se^{\pm i\alpha} \phi_1^\pm + c\phi_2^\pm, \quad (\text{C.10})$$

is given to a very good approximation by

$$M_{H^\pm} = M_H \quad (\text{C.11})$$

and hence cannot be chosen to be as light as 1 TeV as done sometimes in the literature.

D Numerical details for $\Delta F = 2$

Here we give the values of R_{ij} as defined in (3.40) and used in the main part of our numerical analysis. Including all contributions we find for $\epsilon = 0.03$, $s_R = 0.8$ and $s = 0.1$

$$\hat{R}(K) = \begin{pmatrix} -4.3236 \cdot 10^{-9} & -1.2585 \cdot 10^{-6} & -7.8924 \cdot 10^{-5} \\ -1.2585 \cdot 10^{-6} & -6.5793 \cdot 10^{-4} & -4.1333 \cdot 10^{-2} \\ -7.8924 \cdot 10^{-5} & -4.1333 \cdot 10^{-2} & -9.1112 \end{pmatrix}, \quad (\text{D.1})$$

$$\hat{R}(B) = \begin{pmatrix} -2.7079 \cdot 10^{-10} & -7.8847 \cdot 10^{-8} & -4.9574 \cdot 10^{-6} \\ -7.8847 \cdot 10^{-8} & -4.1217 \cdot 10^{-5} & -2.5958 \cdot 10^{-3} \\ -4.9574 \cdot 10^{-6} & -2.5958 \cdot 10^{-3} & -0.5727 \end{pmatrix}. \quad (\text{D.2})$$

For $s = 0.5$ the Higgs contributions get enhanced and the calculation of the R_{ij} yields

$$\hat{R}(K) = \begin{pmatrix} -4.6987 \cdot 10^{-9} & -1.4447 \cdot 10^{-6} & -1.3159 \cdot 10^{-4} \\ -1.4447 \cdot 10^{-6} & -7.5036 \cdot 10^{-4} & -6.7475 \cdot 10^{-2} \\ -1.3159 \cdot 10^{-4} & -6.7475 \cdot 10^{-2} & -16.546 \end{pmatrix}, \quad (\text{D.3})$$

$$\hat{R}(B) = \begin{pmatrix} -2.9439 \cdot 10^{-10} & -9.0565 \cdot 10^{-8} & -8.2716 \cdot 10^{-6} \\ -9.0565 \cdot 10^{-8} & -4.7034 \cdot 10^{-5} & -4.2408 \cdot 10^{-3} \\ -8.2716 \cdot 10^{-6} & -4.2408 \cdot 10^{-3} & -1.0406 \end{pmatrix}. \quad (\text{D.4})$$

Keeping only gauge boson contributions we find (no s dependence)

$$\hat{R}(K, \text{gauge}) = \begin{pmatrix} -3.9343 \cdot 10^{-9} & -1.0653 \cdot 10^{-6} & -2.4264 \cdot 10^{-5} \\ -1.0653 \cdot 10^{-6} & -5.6199 \cdot 10^{-4} & -1.4200 \cdot 10^{-2} \\ -2.4264 \cdot 10^{-5} & -1.4200 \cdot 10^{-2} & -1.3954 \end{pmatrix}, \quad (\text{D.5})$$

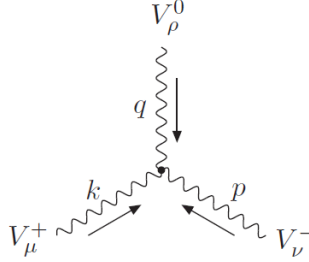
$$\hat{R}(B, \text{gauge}) = \begin{pmatrix} -2.4630 \cdot 10^{-10} & -6.6689 \cdot 10^{-8} & -1.5190 \cdot 10^{-6} \\ -6.6689 \cdot 10^{-8} & -3.5182 \cdot 10^{-5} & -8.8898 \cdot 10^{-4} \\ -1.5190 \cdot 10^{-6} & -8.8898 \cdot 10^{-4} & -8.7355 \cdot 10^{-2} \end{pmatrix}. \quad (\text{D.6})$$

The H^\pm contributions are significantly smaller than gauge contributions.

E Feynman rules

In this part of the appendix we present the Feynman rules up to and including $\mathcal{O}(\epsilon^2)$ corrections, except for the couplings to Higgs bosons where we restrict ourselves to the leading order couplings¹⁰. The Feynman rules are given in mass eigenstates of the particular fields. We want to stress that we keep here the correct notation W and W' , as introduced in appendix B, in spite of using throughout the phenomenological analysis the simplified notation W_L and W_R for the mass eigenstates.

Concerning triple gauge couplings a comment is in order. The Dirac structure of all vertices is the same,



$$\mathcal{C} [\eta_{\mu\nu}(k-p)_\rho + \eta_{\nu\rho}(p-q)_\mu + \eta_{\rho\mu}(q-k)_\nu] ,$$

where $V_\mu^+ = W_\mu^+, W_\mu'^+, V_\nu^- = W_\nu^-, W_\nu'^-, V_\rho^0 = A_\rho, Z_\rho, Z_\rho'$, and k, p, q are their incoming momenta. Therefore in table 12 we collect only the coefficients \mathcal{C} of the respective couplings.

	A_μ	G_μ^a
$\bar{u}_L^i u_L^i X_\mu$	$-i\frac{2}{3}e\gamma^\mu$	$-ig_s\gamma^\mu t^a$
$\bar{u}_R^i u_R^i X_\mu$	$-i\frac{2}{3}e\gamma^\mu$	$-ig_s\gamma^\mu t^a$
$\bar{d}_L^i d_L^i X_\mu$	$-i(-\frac{1}{3})e\gamma^\mu$	$-ig_s\gamma^\mu t^a$
$\bar{d}_R^i d_R^i X_\mu$	$-i(-\frac{1}{3})e\gamma^\mu$	$-ig_s\gamma^\mu t^a$

Table 7. Fermion couplings to the massless gauge bosons X_μ : photon A_μ and gluons G_μ^a

	W^+	W'^+
$\bar{u}_L^i d_L^j X_\mu^+$	$-\frac{ie}{\sqrt{2}s_W} V_{ij}^L \gamma^\mu$	$+\frac{iecs e^{-i\alpha} s_{RCW}}{\sqrt{2}s_W^2} \epsilon^2 V_{ij}^L \gamma^\mu$
$\bar{u}_R^i d_R^j X_\mu^+$	$-\frac{iecs e^{i\alpha}}{\sqrt{2}s_W} \epsilon^2 V_{ij}^R \gamma^\mu$	$-\frac{ie}{\sqrt{2}s_{RCW}} V_{ij}^R \gamma^\mu$

Table 8. Fermion couplings to W^+ and W'^+

¹⁰We would like to thank Jennifer Girrbach for checking the Feynman rules presented here.

	Z	Z'
$\bar{u}_L^i u_L^i X_\mu$	$-\frac{ie}{s_W c_W} \left(\frac{1}{2} - \frac{2}{3} s_W^2 - \frac{1}{24} s_R^2 c_R^2 \epsilon^2 \right) \gamma^\mu$	$ie \left(\frac{1}{6} \frac{s_R}{c_R c_W} + \frac{1}{8} \left(\frac{c_W c_R^3 s_R}{s_W^2} - \frac{c_R^3 s_R}{3 c_W} \right) \epsilon^2 \right) \gamma^\mu$
$\bar{d}_L^i d_L^i X_\mu$	$-\frac{ie}{s_W c_W} \left(-\frac{1}{2} + \frac{1}{3} s_W^2 - \frac{1}{24} s_R^2 c_R^2 \epsilon^2 \right) \gamma^\mu$	$ie \left(\frac{1}{6} \frac{s_R}{c_R c_W} - \frac{1}{8} \left(\frac{c_W c_R^3 s_R}{s_W^2} + \frac{c_R^3 s_R}{3 c_W} \right) \epsilon^2 \right) \gamma^\mu$
$\bar{u}_R^i u_R^i X_\mu$	$-\frac{ie}{s_W c_W} \left(-\frac{2}{3} s_W^2 + \frac{c_R^2}{8} (c_R^2 - \frac{1}{3} s_R^2) \epsilon^2 \right) \gamma^\mu$	$-\frac{ie}{c_W s_R c_R} \left(\frac{1}{2} - \frac{2}{3} s_R^2 + \frac{c_R^4 s_R^2}{6} \epsilon^2 \right) \gamma^\mu$
$\bar{d}_R^i d_R^i X_\mu$	$-\frac{ie}{s_W c_W} \left(\frac{1}{3} s_W^2 - \frac{c_R^2}{8} (c_R^2 + \frac{1}{3} s_R^2) \epsilon^2 \right) \gamma^\mu$	$-\frac{ie}{c_W s_R c_R} \left(-\frac{1}{2} + \frac{1}{3} s_R^2 - \frac{c_R^4 s_R^2}{12} \epsilon^2 \right) \gamma^\mu$

Table 9. Fermion couplings to neutral gauge bosons Z and Z'

	G^+	G'^+
$\bar{u}_L^i d_R^j X^+$	$\frac{e}{\sqrt{2} M_W s_W} \left(m_d^j V_{ij}^L - c s e^{i\alpha} m_u^i \epsilon^2 V_{ij}^R \right)$	$-\frac{e m_u^i}{\sqrt{2} c_W s_R M_{W_R}} V_{ij}^R$
$\bar{u}_R^i d_L^j X^+$	$-\frac{e}{\sqrt{2} M_W s_W} \left(m_u^i V_{ij}^L - c s e^{i\alpha} m_d^j \epsilon^2 V_{ij}^R \right)$	$\frac{e m_d^j}{\sqrt{2} c_W s_R M_{W_R}} V_{ij}^R$

Table 10. Fermion couplings to charged Goldstone bosons

	G^0	G'^0
$\bar{u}_L^i u_R^i X^0$	$\frac{e m_u^i}{2 c_W s_W M_Z} \left(1 - \frac{c_R^4}{4} \epsilon^2 \right)$	$-\frac{e c_R m_u^i}{2 s_R c_W M_{Z'}}$
$\bar{d}_L^i d_R^i X^0$	$-\frac{e m_d^i}{2 c_W s_W M_Z} \left(1 - \frac{c_R^4}{4} \epsilon^2 \right)$	$\frac{e c_R m_d^i}{2 s_R c_W M_{Z'}}$

Table 11. Fermion couplings to neutral Goldstone bosons G^0 and G'^0

	Z	Z'	A
$W^+ W^- X$	$ie \frac{c_W}{s_W}$	$-ie \frac{c_R^3 s_R c_W}{4 s_W^2} \epsilon^2$	ie
$W^+ W'^- X$	$-ie \frac{c s e^{i\alpha} s_R}{s_W^2} \epsilon^2$	$ie \frac{c s e^{i\alpha} c_R}{s_W} \epsilon^2$	0
$W'^+ W^- X$	$-ie \frac{c s e^{-i\alpha} s_R}{s_W^2} \epsilon^2$	$ie \frac{c s e^{-i\alpha} c_R}{s_W} \epsilon^2$	0
$W'^+ W'^- X$	$-ie \left(\frac{s_W}{c_W} - \frac{c_R^4}{4 c_W s_W} \epsilon^2 \right)$	$ie \frac{c_R}{c_W} \left(\frac{1}{s_R} + \frac{c_R^2 s_R}{4} \epsilon^2 \right)$	ie

Table 12. Triple gauge couplings, involving a Z and Z' boson and the photon, respectively

	Z	A
$G^+(p)G^-(q)X_\mu$	$-\frac{ie}{2c_W s_W}(p-q)_\mu \left[1 - 2s_W^2 + \left(\frac{c_R^4}{4} - 2s^2 c^2\right) \epsilon^2\right]$	$-ie(p-q)_\mu$
$G'^+(p)G^-(q)X_\mu$	$\frac{iecse^{-i\alpha}}{\sqrt{2}c_W s_W} \epsilon(p-q)_\mu$	0
$G'^+(p)G'^-(q)X_\mu$	$ie\frac{s_W}{c_W}(p-q)_\mu \left[1 - \frac{1-s_R^2 c_R^2}{4s_W^2} \epsilon^2\right]$	$-ie(p-q)_\mu$

Table 13. Charged Goldstone couplings to the photon and the Z boson

$G^+(p)G^-(q)Z'_\mu$	$-\frac{iec_R}{2s_R c_W}(p-q)_\mu \left[1 - \frac{s_R^2 c_R^4(1-2s_W^2) + 8s^2 c^2 s_W^2(1+s_R^2)}{4c_R^2 s_W^2} \epsilon^2\right]$
$G'^+(p)G^-(q)Z'_\mu$	$\frac{iecse^{-i\alpha}(1+s_R^2)}{\sqrt{2}c_R s_R c_W} \epsilon(p-q)_\mu$
$G'^+(p)G'^-(q)Z'_\mu$	$\frac{ies_R}{c_R c_W}(p-q)_\mu \left[1 - \frac{1+s_R^2(1+c_R^4)}{4s_R^2} \epsilon^2\right]$

Table 14. Charged Goldstone couplings to the Z' boson

	W	W'
$G^0(p)G^-(q)X_\mu^+$	$\frac{ie}{2s_W}(p-q)_\mu \left[1 - \frac{1}{8}(c_R^4 - 8s^2 c^2) \epsilon^2\right]$	$\frac{iecse^{-i\alpha}}{c_W s_R}(p-q)_\mu \left[1 - \frac{1}{2} \left(\frac{c_R^4}{4} + \frac{s_R^2}{s_W^2} - 2s^2 c^2\right) \epsilon^2\right]$
$G'^0(p)G^-(q)X_\mu^+$	$-\frac{iec_R^2}{4s_W} \epsilon(p-q)_\mu$	$\frac{iecse^{-i\alpha}(2-c_R^2)}{2c_W s_R} \epsilon(p-q)_\mu$
$G^0(p)G'^-(q)X_\mu^+$	$-\frac{iecse^{i\alpha}}{\sqrt{2}s_W} \epsilon(p-q)_\mu$	$-\frac{ies_R}{2\sqrt{2}c_W} \epsilon(p-q)_\mu$
$G'^0(p)G'^-(q)X_\mu^+$	$\frac{iecse^{i\alpha}(2+c_R^2)}{2\sqrt{2}s_W} \epsilon^2(p-q)_\mu$	$\frac{ie}{\sqrt{2}c_W s_R}(p-q)_\mu \left[1 - \frac{1}{8}(1+s_R^4) \epsilon^2\right]$

Table 15. Couplings of charged and neutral Goldstone Bosons to the W and W' boson

	G^0	G'^0
$W^+W^-X^0$	0	0
$W^+W'^-X^0$	$-\frac{2ecse^{i\alpha}M_Z}{s_R} g_{\mu\nu}$	$\frac{ec_R^3 cse^{i\alpha}M_{Z'}}{2s_W} \epsilon^2 g_{\mu\nu}$
$W'^+W'^-X^0$	0	0

Table 16. Couplings of charged gauge bosons to the G^0 and G'^0 boson

	G^+	G'^+
$W_\mu^- A_\nu X^+$	$-eM_W g_{\mu\nu}$	0
$W'_\mu^- A_\nu X^+$	0	$-eM_{W_R} g_{\mu\nu}$
$W_\mu^- Z_\nu X^+$	$\frac{es_W M_W}{c_W} g_{\mu\nu} \left(1 - \frac{c_R^4 - 8s^2 c^2}{4s_W^2} \epsilon^2\right)$	0
$W'_\mu^- Z_\nu X^+$	$\frac{2ecse^{i\alpha} M_W}{c_W^2 s_R} g_{\mu\nu}$	$\frac{es_W M_{W_R}}{c_W} \left(1 - \frac{1+s_R^4}{4s_W^2} \epsilon^2\right) g_{\mu\nu}$
$W_\mu^- Z'_\nu X^+$	$-\frac{ec_R M_W}{c_W s_R} g_{\mu\nu}$	$\frac{2ecse^{-i\alpha} M_{W_R}}{c_R s_W} \epsilon^2 g_{\mu\nu}$
$W'_\mu^- Z'_\nu X^+$	$\frac{2ecse^{i\alpha} s_W (1+s_R^2) M_W}{c_W^2 s_R^2 c_R} g_{\mu\nu}$	$\frac{e(1+s_R^2) M_{W_R}}{c_R s_R c_W} \left(1 - \left(\frac{1}{2} + \frac{s_R^4}{4(1+s_R^2)}\right) \epsilon^2\right) g_{\mu\nu}$

Table 17. Couplings of charged and neutral gauge bosons to the G^+ and G'^+ boson

	H_1^0	H_2^0
$\bar{d}_L^i d_R^j X^0$	$-\frac{i}{\sqrt{2}(1-2s^2)v} \left(e^{i\alpha} m_u^a V_{ai}^{L*} V_{aj}^R - 2csm_d^i \delta_{ij}\right)$	$\frac{1}{\sqrt{2}(1-2s^2)v} \left(e^{i\alpha} m_u^a V_{ai}^{L*} V_{aj}^R - 2csm_d^i \delta_{ij}\right)$
$\bar{d}_R^i d_L^j X^0$	$-\frac{i}{\sqrt{2}(1-2s^2)v} \left(e^{-i\alpha} m_u^a V_{ai}^{R*} V_{aj}^L - 2csm_d^i \delta_{ij}\right)$	$-\frac{1}{\sqrt{2}(1-2s^2)v} \left(e^{-i\alpha} m_u^a V_{ai}^{R*} V_{aj}^L - 2csm_d^i \delta_{ij}\right)$
$\bar{u}_L^i u_R^j X^0$	$-\frac{i}{\sqrt{2}(1-2s^2)v} \left(e^{-i\alpha} m_d^a V_{ai}^L V_{aj}^{R*} - 2csm_u^i \delta_{ij}\right)$	$-\frac{1}{\sqrt{2}(1-2s^2)v} \left(e^{-i\alpha} m_d^a V_{ai}^L V_{aj}^{R*} - 2csm_u^i \delta_{ij}\right)$
$\bar{u}_R^i u_L^j X^0$	$-\frac{i}{\sqrt{2}(1-2s^2)v} \left(e^{i\alpha} m_d^a V_{ai}^R V_{aj}^{L*} - 2csm_u^i \delta_{ij}\right)$	$\frac{1}{\sqrt{2}(1-2s^2)v} \left(e^{i\alpha} m_d^a V_{ai}^R V_{aj}^{L*} - 2csm_u^i \delta_{ij}\right)$

Table 18. Fermion couplings to the flavour violating neutral Higgses. Here m_u^a and m_d^a denote the a th up and down quark mass, respectively. Summation over a is understood.

$\bar{u}_L^i d_R^j H^+$	$-\frac{i}{(1-2s^2)v} \left(m_u^i V_{ij}^R - 2cse^{-i\alpha} V_{ij}^L m_d^j\right)$
$\bar{u}_R^i d_L^j H^+$	$\frac{i}{(1-2s^2)v} \left(V_{ij}^R m_d^j - 2cse^{-i\alpha} m_u^i V_{ij}^L\right)$

Table 19. Charged Higgs couplings to fermions. Here m_u^a and m_d^a denote the a th up and down quark mass, respectively.

References

- [1] S. L. Glashow, J. Iliopoulos, and L. Maiani, *Weak Interactions with Lepton-Hadron Symmetry*, *Phys. Rev.* **D2** (1970) 1285–1292.
- [2] A. Bevan, M. Bona, M. Ciuchini, D. Derkach, A. Stocchi, *et. al.*, *The unitarity triangle analysis within and beyond the standard model*, *PoS HQL2010* (2011) 019. Updates available on <http://www.utfit.org>.
- [3] **CKMfitter** Collaboration, J. Charles *et. al.*, *CP violation and the CKM matrix: Assessing the impact of the asymmetric B factories*, *Eur. Phys. J.* **C41** (2005) 1–131, [hep-ph/0406184]. Updates available on <http://ckmfitter.in2p3.fr/>.
- [4] E. Lunghi and A. Soni, *Possible Indications of New Physics in B_d -mixing and in $\sin(2\beta)$ Determinations*, *Phys. Lett.* **B666** (2008) 162–165, [[arXiv:0803.4340](http://arxiv.org/abs/0803.4340)].
- [5] A. J. Buras and D. Guadagnoli, *Correlations among new CP violating effects in $\Delta F = 2$ observables*, *Phys. Rev.* **D78** (2008) 033005, [[arXiv:0805.3887](http://arxiv.org/abs/0805.3887)].
- [6] A. J. Buras, *Minimal flavour violation and beyond: Towards a flavour code for short distance dynamics*, *Acta Phys. Polon.* **B41** (2010) 2487–2561, [[arXiv:1012.1447](http://arxiv.org/abs/1012.1447)].
- [7] G. Isidori, *The challenges of flavour physics*, *PoS ICHEP2010* (2010) 543, [[arXiv:1012.1981](http://arxiv.org/abs/1012.1981)].
- [8] E. Lunghi and A. Soni, *Possible evidence for the breakdown of the CKM-paradigm of CP-violation*, *Phys. Lett.* **B697** (2011) 323–328, [[arXiv:1010.6069](http://arxiv.org/abs/1010.6069)].
- [9] A. Lenz, U. Nierste, J. Charles, S. Descotes-Genon, A. Jantsch, *et. al.*, *Anatomy of New Physics in $B - \bar{B}$ mixing*, *Phys.Rev.* **D83** (2011) 036004, [[arXiv:1008.1593](http://arxiv.org/abs/1008.1593)].
- [10] A. Lenz and U. Nierste, *Numerical updates of lifetimes and mixing parameters of B mesons*, [[arXiv:1102.4274](http://arxiv.org/abs/1102.4274)].
- [11] J. Laiho, E. Lunghi, and R. Van De Water, *Lessons for new physics from CKM studies*, *PoS FPCP2010* (2010) 040, [[arXiv:1102.3917](http://arxiv.org/abs/1102.3917)].
- [12] E. Lunghi and A. Soni, *Demise of CKM and its aftermath*, [[arXiv:1104.2117](http://arxiv.org/abs/1104.2117)].
- [13] J. C. Pati and A. Salam, *Lepton Number as the Fourth Color*, *Phys. Rev.* **D10** (1974) 275–289.
- [14] R. N. Mohapatra and J. C. Pati, *A Natural Left-Right Symmetry*, *Phys. Rev.* **D11** (1975) 2558.
- [15] R. N. Mohapatra and J. C. Pati, *Left-Right Gauge Symmetry and an Isoconjugate Model of CP Violation*, *Phys. Rev.* **D11** (1975) 566–571.
- [16] G. Senjanovic and R. N. Mohapatra, *Exact Left-Right Symmetry and Spontaneous Violation of Parity*, *Phys. Rev.* **D12** (1975) 1502.
- [17] G. Senjanovic, *Spontaneous Breakdown of Parity in a Class of Gauge Theories*, *Nucl. Phys.* **B153** (1979) 334.
- [18] R. N. Mohapatra, F. E. Paige, and D. P. Sidhu, *Symmetry Breaking and Naturalness of Parity Conservation in Weak Neutral Currents in Left-Right Symmetric Gauge Theories*, *Phys. Rev.* **D17** (1978) 2462.
- [19] D. Chang, *A Minimal Model of Spontaneous CP Violation with the Gauge Group $SU(2)_L \times SU(2)_R \times U(1)_{B-L}$* , *Nucl. Phys.* **B214** (1983) 435.

- [20] G. Branco, J. Frere, and J. Gerard, *The value of ϵ'/ϵ in models based on $SU(2)_L \times SU(2)_R \times U(1)$* , *Nucl.Phys.* **B221** (1983) 317.
- [21] H. Harari and M. Leurer, *Left-Right Symmetry and the Mass Scale of a Possible Right-Handed Weak Boson*, *Nucl. Phys.* **B233** (1984) 221.
- [22] K. Kiers, J. Kolb, J. Lee, A. Soni, and G.-H. Wu, *Ubiquitous CP violation in a top inspired left-right model*, *Phys. Rev.* **D66** (2002) 095002, [[hep-ph/0205082](#)].
- [23] G. Beall, M. Bander, and A. Soni, *Constraint on the Mass Scale of a Left-Right Symmetric Electroweak Theory from the $K_L - K_S$ Mass Difference*, *Phys. Rev. Lett.* **48** (1982) 848.
- [24] G. Ecker and W. Grimus, *ϵ, ϵ' in a model with spontaneous P and CP violation*, *Phys. Lett.* **B153** (1985) 279–285.
- [25] J. M. Frere *et. al.*, *$K^0 - \bar{K}^0$ in the $SU(2)_L \times SU(2)_R \times U(1)$ model of CP violation*, *Phys. Rev.* **D46** (1992) 337–353.
- [26] G. Barenboim, J. Bernabeu, and M. Raidal, *Spontaneous CP-violation in the left-right model and the kaon system*, *Nucl. Phys.* **B478** (1996) 527–543, [[hep-ph/9608450](#)].
- [27] R. N. Mohapatra, G. Senjanovic, and M. D. Tran, *Strangeness changing processes and the limit on the right-handed gauge boson mass*, *Phys. Rev.* **D28** (1983) 546.
- [28] Y. Zhang, H. An, X. Ji, and R. N. Mohapatra, *General CP Violation in Minimal Left-Right Symmetric Model and Constraints on the Right-Handed Scale*, *Nucl. Phys.* **B802** (2008) 247–279, [[arXiv:0712.4218](#)].
- [29] G. Barenboim, M. Gorbahn, U. Nierste, and M. Raidal, *Higgs sector of the minimal left-right symmetric model*, *Phys. Rev.* **D65** (2002) 095003, [[hep-ph/0107121](#)].
- [30] P. Ball, J. M. Frere, and J. Matias, *Anatomy of Mixing-Induced CP Asymmetries in Left-Right-Symmetric Models with Spontaneous CP Violation*, *Nucl. Phys.* **B572** (2000) 3–35, [[hep-ph/9910211](#)].
- [31] P. Langacker and S. Uma Sankar, *Bounds on the Mass of W_R and the $W_L - W_R$ Mixing Angle ξ in General $SU(2)_L \times SU(2)_R \times U(1)$ Models*, *Phys. Rev.* **D40** (1989) 1569–1585.
- [32] G. Barenboim, J. Bernabeu, J. Prades, and M. Raidal, *Constraints on the W_R mass and CP violation in left-right models*, *Phys. Rev.* **D55** (1997) 4213–4221, [[hep-ph/9611347](#)].
- [33] Y. Zhang, H. An, X. Ji, and R. N. Mohapatra, *Right-handed quark mixings in minimal left-right symmetric model with general CP violation*, *Phys. Rev.* **D76** (2007) 091301, [[arXiv:0704.1662](#)].
- [34] A. Maiezza, M. Nemevsek, F. Nesti, and G. Senjanovic, *Left-Right Symmetry at LHC*, *Phys. Rev.* **D82** (2010) 055022, [[arXiv:1005.5160](#)].
- [35] K. Hsieh, K. Schmitz, J.-H. Yu, and C. P. Yuan, *Global Analysis of General $SU(2) \times SU(2) \times U(1)$ Models with Precision Data*, *Phys. Rev.* **D82** (2010) 035011, [[arXiv:1003.3482](#)].
- [36] A. Crivellin and L. Mercolli, *$B \rightarrow X_d \gamma$ and constraints on new physics*, [arXiv:1106.5499](#).
- [37] C. Csaki, C. Grojean, L. Pilo, and J. Terning, *Towards a realistic model of Higgsless electroweak symmetry breaking*, *Phys. Rev. Lett.* **92** (2004) 101802, [[hep-ph/0308038](#)].
- [38] Y. Nomura, *Higgsless theory of electroweak symmetry breaking from warped space*, *JHEP* **11** (2003) 050, [[hep-ph/0309189](#)].

- [39] R. Barbieri, A. Pomarol, and R. Rattazzi, *Weakly coupled Higgsless theories and precision electroweak tests*, *Phys. Lett.* **B591** (2004) 141–149, [[hep-ph/0310285](#)].
- [40] H. Georgi, *Fun with Higgsless theories*, *Phys. Rev.* **D71** (2005) 015016, [[hep-ph/0408067](#)].
- [41] A. Crivellin, *Effects of right-handed charged currents on the determinations of $|V_{ub}|$ and $|V_{cb}|$* , *Phys. Rev.* **D81** (2010) 031301, [[arXiv:0907.2461](#)].
- [42] C.-H. Chen and S.-h. Nam, *Left-right mixing on leptonic and semileptonic $b \rightarrow u$ decays*, *Phys. Lett.* **B666** (2008) 462–466, [[arXiv:0807.0896](#)].
- [43] R. Feger, T. Mannel, V. Klose, H. Lacker, and T. Luck, *Limit on a Right-Handed Admixture to the Weak $b \rightarrow c$ Current from Semileptonic Decays*, *Phys. Rev.* **D82** (2010) 073002, [[arXiv:1003.4022](#)].
- [44] A. J. Buras, K. Gemmler, and G. Isidori, *Quark flavour mixing with right-handed currents: an effective theory approach*, *Nucl. Phys.* **B843** (2011) 107–142, [[arXiv:1007.1993](#)].
- [45] M. Nemevsek, F. Nesti, G. Senjanovic, and Y. Zhang, *First Limits on Left-Right Symmetry Scale from LHC Data*, *Phys.Rev.* **D83** (2011) 115014, [[arXiv:1103.1627](#)].
- [46] C. Grojean, E. Salvioni, and R. Torre, *A weakly constrained W' at the early LHC*, *JHEP* **1107** (2011) 002, [[arXiv:1103.2761](#)].
- [47] G. Ecker, W. Grimus, and H. Neufeld, *Higgs induced flavor changing neutral interactions in $SU(2)_L \times SU(2)_R \times U(1)$* , *Phys. Lett.* **B127** (1983) 365.
- [48] F. J. Gilman and M. H. Reno, *Restrictions from the neutral K and B meson systems on left-right symmetric gauge theories*, *Phys. Rev.* **D29** (1984) 937.
- [49] G. Ecker and W. Grimus, *CP Violation and Left-Right Symmetry*, *Nucl. Phys.* **B258** (1985) 328–360.
- [50] W.-S. Hou and A. Soni, *Gauge invariance of the $K_L - \bar{K}_S$ mass difference in left-right symmetric model*, *Phys. Rev.* **D32** (1985) 163.
- [51] D. London and D. Wyler, *Left-right symmetry and CP violation in the B system*, *Phys. Lett.* **B232** (1989) 503.
- [52] P. Ball and R. Fleischer, *An Analysis of B_s decays in the left-right symmetric model with spontaneous CP violation*, *Phys.Lett.* **B475** (2000) 111–119, [[hep-ph/9912319](#)].
- [53] S. Sahoo, L. Maharana, A. Roul, and S. Acharya, *The masses of W_R , triplet Higgs, and Z' bosons in the Left-Right Symmetric Model*, *Int. J. Mod. Phys.* **A20** (2005) 2625–2638.
- [54] G. M. Asatrian and A. N. Ionnisian, *Rare B meson decays in $SU(2)_L \times SU(2)_R \times U(1)$ model*, *Mod. Phys. Lett.* **A5** (1990) 1089–1096.
- [55] G. M. Asatryan and A. N. Ioannisyian, *The decay $b \rightarrow s\gamma$ in the $SU(2)_L \times SU(2)_R \times U(1)$ model*, *Sov. J. Nucl. Phys.* **51** (1990) 858–860.
- [56] D. Cocolicchio, G. Costa, G. L. Fogli, J. H. Kim, and A. Masiero, *Rare B decays in left-right symmetric models*, *Phys. Rev.* **D40** (1989) 1477.
- [57] P. L. Cho and M. Misiak, *$b \rightarrow s\gamma$ decay in $SU(2)_L \times SU(2)_R \times U(1)$ extensions of the Standard Model*, *Phys. Rev.* **D49** (1994) 5894–5903, [[hep-ph/9310332](#)].
- [58] K. S. Babu, K. Fujikawa, and A. Yamada, *Constraints on left-right symmetric models from the process $b \rightarrow s\gamma$* , *Phys. Lett.* **B333** (1994) 196–201, [[hep-ph/9312315](#)].
- [59] K. Fujikawa and A. Yamada, *Test of the chiral structure of the top - bottom charged current*

- by the process $b \rightarrow s\gamma$, *Phys. Rev.* **D49** (1994) 5890–5893.
- [60] G. M. Asatrian and A. Ioannian, *CP-Violation in the Decay $b \rightarrow s\gamma$ in the Left-Right Symmetric Model*, *Phys. Rev.* **D54** (1996) 5642–5646, [[hep-ph/9603318](#)].
 - [61] M. Frank, A. Hayreter, and I. Turan, *B Decays in an Asymmetric Left-Right Model*, *Phys. Rev.* **D82** (2010) 033012, [[arXiv:1005.3074](#)].
 - [62] D. Guadagnoli, R. N. Mohapatra, and I. Sung, *Gauged Flavor Group with Left-Right Symmetry*, *JHEP* **04** (2011) 093, [[arXiv:1103.4170](#)].
 - [63] R. N. Mohapatra and G. Senjanovic, *Neutrino mass and spontaneous parity nonconservation*, *Phys. Rev. Lett.* **44** (1980) 912.
 - [64] R. N. Mohapatra and G. Senjanovic, *Neutrino Masses and Mixings in Gauge Models with Spontaneous Parity Violation*, *Phys. Rev.* **D23** (1981) 165.
 - [65] O. Khasanov and G. Perez, *On neutrino masses and a low breaking scale of left-right symmetry*, *Phys. Rev.* **D65** (2002) 053007, [[hep-ph/0108176](#)].
 - [66] A. Aranda, J. Diaz-Cruz, E. Ma, R. Noriega, and J. Wudka, *Asymmetric Higgs Sector and Neutrino Mass in an $SU(2)_R$ Model*, *Phys.Rev.* **D80** (2009) 115003, [[arXiv:0909.1754](#)].
 - [67] M. Blanke *et. al.*, *Particle antiparticle mixing, ε_K , $\Delta\Gamma_q$, A_{SL}^q , $A_{CP}(B_d \rightarrow \psi K_S)$, $A_{CP}(B_s \rightarrow \psi\phi)$ and $B \rightarrow X_{s,d}\gamma$ in the Littlest Higgs model with T-parity*, *JHEP* **12** (2006) 003, [[hep-ph/0605214](#)].
 - [68] M. Blanke, A. J. Buras, B. Duling, S. Gori, and A. Weiler, *$\Delta F = 2$ Observables and Fine-Tuning in a Warped Extra Dimension with Custodial Protection*, *JHEP* **03** (2009) 001, [[arXiv:0809.1073](#)].
 - [69] A. J. Buras *et. al.*, *Patterns of Flavour Violation in the Presence of a Fourth Generation of Quarks and Leptons*, *JHEP* **09** (2010) 106, [[arXiv:1002.2126](#)].
 - [70] A. J. Buras, M. Misiak, and J. Urban, *Two-loop QCD anomalous dimensions of flavour-changing four-quark operators within and beyond the standard model*, *Nucl. Phys.* **B586** (2000) 397–426, [[hep-ph/0005183](#)].
 - [71] D. Chang, J. Basecq, L.-F. Li, and P. B. Pal, *Comment on the $K_L - K_S$ mass difference in left-right model*, *Phys. Rev.* **D30** (1984) 1601.
 - [72] J. Basecq, L.-F. Li, and P. B. Pal, *Gauge invariant calculation of the $K_L - K_S$ mass difference in the left-right model*, *Phys. Rev.* **D32** (1985) 175.
 - [73] A. J. Buras, S. Jager, and J. Urban, *Master formulae for $\Delta F = 2$ NLO-QCD factors in the standard model and beyond*, *Nucl. Phys.* **B605** (2001) 600–624, [[hep-ph/0102316](#)].
 - [74] M. Gorbahn, S. Jager, U. Nierste, and S. Trine, *The supersymmetric Higgs sector and $B - \bar{B}$ mixing for large $\tan \beta$* , *Phys.Rev.* **D84** (2011) 034030, [[arXiv:0901.2065](#)].
 - [75] A. J. Buras, M. V. Carlucci, S. Gori, and G. Isidori, *Higgs-mediated FCNCs: Natural Flavour Conservation vs. Minimal Flavour Violation*, *JHEP* **10** (2010) 009, [[arXiv:1005.5310](#)].
 - [76] A. J. Buras, G. Isidori, and P. Paradisi, *EDMs vs. CPV in $B_{s,d}$ mixing in two Higgs doublet models with MFV*, *Phys. Lett.* **B694** (2011) 402–409, [[arXiv:1007.5291](#)].
 - [77] D. Becirevic, V. Gimenez, G. Martinelli, M. Papinutto, and J. Reyes, *B-parameters of the complete set of matrix elements of $\Delta B = 2$ operators from the lattice*, *JHEP* **04** (2002) 025,

- [[hep-lat/0110091](#)].
- [78] R. Babich *et. al.*, $K^0 - \bar{K}^0$ mixing beyond the standard model and CP- violating electroweak penguins in quenched QCD with exact chiral symmetry, *Phys. Rev.* **D74** (2006) 073009, [[hep-lat/0605016](#)].
- [79] M. Ciuchini, E. Franco, V. Lubicz, G. Martinelli, I. Scimemi, *et. al.*, Next-to-leading order QCD corrections to $\Delta F = 2$ effective Hamiltonians, *Nucl.Phys.* **B523** (1998) 501–525, [[hep-ph/9711402](#)].
- [80] G. D’Agostini, *Asymmetric uncertainties: Sources, treatment and potential dangers*, [physics/0403086](#).
- [81] W. Altmannshofer, A. J. Buras, S. Gori, P. Paradisi, and D. M. Straub, *Anatomy and Phenomenology of FCNC and CPV Effects in SUSY Theories*, *Nucl.Phys.* **B830** (2010) 17–94, [[arXiv:0909.1333](#)].
- [82] B. Grinstein, M. Redi, and G. Villadoro, *Low Scale Flavor Gauge Symmetries*, *JHEP* **11** (2010) 067, [[arXiv:1009.2049](#)].
- [83] A. J. Buras, D. Guadagnoli, and G. Isidori, *On ε_K beyond lowest order in the Operator Product Expansion*, *Phys. Lett.* **B688** (2010) 309–313, [[arXiv:1002.3612](#)].
- [84] A. J. Buras and D. Guadagnoli, *On the consistency between the observed amount of CP violation in the K and B_d systems within minimal flavor violation*, *Phys.Rev.* **D79** (2009) 053010, [[arXiv:0901.2056](#)].
- [85] **UTfit** Collaboration, M. Bona *et. al.*, *The UTfit collaboration report on the status of the unitarity triangle beyond the standard model. I. Model-independent analysis and minimal flavor violation*, *JHEP* **0603** (2006) 080, [[hep-ph/0509219](#)].
- [86] M. Beneke, G. Buchalla, C. Greub, A. Lenz, and U. Nierste, *Next-to-leading order QCD corrections to the lifetime difference of B_s mesons*, *Phys.Lett.* **B459** (1999) 631–640, [[hep-ph/9808385](#)].
- [87] M. Beneke, G. Buchalla, C. Greub, A. Lenz, and U. Nierste, *The $B^+ - B_d^0$ lifetime difference beyond leading logarithms*, *Nucl.Phys.* **B639** (2002) 389–407, [[hep-ph/0202106](#)].
- [88] M. Beneke, G. Buchalla, A. Lenz, and U. Nierste, *CP asymmetry in flavor specific B decays beyond leading logarithms*, *Phys.Lett.* **B576** (2003) 173–183, [[hep-ph/0307344](#)].
- [89] M. Ciuchini, E. Franco, V. Lubicz, and F. Mescia, *Next-to-leading order QCD corrections to spectator effects in lifetimes of beauty hadrons*, *Nucl.Phys.* **B625** (2002) 211–238, [[hep-ph/0110375](#)].
- [90] M. Ciuchini, E. Franco, V. Lubicz, F. Mescia, and C. Tarantino, *Lifetime differences and CP violation parameters of neutral B mesons at the next-to-leading order in QCD*, *JHEP* **08** (2003) 031, [[hep-ph/0308029](#)].
- [91] A. Lenz, *A simple relation for B_s -mixing*, [arXiv:1106.3200](#).
- [92] **For the CDF** Collaboration, G. Giurgiu, *New Measurement of the B_s Mixing Phase at CDF*, *PoS ICHEP2010* (2010) 236, [[arXiv:1012.0962](#)].
- [93] **D0** Collaboration, V. M. Abazov *et. al.*, *Measurement of the CP-violating phase $\phi_s^{J/\psi\phi}$ using the flavor-tagged decay $B_s^0 \rightarrow J/\psi\phi$ in 8 fb^{-1} of $p\bar{p}$ collisions*, [arXiv:1109.3166](#).
- [94] **LHCb** Collaboration, G. Raven, “B Physics Results from the LHC.” Review talk, rather than LHCb specific, but featuring new LHCb results.

<http://cdsweb.cern.ch/record/1378074?ln=en>, Aug, 2011.

- [95] **Heavy Flavor Averaging Group** Collaboration, D. Asner *et. al.*, *Averages of b -hadron, c -hadron, and tau-lepton Properties*, [arXiv:1010.1589](https://arxiv.org/abs/1010.1589). Updates available on <http://www.slac.stanford.edu/xorg/hfag/>.
- [96] **D0** Collaboration, V. M. Abazov *et. al.*, *Measurement of the anomalous like-sign dimuon charge asymmetry with $9fb^{-1}$ of $p\bar{p}$ collisions*, [arXiv:1106.6308](https://arxiv.org/abs/1106.6308).
- [97] Z. Ligeti, M. Papucci, and G. Perez, *Implications of the measurement of the $B_s^0 - \bar{B}_s^0$ mass difference*, *Phys. Rev. Lett* **97** (2006) 101801, [[hep-ph/0604112](https://arxiv.org/abs/hep-ph/0604112)].
- [98] M. Blanke, A. J. Buras, D. Guadagnoli, and C. Tarantino, *Minimal Flavour Violation Waiting for Precise Measurements of ΔM_s , $S_{\psi\phi}$, A_{SL}^s , $|V_{ub}|$, γ and $B_{s,d}^0 \rightarrow \mu^+\mu^-$* , *JHEP* **10** (2006) 003, [[hep-ph/0604057](https://arxiv.org/abs/hep-ph/0604057)].
- [99] Y. Grossman, Y. Nir, and G. Perez, *Testing New Indirect CP Violation*, *Phys. Rev. Lett.* **103** (2009) 071602, [[arXiv:0904.0305](https://arxiv.org/abs/0904.0305)].
- [100] C. Bobeth, M. Misiak, and J. Urban, *Matching conditions for $b \rightarrow s\gamma$ and $b \rightarrow s$ gluon in extensions of the standard model*, *Nucl. Phys.* **B567** (2000) 153–185, [[hep-ph/9904413](https://arxiv.org/abs/hep-ph/9904413)].
- [101] M. Misiak, H. Asatrian, K. Bieri, M. Czakon, A. Czarnecki, *et. al.*, *Estimate of $B(\bar{B} \rightarrow X_s\gamma)$ at $\mathcal{O}(\alpha_s^2)$* , *Phys.Rev.Lett.* **98** (2007) 022002, [[hep-ph/0609232](https://arxiv.org/abs/hep-ph/0609232)].
- [102] A. J. Buras, L. Merlo, and E. Stamou, *The Impact of Flavour Changing Neutral Gauge Bosons on $\bar{B} \rightarrow X_s\gamma$* , *JHEP* **1108** (2011) 124, [[arXiv:1105.5146](https://arxiv.org/abs/1105.5146)].
- [103] M. Misiak and M. Steinhauser, *NNLO QCD corrections to the $B \rightarrow X_s\gamma$ matrix elements using interpolation in m_c* , *Nucl. Phys.* **B764** (2007) 62–82, [[hep-ph/0609241](https://arxiv.org/abs/hep-ph/0609241)].
- [104] M. Benzke, S. J. Lee, M. Neubert, and G. Paz, *Factorization at Subleading Power and Irreducible Uncertainties in $\bar{B} \rightarrow X_s\gamma$ Decay*, *JHEP* **08** (2010) 099, [[arXiv:1003.5012](https://arxiv.org/abs/1003.5012)].
- [105] T. Hurth, E. Lunghi, and W. Porod, *Untagged $B \rightarrow X_{s,d}\gamma$ CP asymmetry as a probe for new physics*, *Nucl. Phys.* **B704** (2005) 56–74, [[hep-ph/0312260](https://arxiv.org/abs/hep-ph/0312260)].
- [106] J. M. Soares, *CP violation in radiative b decays*, *Nucl.Phys.* **B367** (1991) 575–590.
- [107] A. L. Kagan and M. Neubert, *Direct CP violation in $B \rightarrow X_s\gamma$ decays as a signature of new physics*, *Phys.Rev.* **D58** (1998) 094012, [[hep-ph/9803368](https://arxiv.org/abs/hep-ph/9803368)].
- [108] A. L. Kagan and M. Neubert, *QCD anatomy of $B \rightarrow X_s\gamma$ decays*, *Eur.Phys.J.* **C7** (1999) 5–27, [[hep-ph/9805303](https://arxiv.org/abs/hep-ph/9805303)].
- [109] M. Benzke, S. J. Lee, M. Neubert, and G. Paz, *Long-Distance Dominance of the CP Asymmetry in $B \rightarrow X_{s,d}\gamma$ Decays*, *Phys. Rev. Lett.* **106** (2011) 141801, [[arXiv:1012.3167](https://arxiv.org/abs/1012.3167)].
- [110] M.-C. Chen and J. Huang, *TeV Scale Models of Neutrino Masses and Their Phenomenology*, [arXiv:1105.3188](https://arxiv.org/abs/1105.3188).
- [111] M. Czakon, J. Gluza, and J. Hejczyk, *Muon decay to one loop order in the left-right symmetric model*, *Nucl. Phys.* **B642** (2002) 157–172, [[hep-ph/0205303](https://arxiv.org/abs/hep-ph/0205303)].
- [112] **Particle Data Group** Collaboration, K. Nakamura *et. al.*, *Review of particle physics*, *J. Phys.* **G37** (2010) 075021. Updates available on <http://pdg.lbl.gov/>.
- [113] M. Antonelli, V. Cirigliano, G. Isidori, F. Mescia, M. Moulson, *et. al.*, *An Evaluation of $|V_{us}|$ and precise tests of the Standard Model from world data on leptonic and semileptonic kaon decays*, *Eur.Phys.J.* **C69** (2010) 399–424, [[arXiv:1005.2323](https://arxiv.org/abs/1005.2323)].

- [114] J. Laiho, E. Lunghi, and R. S. Van de Water, *Lattice QCD inputs to the CKM unitarity triangle analysis*, *Phys. Rev.* **D81** (2010) 034503, [[arXiv:0910.2928](#)]. Updates available on <http://latticeaverages.org/>.
- [115] **Fermilab Lattice and MILC Collaboration**, J. A. Bailey *et. al.*, *$B \rightarrow D^* l \nu$ at zero recoil: an update*, *PoS LATTICE2010* (2010) 311, [[arXiv:1011.2166](#)].
- [116] M. Okamoto, C. Aubin, C. Bernard, C. E. DeTar, M. Di Pierro, *et. al.*, *Semileptonic $D \rightarrow \pi/K$ and $B \rightarrow \pi/D$ decays in 2+1 flavor lattice QCD*, *Nucl.Phys.Proc.Suppl.* **140** (2005) 461–463, [[hep-lat/0409116](#)].
- [117] M. Finkemeier, *Radiative corrections to π_{l2} and K_{l2} decays*, [hep-ph/9501286](#).
- [118] **D0 Collaboration**, V. Abazov *et. al.*, *Precision measurement of the ratio $B(t \rightarrow Wb)/B(t \rightarrow Wq)$ and Extraction of V_{tb}* , *Phys.Rev.Lett.* **107** (2011) 121802, [[arXiv:1106.5436](#)].
- [119] **ALEPH, DELPHI, L3, OPAL, SLD, LEP Electroweak Working Group, SLD Electroweak Group, SLD Heavy Flavour Group Collaboration**, *Precision electroweak measurements on the Z resonance*, *Phys.Rept.* **427** (2006) 257–454, [[hep-ex/0509008](#)].
- [120] A. Giri, Y. Grossman, A. Soffer, and J. Zupan, *Determining gamma using $B^\pm \rightarrow DK^\pm$ with multibody D decays*, *Phys.Rev.* **D68** (2003) 054018, [[hep-ph/0303187](#)].
- [121] **Belle Collaboration**, A. Poluektov, “Recent EW results from Belle.” Talk given at Rencontres de Moriond, March 13-20, 2011, slides available on <http://indico.in2p3.fr/conferenceOtherViews.py?view=standard&confId=4403>.
- [122] A. J. Buras, *Flavor physics and CP violation*, [hep-ph/0505175](#).
- [123] S. Faller, M. Jung, R. Fleischer, and T. Mannel, *The Golden Modes $B^0 \rightarrow J/\psi K_{S,L}$ in the Era of Precision Flavour Physics*, *Phys.Rev.* **D79** (2009) 014030, [[arXiv:0809.0842](#)].
- [124] H. Flacher, M. Goebel, J. Haller, A. Hocker, K. Monig, *et. al.*, *Revisiting the Global Electroweak Fit of the Standard Model and Beyond with Gfitter*, *Eur.Phys.J.* **C60** (2009) 543–583, [[arXiv:0811.0009](#)].
- [125] A. Arbuzov, M. Awramik, M. Czakon, A. Freitas, M. Grunewald, *et. al.*, *ZFITTER: A Semi-analytical program for fermion pair production in $e^+ e^-$ annihilation, from version 6.21 to version 6.42*, *Comput.Phys.Commun.* **174** (2006) 728–758, [[hep-ph/0507146](#)]. Updates available on <http://zfitter.desy.de/>.
- [126] M. E. Peskin and T. Takeuchi, *Estimation of oblique electroweak corrections*, *Phys.Rev.* **D46** (1992) 381–409.
- [127] M. Baak *et. al.*, *Updated Status of the Global Electroweak Fit and Constraints on New Physics*, [arXiv:1107.0975](#).
- [128] **The ALEPH, DELPHI, L3, OPAL, SLD Collaborations, the LEP Electroweak Working Group, the SLD Electroweak and Heavy Flavour Groups**, *Precision Electroweak Measurements on the Z Resonance*, *Phys. Rept.* **427** (2006) 257, [[hep-ex/0509008](#)].
- [129] **TWIST Collaboration**, R. Bayes *et. al.*, *Experimental Constraints on Left-Right Symmetric Models from Muon Decay*, *Phys. Rev. Lett.* **106** (2011) 041804.
- [130] **ATLAS Collaboration**, G. Aad *et. al.*, *Search for a heavy gauge boson decaying to a charged lepton and a neutrino in 1 fb^{-1} of pp collisions at $\sqrt{s} = 7 \text{ TeV}$ using the ATLAS*

detector, [arXiv:1108.1316](#).

- [131] **CMS** Collaboration, “Search for W' in the leptonic channels in pp Collisions at $\sqrt{s} = 7$ TeV.” <http://cdsweb.cern.ch/record/1369201?ln=en>, 2011.
- [132] **CMS** Collaboration, “Search for a heavy neutrino and right-handed W of the left-right symmetric model in pp collisions at $\sqrt{s} = 7$ TeV.” <http://cdsweb.cern.ch/record/1369255?ln=en>, 2011.
- [133] **CMS** Collaboration, S. Chatrchyan *et. al.*, *Search for Resonances in the Dijet Mass Spectrum from 7 TeV pp Collisions at CMS*, . <http://cdsweb.cern.ch/record/1370086?ln=en>.
- [134] **ATLAS** Collaboration, G. Aad *et. al.*, *Search for New Physics in the Dijet Mass Distribution using 1fb^{-1} of pp Collision Data at $\sqrt{s} = 7$ TeV collected by the ATLAS Detector*, [arXiv:1108.6311](#).
- [135] E. Lunghi and A. Soni, *Hints for the scale of new CP-violating physics from B-CP anomalies*, *JHEP* **0908** (2009) 051, [[arXiv:0903.5059](#)].
- [136] E. Lunghi and A. Soni, *Unitarity Triangle Without Semileptonic Decays*, *Phys.Rev.Lett.* **104** (2010) 251802, [[arXiv:0912.0002](#)].
- [137] **RBC** Collaboration, D. J. Antonio *et. al.*, *Neutral kaon mixing from 2+1 flavor domain wall QCD*, *Phys. Rev. Lett.* **100** (2008) 032001, [[hep-ph/0702042](#)].
- [138] C. Aubin, J. Laiho, and R. S. Van de Water, *The Neutral kaon mixing parameter $B(K)$ from unquenched mixed-action lattice QCD*, *Phys.Rev.* **D81** (2010) 014507, [[arXiv:0905.3947](#)].
- [139] T. Bae, Y.-C. Jang, C. Jung, H.-J. Kim, J. Kim, *et. al.*, *B_K using HYP-smearred staggered fermions in $N_f = 2 + 1$ unquenched QCD*, *Phys.Rev.* **D82** (2010) 114509, [[arXiv:1008.5179](#)].
- [140] **ETM** Collaboration, M. Constantinou *et. al.*, *B_K -parameter from $N_f = 2$ twisted mass lattice QCD*, *Phys.Rev.* **D83** (2011) 014505, [[arXiv:1009.5606](#)].
- [141] Y. Aoki, R. Arthur, T. Blum, P. Boyle, D. Brommel, *et. al.*, *Continuum Limit of B_K from 2+1 Flavor Domain Wall QCD*, *Phys.Rev.* **D84** (2011) 014503, [[arXiv:1012.4178](#)].
- [142] J. Brod and M. Gorbahn, *ϵ_K at Next-to-Next-to-Leading Order: The Charm-Top-Quark Contribution*, *Phys. Rev.* **D82** (2010) 094026, [[arXiv:1007.0684](#)].
- [143] J. Brod and M. Gorbahn, *The NNLO Charm-Quark Contribution to ϵ_K and ΔM_K* , [arXiv:1108.2036](#).
- [144] R. Barbieri, G. Isidori, J. Jones-Perez, P. Lodone, and D. M. Straub, *$U(2)$ and Minimal Flavour Violation in Supersymmetry*, *Eur.Phys.J.* **C71** (2011) 1725, [[arXiv:1105.2296](#)].
- [145] T. Aushev, W. Bartel, A. Bondar, J. Brodzicka, T. Browder, *et. al.*, *Physics at Super B Factory*, [arXiv:1002.5012](#).
- [146] **SuperB** Collaboration, M. Bona *et. al.*, *SuperB: A High-Luminosity Asymmetric e^+e^- Super Flavor Factory. Conceptual Design Report*, [arXiv:0709.0451](#).
- [147] **SuperB** Collaboration, B. O’Leary *et. al.*, *SuperB Progress Reports – Physics*, [arXiv:1008.1541](#).
- [148] B. Meadows, M. Blanke, A. Stocchi, A. Drutskoy, A. Cervelli, *et. al.*, *The impact of SuperB on flavour physics*, [arXiv:1109.5028](#).

- [149] W. Altmannshofer and M. Carena, *B Meson Mixing in Effective Theories of Supersymmetric Higgs Bosons*, [arXiv:1110.0843](#).
- [150] S. Faller, R. Fleischer, and T. Mannel, *Precision Physics with $B_s^0 \rightarrow J/\psi\phi$ at the LHC: The Quest for New Physics*, *Phys.Rev.* **D79** (2009) 014005, [[arXiv:0810.4248](#)].
- [151] S. Herrlich and U. Nierste, *The Complete $|\Delta S| = 2$ Hamiltonian in the Next-To-Leading Order*, *Nucl. Phys.* **B476** (1996) 27–88, [[hep-ph/9604330](#)].
- [152] A. J. Buras, M. Jamin, and P. H. Weisz, *Leading and next-to-leading QCD corrections to ε parameter and $B^0 - \bar{B}^0$ mixing in the presence of a heavy top quark*, *Nucl. Phys.* **B347** (1990) 491–536.
- [153] J. Urban, F. Krauss, U. Jentschura, and G. Soff, *Next-to-leading order QCD corrections for the $B^0 - \bar{B}^0$ mixing with an extended Higgs sector*, *Nucl. Phys.* **B523** (1998) 40–58, [[hep-ph/9710245](#)].
- [154] **HPQCD** Collaboration, I. Allison *et. al.*, *High-Precision Charm-Quark Mass from Current-Current Correlators in Lattice and Continuum QCD*, *Phys. Rev.* **D78** (2008) 054513, [[arXiv:0805.2999](#)].
- [155] C. Csaki, A. Falkowski, and A. Weiler, *The Flavor of the Composite Pseudo-Goldstone Higgs*, *JHEP* **0809** (2008) 008, [[arXiv:0804.1954](#)].
- [156] R. Barbieri and G. F. Giudice, *Upper Bounds on Supersymmetric Particle Masses*, *Nucl. Phys.* **B306** (1988) 63.
- [157] P. Athron and D. J. Miller, *A New Measure of Fine Tuning*, *Phys. Rev.* **D76** (2007) 075010, [[arXiv:0705.2241](#)].
- [158] D. Guadagnoli and R. N. Mohapatra, *TeV Scale Left Right Symmetry and Flavor Changing Neutral Higgs Effects*, *Phys.Lett.* **B694** (2011) 386–392, [[arXiv:1008.1074](#)].
- [159] A. J. Buras, B. Duling, and S. Gori, *The Impact of Kaluza-Klein Fermions on Standard Model Fermion Couplings in a RS Model with Custodial Protection*, *JHEP* **0909** (2009) 076, [[arXiv:0905.2318](#)].
- [160] B. Duling, *A Comparative Study of Contributions to ϵ_K in the RS Model*, *JHEP* **1005** (2010) 109, [[arXiv:0912.4208](#)].
- [161] K. Agashe, G. Perez, and A. Soni, *Flavor structure of warped extra dimension models*, *Phys.Rev.* **D71** (2005) 016002, [[hep-ph/0408134](#)].
- [162] G. Isidori, Y. Nir, and G. Perez, *Flavor Physics Constraints for Physics Beyond the Standard Model*, *Ann.Rev.Nucl.Part.Sci.* **60** (2010) 355, [[arXiv:1002.0900](#)].
- [163] M. Blanke, B. Shakya, P. Tanedo, and Y. Tsai, *The birds and the Bs in RS: the $b \rightarrow s\gamma$ penguin in a warped extra dimension*, [arXiv:1203.6650](#).
- [164] J. Hubisz, S. J. Lee, and G. Paz, *The Flavor of a little Higgs with T-parity*, *JHEP* **0606** (2006) 041, [[hep-ph/0512169](#)].
- [165] M. Blanke, A. J. Buras, S. Recksiegel, and C. Tarantino, *The Littlest Higgs Model with T-Parity Facing CP-Violation in $B_s - \bar{B}_s$ Mixing*, [arXiv:0805.4393](#).
- [166] M. Blanke, A. J. Buras, B. Duling, S. Recksiegel, and C. Tarantino, *FCNC Processes in the Littlest Higgs Model with T-Parity: an Update*, *Acta Phys.Polon.* **B41** (2010) 657–683, [[arXiv:0906.5454](#)].

- [167] N. G. Deshpande, J. F. Gunion, B. Kayser, and F. I. Olness, *Left-right symmetric electroweak models with triplet Higgs*, *Phys. Rev.* **D44** (1991) 837–858.
- [168] K. Kiers, M. Assis, and A. A. Petrov, *Higgs sector of the left-right model with explicit CP violation*, *Phys. Rev.* **D71** (2005) 115015, [[hep-ph/0503115](#)].